Counteracting Temozolomide resistance in Glioblastoma Multiforme (GBM) through suppression of the base excision repair (BER) pathway

By

Haynes (Shek Hei) Yuan

Thesis submitted to the Faculty of Graduate Studies
Of
The University of Manitoba
In partial fulfillment of the requirements for the degree of
Master in Science

Department of Pharmacology

& Therapeutics
University of Manitoba
Winnipeg, Canada

Contents

1. ABSTRACT 8

2. ACKNOWLEDGEMENTS 10

3. INTRODUCTION 11

3.1. Brain tumours and Glioma. 11
3.2. Glioblastoma Multiforme (GBM). 12
3.3. Epidemiology and occurrence. 13
3.4. GBM mutational profiling and molecular subtypes. 15
3.5. Clinical Presentation and Diagnosis. 16
3.6. Current treatment approaches. 17
3.7. Temozolomide: standard-of-care anti-GBM chemotherapy. 17
3.8. Intratumorally heterogeneity as a driver of resistance. 19
3.9. Advent of recurrence and palliative treatment strategies. 20
3.10. The DNA Damage Response (DDR). 22
3.11. DNA single-stranded break repair 25
3.11.1. Mammalian mismatch repair 26
3.11.2. Base excision repair 26
3.12. DNA double-stranded break repair 27
3.12.1. Homologous recombination repair 27
3.12.2. Alternative non-homologous end-joining repair 28
3.12.3. Non-homologous end-joining repair 29
3.13. Other mechanisms to resolve TMZ-induced DNA damage. 30
3.14. DNA-damage induced cell death. 30
3.15. Parp-inhibitors and their clinical use in cancer management. 33
3.16. On-going GBM research and challenges 35
3.17. GBM models and limitations. 37
1.17.1 *In vitro* 2-D model 37
1.17.2 *In vitro* 3-D cultures and tumour spheroid models 37
1.17.3 *In vivo* xenografts and mouse genetic models 38

4. HYPOTHESIS AND OBJECTIVES 40

Objective 2 40
Objective 3 40

5. MATERIAL AND METHOD 40

5.1. Cell cultures 40
5.2. DNA damaging agents & PARP inhibitors/trappers 41
5.3. Development of fluorescent TMZ-sensitive and resistant U251 lines 41
5.4. Automated system for data collection and analysis 43
5.5. Growth assay 43
5.6. High throughput alkaline comet assay 45
5.7. γ-H2AX staining assay 46
5.8. Zombie cell death assay 48
5.9. Cell migration assay 49
5.10. RNA extraction and Clariom D analysis 50

5.11. PROTEIN EXPRESSION ANALYSIS 51
5.12. GENE KNOCK-DOWN/ OVER-EXPRESSION ANALYSIS 52
5.13. DATA ANALYSIS AND STATISTICS 54
5.14. COMBENEFIT 54

6. RESULTS 55

6.1. DEVELOPMENT OF CELL-BASED ASSAYS & CHARACTERIZATION OF TMZ RESISTANCE 55
6.1.1. CELL GROWTH UNDER TEMOZOLOMIDE 55
6.1.2. ALKALINE COMET ASSAY 56
6.1.3. Γ-H2AX ASSAY 58
6.1.4. ZOMBIE CELL DEATH ASSAY 59
6.1.5. CELL MIGRATION ASSAY 61
6.2. IDENTIFICATION OF PATHWAYS THAT CONTRIBUTE TO RESISTANCE 63
6.2.1. EXPRESSION OF O^6-METHYLGUANINE-DNA METHYLTRANSFERASE (MGMT) 63
6.2.2. DIFFERENTIALLY-EXPRESSED DNA DOUBLE-STRANDED BREAK REPAIR GENES AMONGST SG AND TRR LINES 64
6.2.3. EXPRESSION OF BASE EXCISION REPAIR (BER) PATHWAY-RELATED GENE PRODUCTS 67
6.3. CONTRIBUTION OF MODIFIED PATHWAYS IN TMZ RESISTANCE 69
6.3.1. O^6-METHYLGUANINE-DNA METHYLTRANSFERASE (MGMT) 69
6.3.2. XRCC1-MEDIATED BASE EXCISION REPAIR 71
6.4. RE-SENSITIZING RGBM TO TMZ BY INHIBITING BASE EXCISION REPAIR 79
6.4.1. PJ34 VS TMZ 81
6.4.2. OLAPARIB VS TMZ 86
6.4.3. TALAZOPARIB VS TMZ 91
6.4.4. PAMIPARIB VS TMZ 95
6.4.5. EFFICACY OF PARPI/T TO RE-SENSITIZE RGBM 99
6.5. POTENTIAL ROLE OF XRCC1 IN CELL MIGRATION 100
6.6. TRANSFORMATION OF SG/TRR TO 3-D CULTURES AND VALIDATIONS 102
6.7. PRELIMINARY STUDIES ON PATIENT DERIVED TUMORSPHERE MODEL 103

7. DISCUSSION 104

7.1. DEVELOPMENT AND CHARACTERIZATION OF A TRACTABLE TMZ-RESISTANT MODEL OF GBM 104
7.2. ROLE OF BASE-EXCISION REPAIR IN RGBM DEVELOPMENT AND PROGRESSION 107
7.3. RE-SENSITIZATION OF TRR VIA INHIBITION OF PARP-DEPENDENT BER PATHWAY 108
7.4. XRCC1 AS A POTENTIAL BIOMARKER 110

8. FUTURE DIRECTIONS 111

8.1. INVESTIGATING THE MECHANISM OF CROSS-RESISTANCE TOWARDS SECONDARY THERAPEUTICS 111
8.2. INTRATUMORAL HETEROGENEITY 111
8.3. TRANSLATION TO PATIENT-DRIVEN MODELS AND OTHER CLINICAL MODELS 112
8.4. HIGH-CONTENT SCREENING OF SG VS TRR 113

9. SIGNIFICANCE OF STUDY 114

10. REFERENCES 117

11. SUPPLEMENTAL DATA 128

List of Tables

TABLE 1 WHO CLASSIFICATION OF CNS TUMOURS 11
TABLE 2 INGREDIENTS OF SOLUTIONS 46
TABLE 3 LIST OF ANTIBODIES USED 52
TABLE 4 SEQUENCES OF SHRNZ PLASMIDS USED. 53
TABLE 5 CLARIOM D READOUT OF DSBR PROTEINS 64
TABLE 6 CLARIOM D READOUT OF SSBR PROTEINS 67
TABLE S1 RNA CONCENTRATIONS 128

List of Figures

FIGURE 1 HISTOLOGICAL IMAGE OF GBM 13
FIGURE 2 INSIDENCE RATE AND DISTRIBUTION OF GBM 14
FIGURE 3 WORKING MECHANISM OF TEMOZOLOMIDE 19
FIGURE 4. CELLULAR SINGNALING RESPONSES TRIGGERED BY DNA DAMAGE 23
FIGURE 5.SUMMARY OF TMZ ASSOCIATED DNA REPAIR PATHWAYS 25
FIGURE 6 SIMPLIFIED SCHEMATIC OF SSBR 27
FIGURE 7SIMPLIFIED SCHEMATIC OF DSBR 29
FIGURE 8. SIMPLIFIED PATHWAYS OF DNA DAMAGE INDUED APOPTOSIS 32
FIGURE 9. SIMPLIFIED WORKING MECHANISMS OF PARP INHIBITOR/TRAPPER 34
FIGURE 10 DEVELOPMENT OF 2-D RESISTANT GBM MODEL 42
FIGURE 11 AUTOMATED SYSTEM USED IN THE EXPERIMENT 43
FIGURE 12 EXAMPLE IMAGES OF GTOWTH ASSAY 44
FIGURE 13 EXAMPLE IMAGES AND COMET TAIL MOMENT DETERMINATION OF COMET ASSAY 46
FIGURE 14 EXAMPLE IMAGES OF Γ-H2AX ASSAY 47
FIGURE 15 EXAMPLE IMAGES OF ZOMBIE DEATH ASSAY 49
FIGURE 16. EXAMPLE IMAGES OF CELL MIGRATION ASSAY 50
FIGURE 17 VALIDATION OF RESISTANCE WITH GRWOTH ASSAY 56
FIGURE 18 VALIDATION OF RESISTANCE WITH COMET ASSAY 57
FIGURE 19 VALIDATION OF RESISTANCE WITH Γ-H2AX ASSAY 59
FIGURE 20 VALIDATION OF RESISTANCE WITH DEATH ASSAY 60
FIGURE 21 CHARACTERIZATION OF RESISTANCE LINE WITH MIGRATION ASSAY 62
FIGURE 22 EXPRESSION LEVEL OF MGMT 63
FIGURE 23 PROTEIN EXPRESSION FOR DSBR PROTEINS 66
FIGURE 24 PROTEIN EXPRESSION OF BER PROTEINS 68
FIGURE 25 COMET ASSAY WITH MGMT KNOCK-DOWN IN SG/TRR 70
FIGURE 26 PROTEINASE-K COMET ASSAY WITH 72 HOURS TMZ PRE-TRETMENT IN TRR 73
FIGURE 27 PROTEINASE-K COMET ASSAY WITH XRCC1 OVER-EXPRESSION IN SG 75
FIGURE 28 PROTEINASE-K COMET ASSAY WITH XRCC1 KNOCK-DOWN IN SG/TRR 77
FIGURE 29 GROWTH ASSAY WITH XRCC1 KNOCK-DOWN IN SG/TRR 78
FIGURE 30 DEATH ASSAY WITH 72 HOURS PRE-TREATMENT IN TRR 79
FIGURE 31 PARP TRAPPING CAPABILITIES OF INHIBITORS 80
FIGURE 32 GROWTH ASSAY WITH TMZ-PJ34 CO-TREATMENT 82
FIGURE 33 DNA DAMAGE ASSAYS WITH TMZ-PJ34 CO-TREATMENT 84
FIGURE 34 DEATH ASSAY WITH TMZ-PJ34 CO-TREATMENT 85
FIGURE 35 GROWTH ASSAY WITH TMZ-OLAP CO-TREATMENT 87
FIGURE 36 DNA DAMAGE ASSAYS WITH TMZ-OLAP CO-TREATMENT 89
FIGURE 37 DEATH ASSAY WITH TMZ-OLAP CO-TREATMENT 90
FIGURE 38 GROWTH ASSAY WITH TMZ-TALAZOPARIB CO-TREATMENT 92
FIGURE 39 DNA DAMAGE ASSAYS WITH TMZ-TALAZOPARIB CO-TREATMENT 93
FIGURE 40 DEATH ASSAY WITH TMZ-TALAZOPARIB CO-TREATMENT 95
FIGURE 41 GROWTH ASSAY WITH TMZ-PAMIPARIB CO-TREATMENT 96
FIGURE 42 DNA DAMAGE ASSAYS WITH TMZ-PAMIPARIB CO-TREATMENT 98
FIGURE 43 DEATH ASSAY WITH TMZ-PAMIPARIB CO-TREATMENT 99
FIGURE 44 RE-SENSITIZATION EFFECT OF PARPI/T WITH TMZ 100
FIGURE 45 CELL MIGRATION ASSAY WITH XRCC1 KD AND/OR PAMIPARIB UNDER TMZ 101
FIGURE 46 PRELIMIARY PROTEIN EXPRESSION ASSAY WITH 3-D SG/TRR MODELS... 錯誤! 尚未定義書籤。
FIGURE 47 PRELIMIARY PROTEIN EXPRESSION ASSAY WITH 3-D BTIC MODELS錯誤! 尚未定義書籤。

FIGURE S1 RNA PURITIES **128**
FIGURE S2 RNA CONTENTS (1) **129**
FIGURE S3 RNA CONTENTS (2) **130**
FIGURE S4 RNA CONTENTS (3) **131**
FIGURE S5 RNA CONTENTS (4) **132**
FIGURE S6 RNA CONTENTS (5) **133**

Table of abbreviations

Abbreviations/jargon	Expanded form	Abbreviations/jargon	Expanded form
ADP	Adenosine diphosphate	MGMT	O^6-methylguanine-DNA methyltransferase
AIC	4-amino-5-imidazole-carboxamide	MMR	Mammalian mismatch repair
AIF	apoptosis inducing factor	MPG	N-methylpurine DNA glycosylase
ANOVA	Analysis of variance	Mre11	Meiotic recombination 11
APAF-1	apoptosis protease activating factor	MTIC	5-(3-methyltriazen-1-yl)imidazole-4-carboxamide
Ape1	Apurinic endonuclease 1	MutH	Mytator H
ATM	Ataxia telangiectasia Mutant	MutL	Mytator L
BAX	Bcl-2 associated protein X	MutS	Mytator S
Bcl-2	B-cell lymphoma 2 gene	NBS1	Nijmegen breakage syndrome 1/ Nibirin
BER	Base-excision repair	NHEJ	Non-homologous end joining
BRCA1/2	Gene for Breast cancer 1/2	PARP	Poly ADP-ribose polymerase
Caspase	Cysteinyl, aspartate specific proteases	PARPi/t	PARP ihibitor/ trapper
CDK1/2	Cyclin Dependent Kinase 1/2	pATM	Phosphorylated (Ser1981) ATM
chk1/2	Checkpoint kinase 1/2	PFA	Paraformaldehyde
CNS	Central nervous system	PGP	Phospho-glycoprotein
CSCs	Cancer stem cells	PIKK	phosphatidylinositol-3-kinase like protein kinase
CT	computed tomography	polβ	DNA polymeraseβ
CtBP	C-terminal binding protein	PTEN	Phosphatase and tensin homolog
CtIP	C-terminal binding protein interacting protein	PUMA	p53 upregulated modulator of apoptosis
Cyt c	Cytochrom C	RFC	Replication factor C
DDR	DNA damage responses	ROS	Reactive oxygen species
DNA-PK	DNA depedent protin kinase	RT	Room temperature
DSB	DNA double-stranded break	SG	TMZ sensitive green fluorescent U251 cell
DSBR	Double-stranded break repair	sGBM	Secondary Glioblastoma multiforme
EGFR	Epidermal growth factor receptor	Smac	second mitochondria-derived activator of caspases
Exo1	Exonuclease 1	SSB	DNA single-stranded break
GBM	Glioblastoma multiforme	SSBR	Single-stranded break repair
GFP	Green fluorescent protein	TAC	Transcriptom analysis console
H2AX	Histon 2A analog	TMZ	Temozolomide
HRR	Homologous recombination repair	TRR	TMZ resistant red fluorescent U251 cell
IDH1/2	Isocitrate dehydrognase 1/2	VEGF	Vessel endothelial cell growth factor
LigIII	DNA ligase III	WHO	World Health Organization
LigIV	DNA ligase IV	XRCC1/4	X-ray repair cross-complementing protein 1/4
MDR1	Multiple drug resistance gene 1	γH2AX	Phosphorylated (Ser139) H2AX

1. Abstract

Background

Glioblastoma Multiforme (GBM) is an aggressive cerebral cancer. Standard treatment includes surgery, radiation and Temozolomide; a DNA alkylating agent. Patients relapse mostly due to recurrence of a drug-resistant tumour. As GBM resistance may involve DNA repair pathways that become hyperactivated, my project seeks to understand the molecular underpinnings of GBM resistance and recurrence in order to identify novel treatment paradigms that may serve to counteract drug-resistant GBM.

Methods and Materials

TMZ sensitive/resistant GBM models with nuclear fluorescent were generated, and resistance was validated with growth, DNA damage and death assays. Furthermore, RNA/protein expression was compared to identify modifications in TMZ-resistant cells; significant changes were functionalized via RNAi. PARP inhibitors (PARPi) were used in cell-based assays to evaluate the relative contribution of BER to TMZ resistance in GBM.

Results

TRR cells demonstrated robust performance toward TMZ in terms of growth, tolerance against DNA damage and resistance to TMZ-induced cell death. With RNA /protein analysis assays, XRCC1-mediated BER expression and activity was enhanced in TRR, and further stimulated under subsequent treatment of TMZ indicating a plastic response to *de novo* DNA damage despite acquired resistance.

Validation studies using XRCC1 knockdown in TRR and over-expression in SG suggested XRCC1 plays a critical role in TMZ-resistance. Furthermore, effects of 4 independent PARP inhibitors/trappers (PARPi/PARPt) were tested on this cell model to study the efficacy of chemical-mediated BER inhibition as a co-treatment strategy to re-sensitize TRR toward TMZ. PARPi/PARPt demonstrated cooperativity with TMZ, displaying growth suppression, enhanced DNA damage, and increased cell death in TRR.

Conclusion

In my study, base excision repair pathway was found to significantly contribute to TMZ resistance in rGBM. By inhibiting BER using PARPi/PARPt, re-sensitization to TMZ was restored in TRR, while the efficacy of TMZ was enhanced in SG. These data have potential implications on treating recurrence of rGBM. Furthermore, this novel cell-based model of pGBM/rGBM can be used in a variety of fluorescence-based high throughput small molecule drug screens to identify novel anti-GBM treatments.

2. Acknowledgements

At the completion of this Master's thesis, I would like to express my deepest gratitude to my supervisor, Dr. Sachin Katyal, for offering this opportunity to me, his kind support and guardiancy, particularly in improving my scientific writing skills.

In the same light, I really appreciate all the help and assistance from my fellow lab members, who taught and guided me through all the research techniques and novel e-cutting-edge technologies.

I would also like to extend my thanks to Mr. Mike Wakem, who aided in the analysis of the Clariom D transcriptome, and Dr. Judy Anderson, supervisor of the Honor's thesis in my undergrad, for her friendly advice, support and presence at my thesis defense.

Lastly, I would like to dedicate this thesis to my family, mentors and friends, in honor of all the support, patience and opportunities they have provided me over the years.

3. Introduction

3.1. Brain tumours and Glioma.

There are a variety of tumours of the central nervous system. These are most often and best classified based on the location in CNS and/or the cell type of origin or area that is affected (See table 1.).

Table 1. WHO classification of CNS tumours. [Table modified from (Reifenberger et al. 2010; Louis et al. 2016)].

Origin	Subtypes	Origin	Subtypes
Astrocytic tumours	Pilocytic astrocytoma	**Neuronal and mixed neuronal-glial tumours**	Dysplastic gangliocytoma of cerebellum
	Pilomyxoid astrocytoma		Desmoplastic ingantile astrocytoma/ganglioglioma
	Subependymal giant cell astrocytoma		Dysembryoplastic neroepithelial tumour
	Pleomorphic xanthoastrocytoma		Gangliocytoma
	Diffuse astrocytoma		Gangioglioma
	Anaplastic astrocytoma		Anaplastic ganglioglioma
	Glioblastoma		Central neurocytoma
	Gliomatosis cerebri		Extraventricular neurocytoma
			Cerebellar liponeuronal tumour
Oligodendroglial tumours	Oligodendroglioma		Rosette-forming glioneuronal tumour of the forth centricle
	Anaplastic oligodendroglioma		Paraganglioma
Oligoastrocytic tumours	Oligoastrocytoma	**Tumouurs of the pineal region**	Pineocytoma
	Anaplastic oligoastrocytoma		Pineal parenchymal of intermediate differentiation
			Pineoblastoma
Ependymal tumours	Subpendymoma		Papillary tumour of pineal region
	Myxopapillary ependymoma		
	Epenymoma	**Embryonal tumours**	Desmoplastic/nodular medulloblatoma
	Anaplastic ependymoma		Medulloblatoma with extensive nmodularity
			Anaplastic medulloblastoma
Choroid plexus tumous	Coroid plexus papilloma		Large cell medulloblastoma
	Atypical choroid plexus papilloma		CNS neuroblastoma
	Choroid plexus carcinoma		CNS ganglioneuroblastoma
			Medulloepithelioma
Other neuroepitelial tumours	Astroblastoma		Ependymoblastoma
	Chordoid glioma of the third venticle		Atypical teratoid/rhabdiod tumour
	Angiocentric glioma		

Glioma is a general term describing tumours that originate from different types of glial cell, including astrocytes, from within the brain. Astrocytes are a specific sub-class of glia, that are neural (yet non-neuronal) and provide physical and physiological support to neurons. Gliomas[3] account for approximately 80% of all primary malignant brain tumours [4]. The World Health Organization (WHO) classifies gliomas (glial cell of origin) and astrocytomas (astrocyte cell of origin) based on a four-tier system, primarily on the tumour's histopathological

characteristics. Grade I gliomas include benign astrocytoma lesions such as pilocytic astrocytoma and subependymal giant cell astrocytoma. Diffuse astrocytoma is the most common grade II astrocytoma, which is a slow growing cancer with the capability to transform into higher grade glioma after treatment [5]. Grade III anaplastic astrocytoma is characterized by prominent hypercellularity, mitotic activity and nuclear atypia. Lastly, the malignant astrocytoma subtype with vascular proliferative properties, such as Glioblastoma multiforme are considered a grade IV tumours [2,6,7].

Additional to *de novo* development of high grade tumours, approximately 70% low grade brain tumour (Grade I and II) that present as relatively benign tumour and inert behavior, do ultimately progress to a high grade tumour 5-10 years after diagnosis [8].

3.2. Glioblastoma Multiforme (GBM).

Central nervous system malignancy is a commonly occurring neural-origin solid neoplasm prevalent during the course of human history. Glioblastoma Multiforme (GBM) is a highly invasive, undifferentiated, and highly lethal form of brain cancer [9]. GBM is the most frequently-diagnosed primary astrocytoma comprising of approximately 60% of all newly diagnosed cases [10], and classified as a grade IV malignancy according to the World Health Organization classification system [2]. GBM have distinct neuropathological features, such as active mitotic events, pseudopalisading and central region necrosis, diffuse infiltration into surrounding

tissues, and microscopic angiogenic events, which were commonly considered diagnostic factors [11](See figure 1).

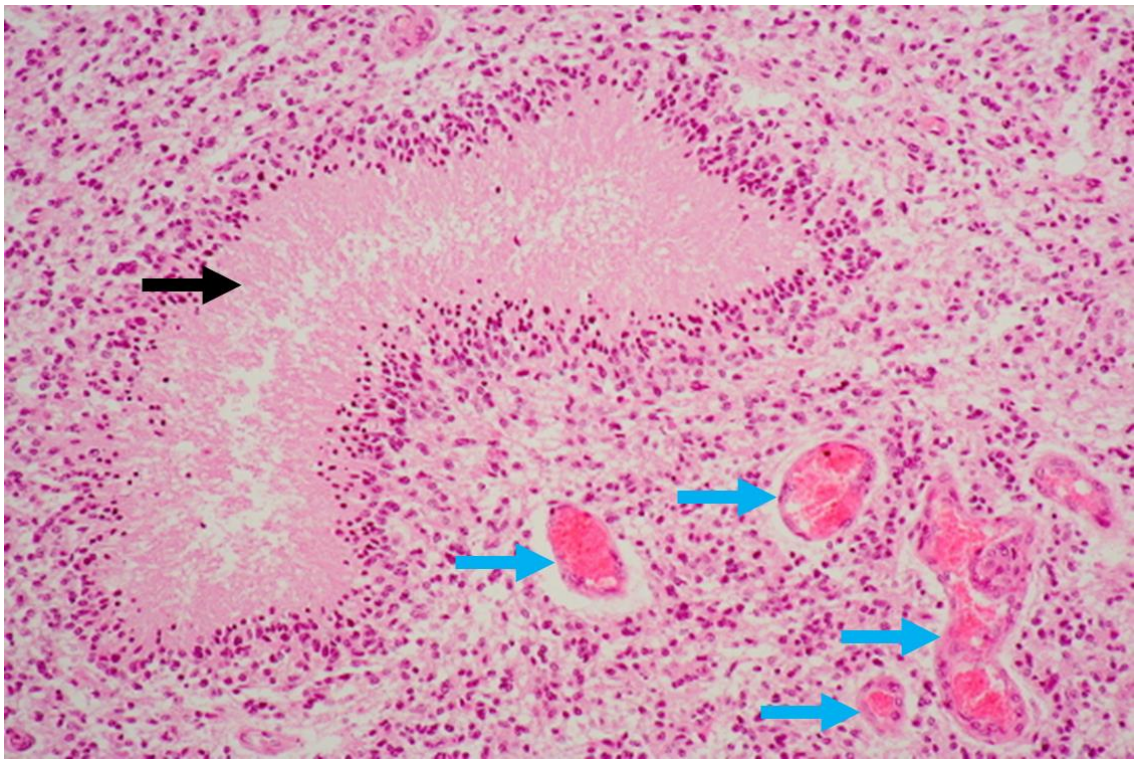

Figure 1. Histological image of GBM. Highly active mitotic events in the parenchymal area, necrotic zone (Black arrow) and the microvasculatures are indicated by blue arrows [Image adapted from Abdelzaher, E. Glioblastoma multiforme. PathologyOutlines.com website. http://www.pathologyoutlines.com/topic/cnstumorglioblastoma.html. Accessed April 23rd, 2019.]

3.3. Epidemiology and occurrence.

Glioblastoma Multiforme can manifest at any age, and accounts for 15.7% of all primary brain tumour cases. The peak incidence is around 45-75 years old [12], and the site of incidence is usually located in frontal, temporal and parietal lobes (Fig 2). Moreover, disproportionally to its overall incidence [4.06 per 100,000 people,[13]],

GBM has an abysmal prognosis with an overall survival rate of 14.6 months upon diagnosis [14]. Following surgical resection of the tumour mass, standard GBM treatment, consisting of chemo-radio-therapy, incurs costs of ~$10,000/month; a heavy economic burden to patients and public health care systems [15,16]. The etiology of GBM remains unclear, as no underlying carcinogenic factor is identified as a direct cause for GBM. Although some studies have suggested that exposure to therapeutic grade ionizing radiation is a risk factor for GBM, most GBM cases are considered to be spontaneous [2,17,18].

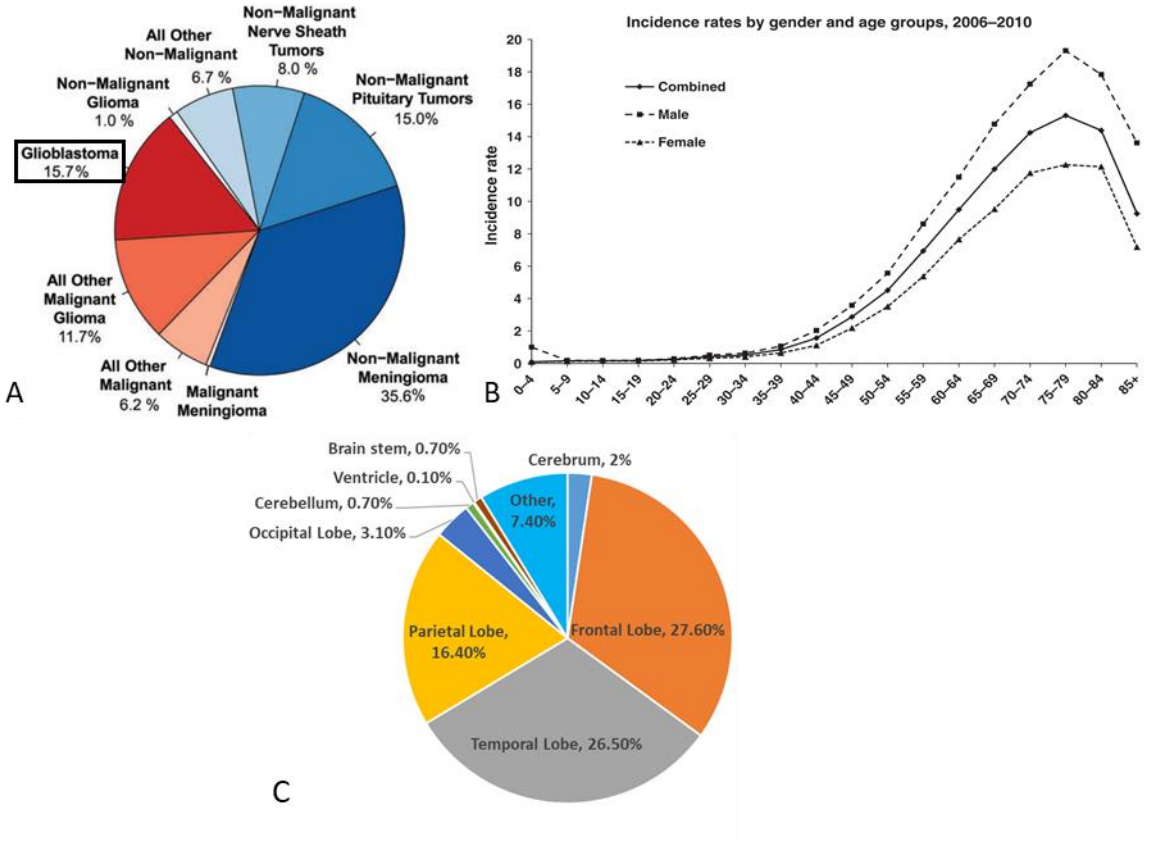

Figure 2. (A) Diversity of primary CNS and brain tumours, GBM accounts for a significant fraction. (B) Incidence rate by gender and age for GBM, which the incident rate is highest around age 65. (C) Site distribution of GBM, figures adopted from National Cancer Registry and [17,19].

3.4. GBM mutational profiling and molecular subtypes.

Like most cancers, the accumulation of genetic alterations (loss of function, amplification of gene, etc.) contributes to the development of GBM. Mutations in genes, such as, IDH1/2, p16, p53, PTEN, VEGF (vascular endothelial cell growth factor) and EGFR (epidermal growth factor receptor) are frequently identified [20]. These genetic modifications contribute to the poor patient prognosis and lethal characteristics of this deadly disease (Sonoda et al. 2011; Lam et al. 2009). Isocitrate dehydrogenase 1/2 (IDH1/2) are critical enzymes related to glucose metabolism and oxidative stress. Mutations in IDH 1/2 are frequently identified in GBM genetic profiling analyses [23], and they are more common in high-grade/recurrent GBM (~70%) than in low-grade/primary tumour (~12%)[24], which makes the IDH status a strong prognostic factor in high-grade GBM. However, studies suggest that GBM patients with IDH mutations tend to fare better with relatively longer overall survival [21,24]. The underlying mechanisms of how IDH mutations improve patient outcome are unclear, but there are recent studies suggesting that, an enzymatic product of mutated IDH, 2-hydroxyglutarate (2-HG), inhibited effects of DNA demethylating enzymes, including MGMT. The inhibition of MGMT might provide survival advantages to GBM patients [25,26].

PTEN, p16 and p53 are tumour suppressor genes that regulate cell migration, genome integrity, cell cycle, proliferation and death. Mutations of these genes play important roles in tumour development and aggressiveness, which lead to worse prognostic features, including dysregulated cell cycle and cell proliferation [9,27], diffuse infiltration, [9,28], genetic aberration [29], and resistance to cell death [30].

Angiogenesis is a primary definitive characteristic of high-grade GBM, as rapid angiogenic events close to the tumour site is commonplace. This may due to modulation of expression of the pro-angiogenic factor, VEGF [31,32]. Anti-VEGF compounds have been incorporated in some GBM treatment regimens but with limited success [33]. The epidermal growth factor receptor (EGFR) is overexpressed in GBM [34]; the most common mutation of which is the extracellular domain mutation in EGFR vIII. Dysregulated EGFR vIII signaling that over-regulates and promotes cancer proliferation [35] is often associated with tumour progression and is correlated with poor prognosis [36].

3.5. Clinical Presentation and Diagnosis.

In most cases, GBM is asymptomatic at earlier stages of tumour development; therefore, the majority of primary GBM patients present with limited adverse clinical history of only a few months, while patients incurring secondary GBM arising from earlier occurring low-grade glioma tend have a longer clinical history [9,28]. Common signs of GBM include dizziness, vomiting, vertigo and headache, but none of these, alone, are specifically an indicator of GBM. These sorts of neurological symptoms may be initiated by neural tissue necrosis arising from the tumour or by increased inter-cranial pressure arising from the growing cell mass [27,28].

Due to a lack of active screening, surveillance or initial symptom-free detection there are no known or effective diagnosis or biomarkers of GBM. As such, usually GBM is discovered via brain imaging techniques, such as MRI (Magnetic resonance imaging), or CT (computed tomography) scans either coincidently with other events

are when patients present with neurological symptoms [9,28]. Ultimately, accurate definitive diagnoses occurs following surgical extraction of brain material and subsequent histological examination of these samples [28].

3.6. Current treatment approaches.

GBM treatment remains enigmatic in clinical oncology, mainly because of the lack of accessibility to the tumour, the complexity and heterogeneity of the disease [30]. The current standard of care for GBM involves surgical resection of cancer tissue followed by radio- and chemotherapy [14,37]. Surgery that remove cancerous tissue is a critical to anti-GBM treatment. However, as a highly invasive malignancy and its tendency to encroach on critical structures and vasculature, GBM is extremely difficult to completely resect [38], resulting in a high probability of recurrence [33]. To kill/suppress the remaining cancer cells after surgery, radio- and chemotherapy is employed [10]. Radiotherapy uses a total course of 60 Gy (2Gy/day, 5 days/week for 6 weeks) leads to an improvement in the patient's overall survival [39]. In addition, chemotherapy utilizing the FDA approved alkylating agent, Temozolomide (TMZ), is sole agent used; a dose of 75mg/m^2 is recommended alongside with radiotherapy course, or an adjuvant dose of 150mg/m^2 for 6 x 5/28day cycle[40].

3.7. Temozolomide: standard-of-care anti-GBM chemotherapy.

Temozolomide (TMZ) is a DNA alkylating agent proven to significantly improve patient survival (~25% increase in 2-yr survival post-diagnosis) when combined

with radiotherapy[10,39]. With consideration of several determining factors, such as the tumour mutational profile, immune system [41] of the patient and epigenetic status of oncogenes (p53, EFGR, PTEN,IDH1/2 chromosomal 1p/19q deletion)[7,42–44] and resistant genes (MGMT, MDR1)[45], oral administration of TMZ is prescribed in most cases as an adjuvant to surgery and radiotherapy [39].

TMZ methylates guanine on either its O^6- and N^7- position (See figure 3.); a nucleotide modification that triggers the DNA mismatch repair (MMR) system, a DNA repair process often used to eliminate replicational errors to maintain genome integrity. However, a lack of base complementarity towards the methylated guanine, results in incomplete MMR and a failure to resolve the DNA damage. This failure consequently induces a nick on the DNA strand, progressing to a to single strand break if it remains unrepaired. This DNA lesion can further disintegrate into a DNA double-stranded break as a result of DNA replication. When these DNA breaks are detected, they trigger DNA damage responses that may interrupt the cell cycle, or induce cell apoptosis if the damage is significant [46,47]. Resolution of this damage can occur via multiple mechanisms, thereby counteracting TMZ's therapeutic benefit. In addition to the inbound DNA damage repair pathways (DNA single/double strand break repair), the best studied enzymatic modifier of this damage-type is O^6-methylguanine-DNA methyltransferase (MGMT) which is often epigenetically modified to enhance repair and correlates with therapeutic resistance. MGMT is an enzyme, coded by the gene of the same name, that can reverse the methylating action of TMZ on DNA. While this genetic locus usually undergoes methylation, epigenetic demethylation of this gene will enhance hyperactivity of MGMT thus

contributing to TMZ resistance [2,38,48,49]. A more detailed description of how TMZ-induced damage is resolved and repaired is covered in section 1.13.

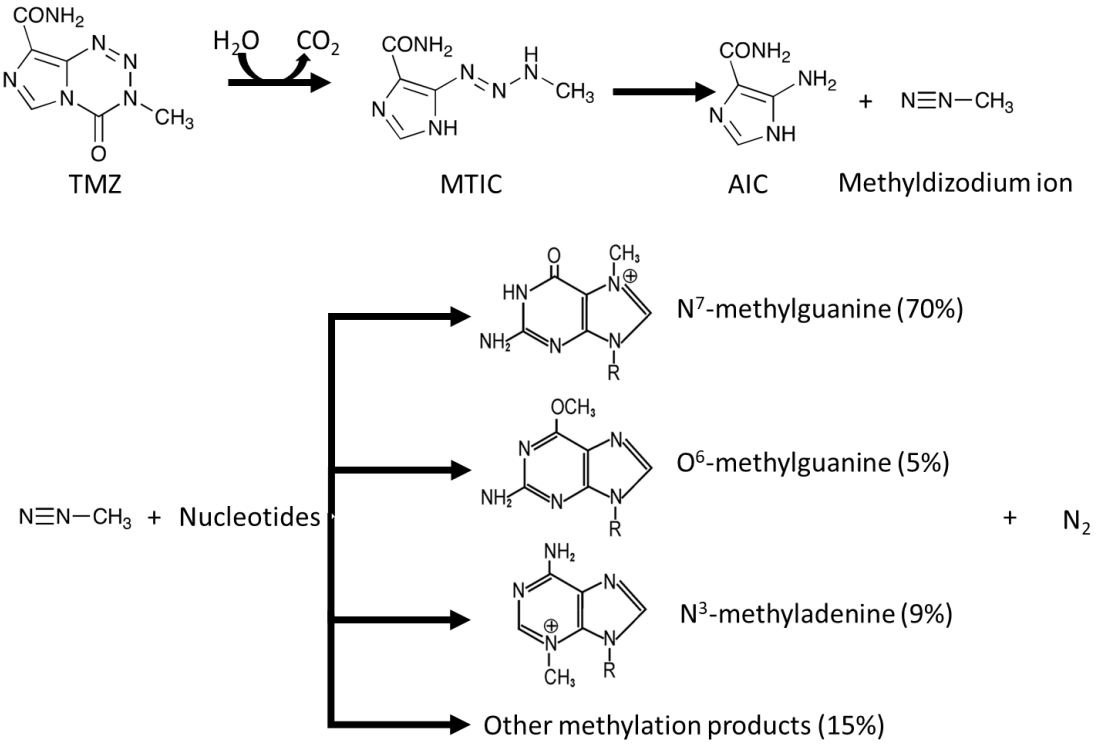

Figure 3. The chemical conversion of Temozolomide and the methylation product of DNA. Temozolomide (TMZ) is hydrolyzed to is intermediate compound, 5-(3-methyltriazen-1-yl)imidazole-4-carboxamide (MTIC), and further decompose to 4-amino-5-imidazole-carboxamide (AIC) and methyldizodium, the active compound that methylate DNA. Methyldizodium methylate nucleotides and release Nitrogen, major methylated products include N^7-methylguanine (70%), O^6-methylguanine (5%) and N^3-methyladenine (9%). [modified from [46,50,51]].

3.8. Intratumorally heterogeneity as a driver of resistance.

As evidenced by the name, Glioblastoma **multiforme** is recognized as a heterogenetic tumour. GBM growth is thought to be driven by cancer stem cells

(CSCs) that are able to self-renew and proliferate[6,52]. Lineages of CSCs with diverse mutation states develop subpopulations of clusters within a tumour mass, containing varieties of genotypic and phenotypic characteristics [53].

The currant prevailing theory is that intratumorally heterogeneity is foundational for therapeutic resistance in GBM: sub-clonal populations in primary tumours may diverge at difference periods during tumorigenesis, or even during therapy [54]. The diversity of the genetic mutation profile (e.g. p53, EGFR, IDH, MGMT, PTEN etc) within the same tumour mass may have divergent effects on cell survival, growth and response to therapies [55,56]. Upon the therapeutic selection pressure, these fitness characteristics might ultimately lead to a better clonal evasion of treatments/drug effects, with surviving resistant clones driving tumour recurrent[6,43,54,57]. Whether these clones pre-exist prior to therapy or emerge as a function of therapy remains controversial [58,59]; but likely, both mechanisms were involved [54].

3.9. Advent of recurrence and palliative treatment strategies.

The majority of patients survive the standard treatment for primary GBM, but ultimately incur GBM recurrence [14]. Most recurrent GBM (rGBM) arise from intercranial primary tumours (GBM or other low-grade glioma)[60], where glioblastoma stem cells that survive treatment form clones that undergo expansion. [54,61]. Usually, the recurrence is located within 2 cm from the primary site [62,63], however, some tumour cells are able to infiltrate and migrate to other intracranial sites, thus developing secondary tumours [28,64]. Although rare, some GBM tumour cells can invade and migrate across the blood-brain barrier, and enter the

circulating blood stream as circulating tumour cells; thus, leading to extracranial metastasis [64–66].

There are a few distinct mutation features commonly found in rGBM; approximately 85% of rGBM contain a mutation in *IDH1* [61], while *p53*, *PTEN*, and *EGFR* also show frequent mutation in rGBM [44,54,60,61,67,68]. Combined, mutation of these genes are implicated in tumour progression,, treatment resistance and poor outcome [17,44,47,52,60]. To date, there exists no standard treatment protocol for dealing with rGBM; TMZ still remains the most commonly used rGBM therapeutic although its efficacy is significantly lower in recurrent GBM [57]. Additional agents as an adjuvant to TMZ are utilized, including Topoisomerase-1 inhibitors (ie. Topotecan, Irinotecan, SN-38), EGFR inhibitors (ie. Gefitinib, erlotinib), mTOR inhibitors (ie.Temsirolimus, Everolimus), Platelet-derived growth factor receptor inhibitors (ie. Imatinib mesylate, PTK787), VEGFR inhibitors (ie. Sorafenib, Sonitinib), etc [69–71]

The recurrent tumour relies greatly on nutritional supply and a variety of external trophic factors, including EGF, VEGF and PDGF, However, attempts to use inhibitors against these factors (ie. Avastin against VEGF) and signaling pathways (ie. Gefintinib/Lapatinib against EGFR) have had limited success against recurrent GBM [32,43,68]. The integration of chemotherapeutics agents that induce DNA damage have also been used to suppress rGBM, such as topoisomerase inhibitors [72], radiolabeled vectors and seeds [73], Cannabinoids [74,75], and other DNA alkylating agents [76].

Recently, surgeons have applied drug-coated wafers to deliver chemotherapeutics locally via insertion of biodegradable wafers containing the drug-of-choice (ie. TMZ, Carmustine or other anticancer agents) during surgical resection of the tumour. The

wafers release drug up to 4 weeks locally at the location of the primary tumour, and some studies showed positive results: however, wafers have limited potential to prolong patient survival [12,77]. As such, due to the heterogeneic nature of this disease, overall treatment success so far has been limited with results varying greatly amongst individual patients.

3.10. The DNA Damage Response (DDR).

As indicated above, the vast majority of chemotherapeutics counteract cancer via the induction of DNA damage with ultimate purpose of killing tumour cells [78,79]. However, cells already are pre-programmed with inborn mechanisms to deal with exogenously and endogenously-occurring DNA damage. DNA damage can occur via a multitude of mechanisms, which can induce a variety of DNA lesions. The cellular DNA damage repair response is composed of phases that act to detect, transduce and respond to the damage signal, in order to repair DNA lesions, and ultimately, to restore DNA integrity to achieve cell survival [80,81]. These involve the convergence of many cellular pathways (ie. cell cycle, DNA replication, metabolism, apoptosis) that act in concert (Cellular responses to TMZ-induced damage were showed in figure 4). If the damage is too great for repair or overwhelms the repair system, a cell death signal is initiated to remove the aberrantly damaged cells from the organ system. The goal of cancer radio- and chemotherapy is to promote DNA damage and cell death of tumour cells by exploiting unique tumour features while sparing/minimizing impact on normal cells. However, specific tumour types and following primary therapy, the tumour cell's DNA damage detection/repair

mechanisms may become hyperactivated and develop resistant to DNA damaging agents, thus making the tumour increasingly difficulty to treat [52,79,82,83].

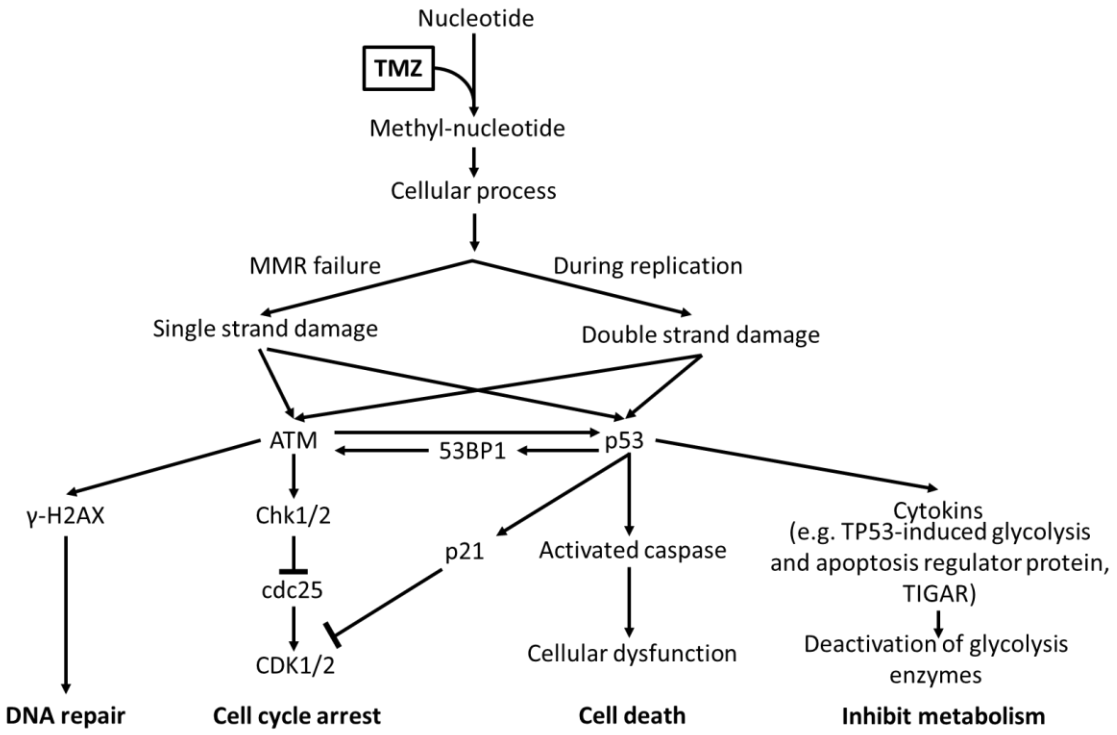

Figure 4. The molecular signaling schematic of cellular responses triggered by DNA damage (ie. TMZ treatment). TMZ induces both single and double stranded breaks, which will activate ATM (Ataxia Telangiectasia Mutant protein) and p53, these activated proteins further regulate/alter cell cycle by activating check point kinase proteins (chk1/2) or p21. Activation of ATM can also trigger DNA repair pathways and activate p53-mediated cell cycle regulation, cellular metabolism and apoptosis. [integrated from[9,18,84–87]]

The main types of DNA lesions occurring within cells includes nucleotide mismatch, bulky lesions, DNA single stranded breaks and double stranded breaks [81,84]. These lesion-types are recognized and repaired by dedicated repair pathways (Figure 5).

An accumulation of DNA damage triggers a cell cycle signaling cascade which include key effector proteins such as, p53, p21, CDK1/2, chk1/2, etc [88]. These have critical roles in the cell cycle checkpoint pathway (see above figure 4 and 5), which ultimately, can arrest the cell cycle at check points to allow for DNA repair to complete thus allowing resumption of the cell cycle[89]. Alternatively, should these damage fail to fully repair, cell cycle checkpoints will induce cell death in order to clear the damaged, irreparable cells.

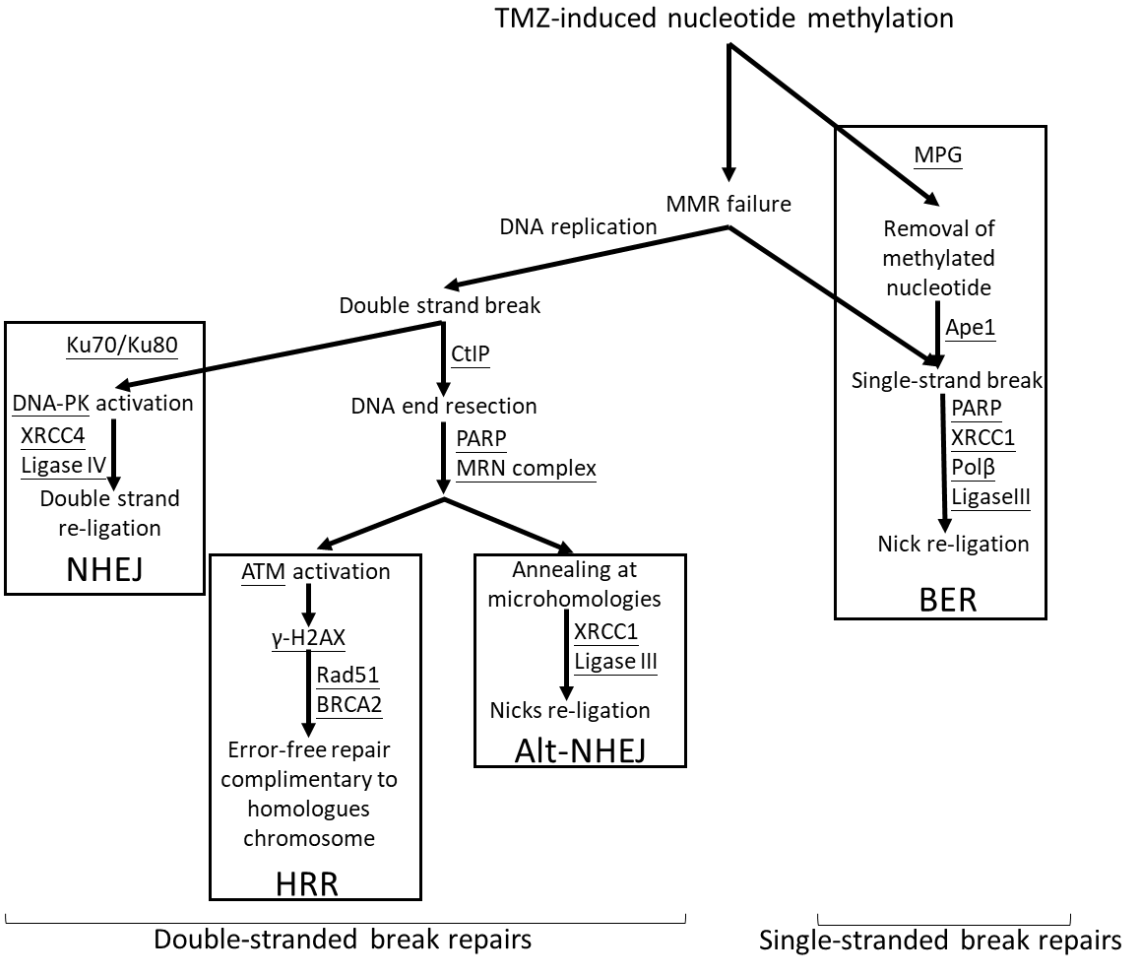

Alt-NHEJ	Alternative non-homologous end joining repair	MMR	Mismatch repair
Ape1	Apurinic endonuclease	MPG	N-methylpurine DNA glycosylase
ATM	Ataxia telangiectasia Mutant protein	MRN complex	MRE11, Rad50, NES1
BER	Base excision repair	NHEJ	Non-homologous end joining repair
BRCA2	Mutation in breast cancer gene 2	PARP	Poly ADP-ribose polymerase
CtIP	C-terminal binding protein interacting protein	Pol β	DNA polymerase β
DNA-PK	DNA depedent protein kinase	XRCC1	X-ray repair cross-complementing protein 1
HRR	Homologous recombinantion repair	XRCC4	X-ray repair cross-complementing protein 4
MGMT	O6-methylguanine-DNA methyltransferase		

Figure 5. Summary of major DNA repair pathways and their responsibility in the context of TMZ-induced methylation and TMZ-associated DNA damage. [Modified from [50,90–95]].

3.11. DNA single-stranded break repair

DNA single stranded breaks (SSB) refer to damage of the DNA sugar backbone or nucleotide base within one strand of the DNA molecule. SSBs are induced in daily metabolic events, such as replicational errors, reactive oxygen species (ROS), ionizing radiation, and other carcinogens [96,97]. Radiotherapy, radiomimetics and a variety of chemotherapeutics induce SSB to achieve cancer suppression [13,98,99]. These DNA SSB inducers generate single strand nicks, bulky lesion or cross-linkages on the DNA strand, which can burden cellular activities [100,101]. Should SSB remain unresolved and the damaged DNA undergo replication, lethal DNA double stranded breaks may result due to replication fork collapse [96,102]. To eliminate SSBs before replication, there are two major DNA single stranded break repairing mechanisms that may be engaged: mammalian mismatch repair (MMR) and base excision repair (BER) [47,50].

3.11.1. Mammalian mismatch repair

Mammalian mismatch repair acts as a prove-reading system for replicating DNA. MutS proteins recognize nucleotide mismatches (i.e. methylated nucleotides), and the MutL proteins stabilize the DNA-protein complex. With the help of MutH, exonuclease 1 and other proteins, a section of the DNA strand with the mismatched nucleotide is removed, and the molecule is repaired in conjunction with DNA polymerase and ligases[90,103,104] (see figure 6).

3.11.2. Base excision repair

In addition to MMR, damaged or transformed nucleotides can also be repaired via DNA single stranded break repair, particularly base excision repair (BER). The mismatched base is first recognized by N-methylpurine DNA glycosylase (MPG), whereby the deoxyribose backbone is removed by Apurinic endonuclease (Ape1) resulting in a prototypical DNA single stranded break. This lesion is then detected by Poly ADP-ribose polymerase (PARP), which catalyzes the formation of polymers of ADP ribose (PAR) onto the XRCC1 scaffolding protein to mediate its breaksite recruitment. Accompanying XRCC1 are DNA polymeraseβ (polβ) and DNA ligase III to the breaksite which are assembled to repair the DNA break [95,105] (See figure 6). As such, prior work has shown that BER is critical to resolve TMZ-induced DNA damage [50,95].

3.12. DNA double-stranded break repair

A failure to resolve SSBs may lead to the generation of the particularly genotoxic DNA double-stranded breaks (DSBs) [96,98,102]. Cellular detection of DSBs triggers a DSB repair cascade that efficiently repairs via two major mechanisms: homologous recombination repair (HRR) and non-homologous end joining (NHEJ) [100]. In certain contexts, an alternative-NHEJ pathway also contributes to DNA double stranded break repair [93].

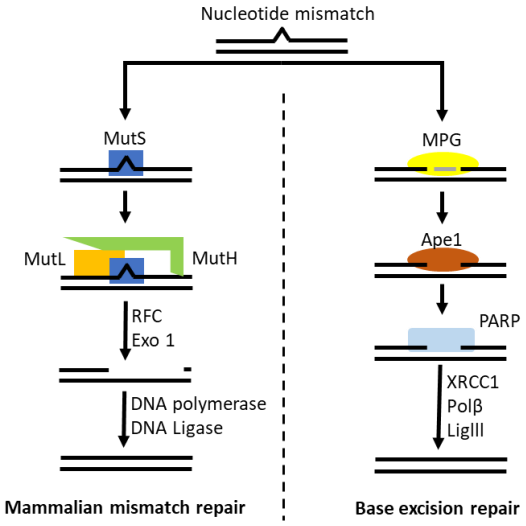

Ape1	Apurinic endonuclease
Exo1	Exonuclease 1
LigIII	DNA Ligase III
MPG	N-methylpurine DNA glycosylate
MutH	Mytator H
MutL	Mytator L
MutS	Mytator S
PARP	Poly ADP-ribose polymerase
Pol β	DNA polymerase β
RFC	Replication factor C
XRCC1	X-ray repair cross-complementing protein 1

Figure 6. A simplified schematic of the DNA single-stranded break repair pathways, including mammalian mismatch repair (MMR) and base excision repair (BER). [Modified from [103–107]]

3.12.1. Homologous recombination repair

In terms of repairing TMZ-induced damage, DNA double-stranded breaks can arise from MMR failure followed by DNA replication. Most DNA double-stranded breaks contain an exposed C-terminus, which can be recognized by C-terminal binding

protein (CtBP) and C-terminal binding protein interacting protein (CtIP): two proteins involved in the resection of the DNA ends [92], followed by recruitment of poly ADP-ribose polymerase (PARP) and the MRN complex. The MRN complex (MRE11, RAD50 and NBS1) detects this lesion and subsequently phosphorylates the dimeric ATM (Ataxia telangiectasia Mutant) serine/threonine phosphatidylinositol-3-kinase-like protein kinase (PIKK). When the cell is under stress from DNA damaging agents, ATM is activated by phosphorylation on its serine-1981 site within the FAT domain upstream to the kinase catalytic domain [108], thus disassembling the dimeric (inactive) proteins into its mono-meric active form which is then recruited to the DNA double-stranded break site. Activated ATM (p-ATM) is responsible for the phosphorylation of neighboring alternative histone H2A.X at serine-139 site [109], resulting in the formation of γH2AX, stimulation of Rad51 and BRCA2, resulting in activation of ATM-dependent homologous recombination repair (HRR) [84,102]. Mediated by the Rad51, BRCA2 and XRCC2 tri-partite recombinase, the double-stranded break is repaired with guidance of the undamaged homologous sister chromatid used as template thus enabling error-free repair [110,111,94] (see figure 5).

3.12.2. Alternative non-homologous end-joining repair

In cells that inadequately express Rad51/BRCA2, HRR is not efficient thus allowing alternative repair via BER protein-members to guide double-stranded break repair. Mediated by PARP, X-ray repair cross-complementing protein 1 (XRCC1) and Ligase III, the double stranded break is repaired and ligated; however, with an increased

probability of insertion/deletion of the associated sequence at the repair site. This repair pathway is named alternative-NHEJ [93] (See figure 5).

3.12.3. Non-homologous end-joining repair

Depending on the phase of the cell cycle with which the DSB is incurred, another double-stranded repair pathway that may predominate is non-homologous end joining (NHEJ)[92,102]. The breaksite is recognized and modified by a pair of heterodimers, ku70/ku80 and other end-processing factors. The ligateable ends will then be joined via an XRCC4/ Ligase IV mediated mechanism [91] (See figure 5). As there is guidance of undamaged DNA/sister chromatid, the goal of this repair is simply to re-established the intact DNA backbone; therefore, this repair pathway is prone to errors.

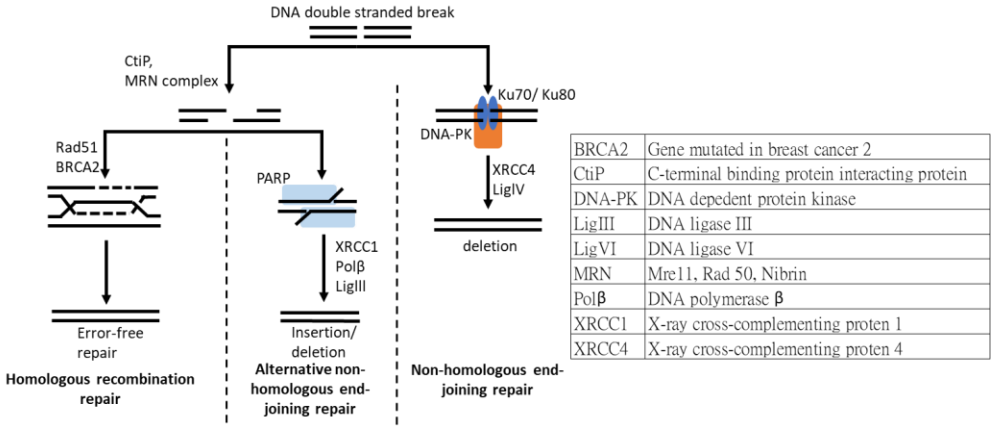

Figure 7. Simplified schematic of DNA double strand break repair pathways, including Homologous recombination repair (HRR), Alternative non-homologous end joining repair (Alt-NHEJ) and Non-homologous end joining repair (NHEJ). [Modified from (Amunugama 2012; Davis andDavid J 2013; Zhao et al. 2017, Mckinnon 2009)]

3.13. Other mechanisms to resolve TMZ-induced DNA damage.

A multitude of DNA repair mechanisms are employed in cells to combat TMZ-induced DNA lesions. In addition to DNA single/double-stranded break repair, one of the best-studied approaches is the epigenetic up-regulation of O^6-methylguanine-DNA methyltransferase (MGMT) [29,113]. MGMT is responsible for maintaining genome stability; it recognizes O^6-methylguanine (one of the major products of TMZ methylation) and catalyzes the removal of this methyl-group to restore guanine and base-pairing potential to prevent nucleotide mismatch and transcriptional/ replicational errors [14,29,47]

The gene coded for MGMT located on chromosome 10, where methylation of the associated promoter suppress MGMT expression, which lead to poor patient outcome, and short survival time relative to unmethylated population[114]. Methylation of MGMT were found in a majority (~70%) of high-graded glioma and recurrent tumours[115,116], which had a limited expression and function of the protein, and lead to the low response rate of TMZ in primary GBM [70,117].

3.14. DNA-damage induced cell death.

When the amount of accumulated damage reaches a certain threshold that cannot be effectively repaired, a resulting DNA repair-pathway-mediated signal is to stimulate programmed cell death pathways [47,102]. Apart from its regulatory function in the cell cycle pathway, p53 also responsible to induce cell death (Fig 8) [118]. Cell death can be further classified into 3 types, autophagy, necrosis and apoptosis [119].

However, with respect to TMZ-induced damage the majority of cell death events occur via apoptotic pathways [10,57].

In the cellular apoptosis signaling pathway, alterations in the mitochondrial system and the activation of caspases (Cysteinyl, aspartate specific proteases) are crucial to complete this process. Upon induction of stress signal, the ATM-p53 signaling axis induces expression and activity of pro-apoptotic factors, such as PUMA, Noxa and Bax, resulting in alterations to the mitochondrial membrane potential [120,121]. Mitochondrial permeabilization leads to leakage of contents of the intermembranal space into cytoplasm, leading to disturbance of the electrochemical balance, acidification of the cytoplasmic environment, an increase in reactive oxygen species, and release of cell death factors [118] (See figure 8). Key death factors released during permeabilization of the mitochondrial outer membrane include cytochrome c (cyt c), second mitochondria-derived activator of caspases (Smac), apoptosis inducing factor (AIF) and DNA endonuclease G (Endo G).

Cytochrome c is a well-studied mitochondrial protein, which is released from the mitochondrial intermembranal space during apoptosis. The major effect of cyt c release into the cytoplasmic space is the formation of apoptosomes, including apoptosis protease activating factor (APAF-1), thereby activating the caspase system [122]. Smac (also named Diablo protein) can indirectly activate caspases [118]. Caspases are effector proteases that execute “cell suicide”, by cleaving and degrading multiple proteins and substrates; the caspase system alters the internal environment of cells, ultimately causing cell death.

Apoptosis inducing factor (AIF) release from the ruptured mitochondria will undergo transport to the nucleus where AIF induces condensation of chromosomes in an ATP-independent manner [123]. In conjunction with caspases and endonuclease G, condensed chromosomes in an apoptotic cell are cleaved into pieces, resulting in DNA fragmentation followed by completion of the apoptotic process [118,124](See figure 8).

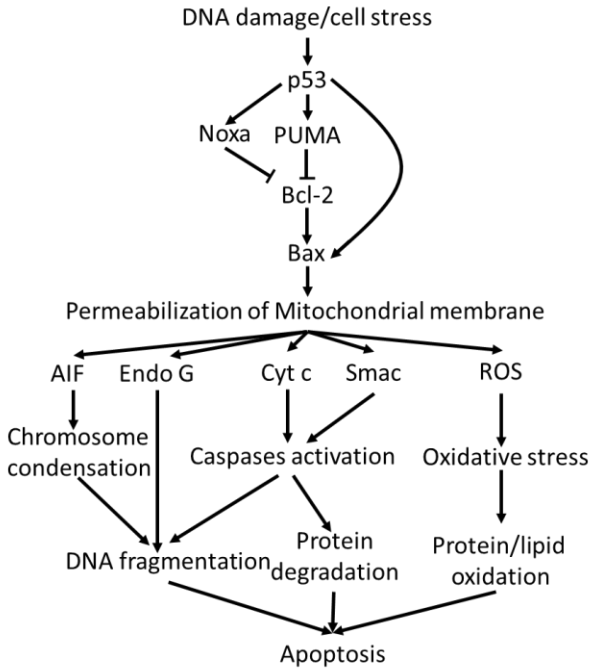

Figure 8. Simplified pathways of DNA damage induced apoptosis. P53 is stimulated by extrinsic damage, thereby regulating the expression of PUMA and Noxa, which inhibit the anti-apoptotic activity of Bcl-2, which unbalances pro-apoptotic and anti-apoptotic equilibrium. The pro-apoptotic protein Bax leads to mitochondrial dysfunction, further stressing the cell by increasing reactive oxygen species (ROS) and releasing of cell death factors such as apoptotic inducing factor (AIF), endonuclease G (Endo G), cytochrome C (cyt c) and second mitochondria-driven caspases activator (Smac). These death factors induce apoptosis via the decomposition of DNA, proteins and lipids. (Modified from [83,118,121,122,124,125])

3.15. Parp-inhibitors and their clinical use in cancer management.

PARP is a key player in both the DNA single-stranded and double-stranded break repair process (Fig 3). PARP recognizes DNA lesions, physically binds to the breaksite, generates poly ADP-ribose polymers on targets, and stimulates the recruitment of specific repair proteins [126]. Recently, small drug compounds specifically designed to inhibit the function of PARP have been develop which act to suppress DNA repair response *in vitro* and *in vivo* [127].

Clinically, PARP inhibitors (PARPi) have been commonly used in eliciting synergistic cell death (termed synthetic lethality) in cancers with specific DNA damage repair deficiency, such as BRCA1/BRCA2 mutation in breast and ovarian cancer [128,129]. In these BRCA-mutated cancers, DNA DSB repair mechanisms, specifically HRR, are defective thereby inducing these cells to rely on SSB repair to resolve DNA damage for cell survival. PARP, an essential factor in SSBR is an appropriate target (via PARPi) to inactivate this alternative repair pathway thus achieving synthetic lethality in BRCA-deficient/mutant cells. As the tumour cells specifically show BRCA inactivation, somatic cells with wildtype/functional BRCA protein remain unharmed [128,130]. In other cases, PARPi are used to hypersensitize tumour cells to SSB-inducing therapeutics (such as TMZ, radiation and radiomimetics). Through inhibition of PARP-dependent DNA repair, the efficacy of the drug is enhanced [131–133]

Amongst PARPis, there are two main properties of PARP that are targeted: catalytic inhibition and PARP trapping [134]. By definition, most PARPis are able to inhibit the catalytic function of PARP through reversable binding on the active site of PARP, which competitively reduced the enzyme-substrate interaction. PARPi can slow

down the formation of poly ADP-ribose, and reduce PARP-dependent DNA repair pathway activity thereby achieving its intended therapeutic effect [135] (Figure 9). However, not all PARPi demonstrate PARP trapping capability as some PARPis (e.g. Talazoparib, BMN 673 and Pamiparib, BGB290)[136–138] have strong affinity to PARP which stably, almost irreversibly bind to PARP, and significantly suppress the enzymatic function of PARP and "trap" PARP at the DNA break-site [134]. The collision between DNA replication fork and trapped PARP induces fork collapse and DNA double-stranded break formation [139]; damage that enhances cell death [140,141] (see figure 9).

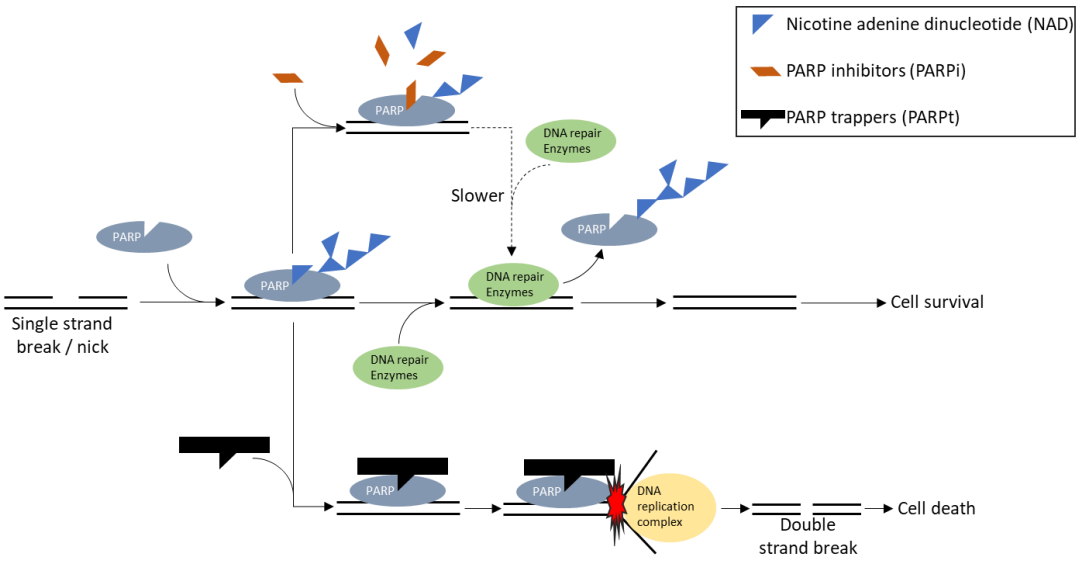

Figure 9. Simplified schematic demonstrating the critical role of PARP in DNA repair, and the working mechanism of PARP inhibitors (PARPi) and trappers (PARPt). [Modified from [126,127,134,135,139]].

3.16. On-going GBM research and challenges

A tumour-specific, non-invasive biomarker, would dramatically improve clinical diagnosis and the prediction of patient outcome. However, the discovery of such a GBM-specific marker for either/or diagnosis and treatment of the disease remains elusive[23,52]. Subsequently, patients diagnosed with GBM are mostly at mid-age [14], whereby the ability to recover from the aggressive treatment is unfavorable with increased age. Even when GBM patients complete standard-of-care therapy, comprised of the surgery, radiation and chemotherapy with severe systemic harm, recurrence is commonplace, resulting in a mean survival rate of 14.6 months [14].

Although standard anti-GBM treatment is crucial to fight the tumour as well as to save the patient, the heterogeneic nature of GBM promotes cancer cell survival despite treatment. The difficulty in resecting the GBM tumour to minimize surgical damage already provides the a tumour a survival advantage[142]. GBM cells are highly motile and invasive, and able to invade to neighboring tissue [27,143] Ablating the residual tumour requires additional therapeutic avenues such as radiotherapy and chemotherapy. Radiotherapy is the use of high-energy radiation to stimulate oxygen molecule is targeted tissue to induce oxidative stress and damage the genetic material. However, the central area of tumour mass is often hypoxic, there is a lack of excitable oxygen to generate reactive oxygen species (ROS) to achieve therapeutic effect [144]. Furthermore, the chemotherapeutic effects and dosage of drugs needs to overcome the fact that the target is within the CNS, since the brain and the tumour are protected by the blood-brain-barrier: a layer of cells and connective tissue that

have selective permeability [47]. There also exist enhanced mechanisms of drug removal from GBM cells. Highly active P-glycoprotein (PGP), encoded by *MDR1,* is a membrane-associated efflux transporter that can evacuate TMZ from the tumour site, thus reducing its anti-tumour efficacy at the target-site [47,145]..

Generally, as a disease with high heterogeneity, cells within a tumour mass may develop different means to evade therapies (e.g., increase expression of drug removing transporters, enhancing damage repair, or neutralization of drugs) [2,28], some subpopulations might also be relatively inert toward treatments due to the low metabolic activities (e.g. Cancer stem cells), these populations might survive under treatments, expand and contribute to recurrent [79].

On the whole, the current standard of anti-GBM therapy is not very effective, while being highly intrusive and presenting a great burden to patient's life and their family. Recurrence of treatment-resistant tumours is commonplace and will continue to be an ongoing challenge for clinicians and GBM patients. As there are no specific effective therapies for rGBM, follow-up treatment is limited to palliation. Despite the arsenal of over 1600 FDA approved drugs available, a major confounding reason for a failure to advance rGBM research and identification of effective treatments is due to a lack of effective rGBM model systems that adequately mimic rGBM and mediate drug discovery.

3.17. GBM models and limitations.

1.17.1 *In vitro* 2-D model

Cell-based models are the most commonly-used system for cancer drug studies. Monolayers of cancer cells are simple to culture, and are highly adaptive for a variety of assays. Furthermore, they are amenable to cytotoxicity assays which can be scaled up for high throughput capability [6,47,52]. On the other hand, these 2-D patient-derived cell lines lack the representative structural characteristics and microenvironment to adequately represent the native cancer or tumour[146]. In an attempt to better model this environment, a co-culture model featuring cancer cells growing in contact with other normal cells (ie. fibroblasts, glia, astrocytes) has been developed for specific assays [147]. While this has yielded promising data and findings, their use is still limited by the fact that the 3-D GBM microenvironment is not fully recapitulated.

1.17.2 *In vitro* 3-D cultures and tumour spheroid models

To fill the gap between monolayer cell-based study and animal trials, a 3-D culture was developed to better mimic the architecture and microenvironment of the GBM cancer cell. This involves the use of culturing matrices that mimic the composition of tumours extracellular matrix, thus creating a supportive platform for cancer cells to thrive in a tissue-like manor [32,143]. Although these models are not amenable for typical image-based studies, these models do better mimic the physiological environment of tumour tissue by promoting 3-D cell-cell interactions [147].

Another commonly used 3-D model are GBM cells grown as tumour spheroids (tumorspheres), which are aggregates of cells that phenocopy a microtumour [11]. These spheroids are usually achieved by using low-adherent culturing plastic-ware and suitable extracellular growth factors (ie. FGF and HGF), thus promoting cell attachment to each other into cell clusters or a microtumour mass [148]. Although spheroid cultures provide 3-D architecture, cell interactions and microenvironment, these models too are less trackable, harder to culture and less adaptive to image-based assays. Additionally, due to lack of willingness of rGBM patients to undergo re-surgery, it is highly difficult to obtain patient-derived rGBM models [54,148].

1.17.3 *In vivo* xenografts and mouse genetic models

Animal models are a critical translational step for delivery of drug study results to the bedside. Compounds need to undergo *in vivo* pre-clinical analysis and validation, usually in small animals, with similar physiological systems to humans' [149,150]. Animal models commonly used to mimic disease pathology, include mouse brain stereotactic xenografts and genetic tumour-bearing models.

A xenograft is the introduction of heterologous cell, tissue or organs into mouse to mimic the phenotype of diseases (Cancer tumours) using an appropriate *in vivo* environment [151]. Xenograft models provide a pathophysiological condition that resembles human disease. However, as each mouse represents one individual replicate in any study, drug testing and animal experimentation incur high costs in contrast to other 2-D/3-D model systems [152].

Mouse tumour-bearing genetic models have been developed by intercrossing genetically-engineered transgenic lines to yield mice that develop highly invasive GBM tumours[153,154]. To phenocopy disease-specific genetic mutations, genetically modified mice often undergo routine image-based tracking, MRI and behavioral analysis to determine tumour establishment and analysis. Some of the common lines developed include GL261 (C57BL/6), GL26 (C57BL/6) CT-2A (C57BL/6), SMA-560 (VM/Dk), and 4C8 (B6D2F1)[155]. There are added challenges to working with these systems including inconsistency in tumour development, size and time-to-establishment. These systems are also not amenable for high throughput drug discovery.

To date, resistant GBM remains challenging to treat, due to the aggressive progression rate, heterogeneity of the disease, and the lack of effective therapeutic means. The standard regimen of treatment is only able to improve a patient's overall survival by a few of months. Meanwhile, mechanisms that contribute to therapeutic resistance remain largely unclear and understudied, as such, a representative model that is tractable and adaptive to multiple experimental methods is needed to improve analysis of rGBM and the identification of potential therapeutics.

To satisfy the urgent demand of for these studies and, in light of the inherent limitations in obtaining relevant patient-derived treatment-resistance models, I seek to develop models that resemble the rGBM phenotype. Potential mechanisms that encourage resistance in GBM will be identified and studied. Key genes that are

related to TMZ resistance will be determined and their potential as either prognostic markers and/or therapeutic targets will also be investigated.

4. Hypothesis and Objectives

I hypothesize that TMZ resistance in GBM is mediated by enhanced DNA damage repair mechanisms. My project aims to establish tools to study drug resistance in GBM, and to build the foundation of an automated high throughput platform to identify novel treatments against resistant GBM.

Objective 1: To develop and validate a fluorescent cell model for TMZ resistance GBM

Objective 2: To investigate the molecular mechanisms that contribute to TMZ resistance in GBM

Objective 3: To identify new treatments that could counteract TMZ resistance in GBM

5. Material and Method

5.1. Cell cultures

Human glioblastoma derived cell line U251 (astrocytoma subtype, Sigma, Saint Louis, MO) [156] was selected due to its TMZ sensitivity [51]. All U251 derivatives were cultured with supplemented Dulbecco's Modified Eagle Media (DMEM)-high glucose

(Detailed composition of solutions were listed in Table 2.) Cells were cultured at 37°C, 5% CO_2 in a humidified chamber. At 75-90% confluence, cells were washed with PBS (Sigma), harvested with Trypsin-EDTA (Sigma, USA), and re-passaged at ~95% confluence in 10 cm dish (approximately every 3 days).

Patient-derived primary GBM spheroids (BTIC cells) were provided by Dr. Sheila Singh, and the tumorspheres were cultured according to the method described in Dr. Singh's publication [148]. Tumorspheres were cultured in ultra-low attachment plates (Corning) with neuro-culture medium showed in table 2.

5.2. DNA damaging agents & PARP inhibitors/trappers

To phenocopy anti-GBM therapy, Temozolomide (TMZ, Sigma, T2577) was used as treatment. Hydrogen peroxide (Sigma, #216763) was used to mimic oxidative stress induced single stranded break, while the topoisomerase II poison, Etoposide (Sigma, E1383) was used to induce DNA single and double stranded breaks. To inhibit PARP, the PARP inhibitor PJ34 (EMD Millipore Corp), PARP inhibitor/trapper intermediate Olaparib (Cedarlane), and PARP trapper Talazoparib (BMN 673, AdooQ, A11243) and Pamiparib (BGB290, Selleckchem, #58592) were used.

5.3. Development of fluorescent TMZ-sensitive and resistant U251 lines

Parental U251 cells were transfected with either H2B-GFP (Addgene, #55055) or pmCherry-H2B (Addgene, 11680) plasmids, using Polyjet transfection reagent (FroggaBio, SL100688). Cells were incubated with the plasmid and transfecting

reagent mixture for 48 hours, followed by a selection with 300µM G418 (Gibco, #10131035) until >95% fluorescence expression. Subsequent passaging in G418 media confirmed the establishment of these stable cell lines.

To mimic the drug resistance in GBM, the red fluorescent (pmCherry-H2B transfected) U251 line underwent differential TMZ selection for 3 weeks. Three outgrowing clones within the 200µM TMZ selection condition were isolated and cultured separately. The subclone culture with the strongest fluorescent signal was chosen to represent as the TMZ Resistant Red fluorescent population (TRR). The green fluorescent U251 cells (H2B-GFP transfected) were treated with DMSO during TMZ selection phase; retaining sensitivity toward TMZ and are designated Sensitive Green (SG) cell (See figure 10.)

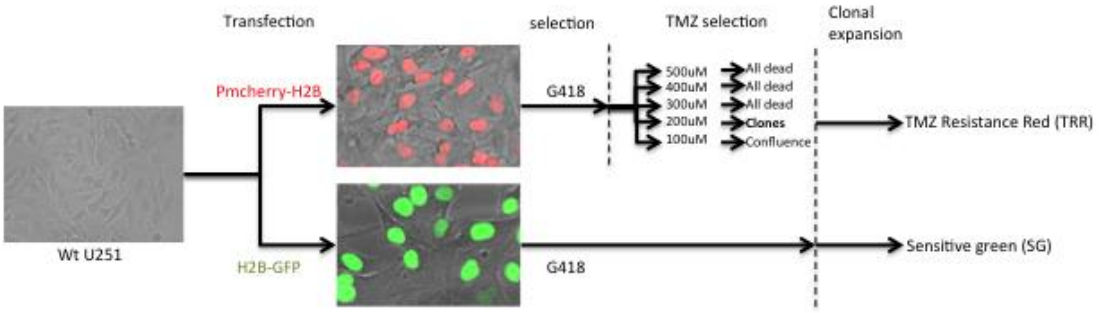

Figure 10. Development of the TMZ resistant red fluorescent line and the TMZ naive sensitive green fluorescent line. Parental U251 lines were transfected with Pmcherry-H2B and H2B-GFP plasmid, respectively, followed by G418 selection for 3 passages. The red fluorescent line underwent TMZ treatment at different drug concentrations. Outgrowing cell clones that developed at 200µM TMZ were used to develop the TMZ resistance model. For both green sensitive and TMZ red resistant lines, cells with strong fluorescence intensity were specifically selected and underwent expansion.

5.4. Automated system for data collection and analysis

Automated data collection and analysis took place on a high throughput analysis suite composed of key components: the BioSpa 8 (Biotek, USA), Cytation V (Biotek) and Gen5 software (Biotek) (See Figure 11). BioSpa 8 combines automated incubation with a robotic arm that transfers multi-well plates into the Cytation V plate holder according to prescribed protocols. Cytation V is an automated multi-mode plate reader that enables automatic data collection. In this case, fluorescence imaging data is collected using a variety of filters according to experimental design. Data collected is processed and analyzed via Gen 5 software, which generates quantitative outputs for interpretation and presentation.

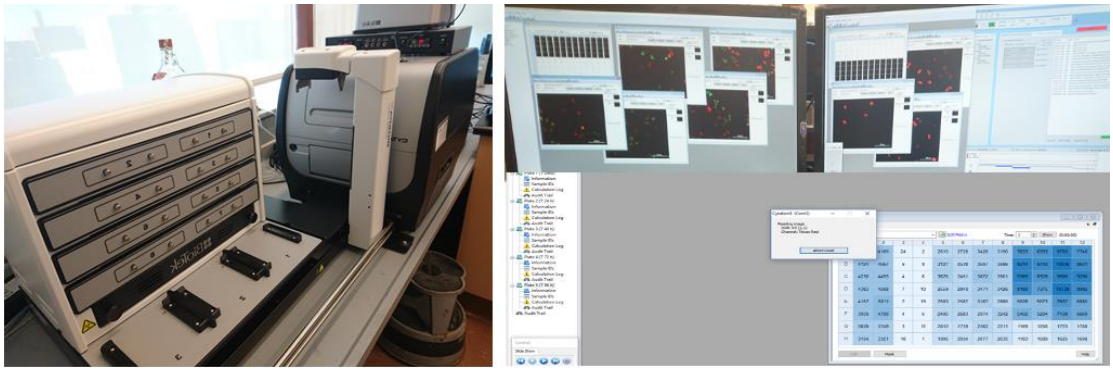

Figure 11. The BioSpa 8 incubator (White) with the robotic arm to transfer plates to the Cytation V (Black) for data collection. The inset image (bottom right) is a screenshot from Gen 5 software.

5.5. Growth assay

Cell survival and proliferation is an important indicator of cell response to drug treatments, thus, a semi-automated kinetic growth assay was developed to monitor cell proliferation. The nuclear fluorescence of SG/TRR was used to mark and

enumerated cell counts at different time-point. This method requires minimal handling and is non-invasive (unlike MTT-like assays), thus allowing real-time monitoring of cell number/count in 96-well plate formats without the need to pipet, manipulate or fix cells. The counts of each time-point were normalized to the baseline reading (Time 0) to give a relative growth value; a more accurate and better representation of proliferative rate of the lines.

TMZ sensitive (SG) and resistant (TRR) cells were seeded in approximately 1:1 ratio (A total of 700 cells/well) in a 96-well flat-bottomed imaging plate (Corning, USA) at time 0. Three hours after cell seeding, drug treatments were applied according to experimental design (see Results), and the plate(s) was/were introduced to the BioSpa 8 incubator with readings occurring at each specified time-point automatically (depending on the experimental design, usually 24 hours for growth assay). Figure 12 (below) demonstrates how the collected images are masked and analyzed to generate the cell count data.

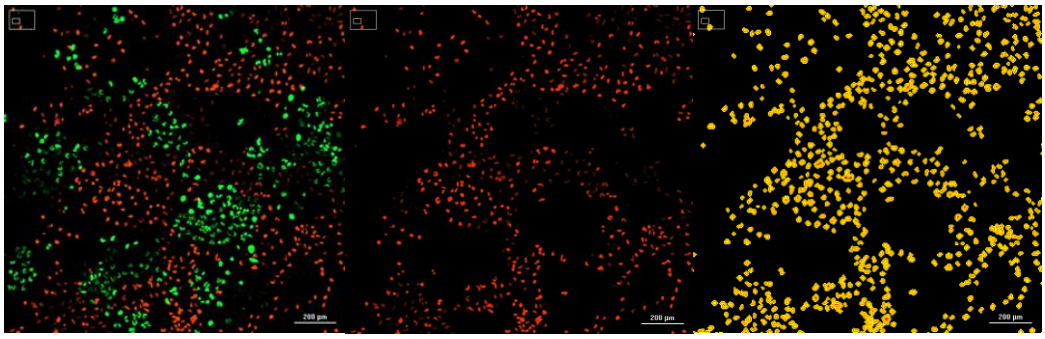

Figure 12. Representative images of the mixed culture under control conditions (Left); the red channel (Middle) demarcates the TRR signal. Gen5 system analysis (Right) with masking/selecting the fluorescent signal to generate the cell count readout.

5.6. High throughput alkaline comet assay

Most of the cancer chemotherapeutics kill cancer cells via direct or indirect induction of DNA damage, thus, quantification of DNA damage following treatment correlates with therapeutic efficacy. The alkaline comet assay, also referred to ase single cell get electrophoresis, directly quantifies DNA damage [157].

U251 cells (3500 cells/well) were seeded in 96-well flat-bottomed plates (Sigma) and incubated overnight. Treatments were applied according to experimental plans (detailed in the relevant sections within Results). Immediately following treatments, cells were washed twice with 50 uL of PBS, trypsinized and quenched with 150uL ice cold culture medium (see Table 2). Cells were pelleted by centrifuging the cell suspension at 250 RPM for 2 minutes, 130uL of supernatant was removed carefully from each well, and the remaining cells were resuspended in 300uL of warm agarose solution (Table 2.). 14uL of cell-agarose mixture were transferred to 96-well comet slide (Trevigen) and incubated at 4^{o}C for 5 mins. Cells were lysed in comet lysis buffer (Table 2.) for 20 mins at room temperature (RT), and the slides were transferred to the alkaline unwinding buffer (Table 2.) for 20 mins at RT. Electrophoresis was conducted in an electrophoresis tank (Trevigen-425-0050-ES) with electrophoresis buffer (Table 2.) for 40 mins at 21V. Slides were then washed with double distillated water (ddH_2O) for 2 x 5 mins. Slides were then dried at 37^{o}C for 5 mins, and stained with Sybr Green (1:10,000 in 0.4M Tris buffer, 30uL/well, 10 mins in dark, RT, Sigma), followed by a ddH_2O wash for 60 mins. The slide were dried again at 39^{o}C for 5 mins, and images were collected and analyzed by the

Cytation V-Gen 5 system, Figure 13 shows an example of these comet images; more details can be found in [157].

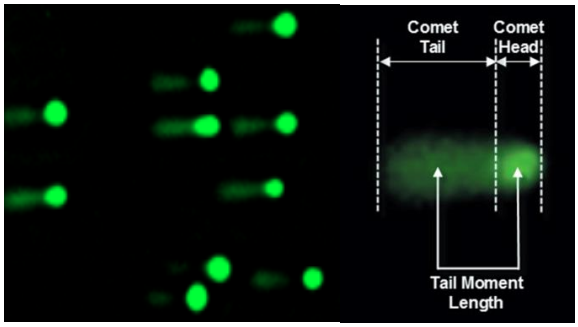

Figure 13. Images showing the stained DNA following electrophoresis (Left), and schematic demonstrated how the analysis program recognizes DNA comets for calculation of tail moment (Right, Larson et al., 2016). Comet tail moment = (% DNA_{tail} x Tail moment length)/100. Proteinase-K comet assay uses an addition step of proteinase-K (25ng/mL Proteinase-K in PBS, 37°C, 30 mins) digestion prior to the lysis incubation step.

Table 2. Ingredients of solutions and buffers used in this experiment

Solutions/buffer	Ingredients
Agarose solution for Comet assay	1% Low-melting point agarose in PBS
Alkaline unwinding buffer	0.2M NaOH, 250mM EDTA
Culture medium	10% Fetal bovine serum, 1% Penicillin /streptomycin, 1% Gluta-Go in DMEM
Electrophoresis buffer	1mM EDTA, 0.5M NaOH, 1% DMSO
Lysis buffer for Comet assay	2.5M NaCl, 0.1M EDTA, 10mM Tris, 3% Triton X-100, 3% DMSO, pH 10
Lysis buffer for Western blot	50 mM Tris, 200 mM NaCl, 0.2% NP-40, 1% Tween-20, 1 mM NaF, 1 mM NaV, 50 mM β-glycerophosphate, 2 mM PMSF, and protease inhibitor
Neuro-culture medium	1x Antibiotic/antimycotic, 1x Mycozap, 10 % NS-A supplement, 20ng/mL EGF, 10ng/mL FGF, and 50uL Heparin in 50mL Medium
Running buffer	50mM**MOPS**, 50mM Tris, 1.025mM EDTA, 0.1%SDS
TBE buffer	90 mM TRIS, 90 mM Boric acid, 2mM EDTA
TBST	20mM Tris, 150mM NaCl, 0.1% Tween 20, pH 7.4
Transfer buffer	25mM TRIS-HCL, 192mM Glycine, 0.03% SDS in 20% methanol

5.7. γ-H2AX staining assay

As an alternative approach to detect DNA lesions, the phosphorylation of alternative histone H2A.X at serine-139 (referred to as γ-H2AX) is a well-described indirect method to detect DNA double stranded breaks. Cells were seeded at 3500 cells/well,

in 96-well flat-bottomed imaging plate and incubated overnight, treatments (as outlined in Results) were applied after incubation with respect to the design of experiment. Following the removal of drug/medium, the treated cells were washed twice with PBS (50uL/well) and fixed with 1% paraformaldehyde (PFA) in PBS. Fixed cells were then washed (2 x 50uL PBS) and permeabilized with 0.1% Triton-X 100 (Thermo-fisher) in PBS for an hour at 4°C. Permeabilized cells were washed (1 x 50uL PBS), Alexa Fluor 647 pre-conjugated anti-γ-H2AX antibody (1:1000, Biolegend, #93144) was applied (in 3% BSA in PBS), and incubated overnight at 4°C. Before imaging, immunolabeled cells were washed with 0.1% Triton-X 100 in PBS, and 50uL PBS was added to each well to maintain a moist environment in the plate. The plate was read with the automated dual-mask spot counting protocol [158] to quantify DNA damage after drug treatment. A simplified spot count analysis is outlined in figure 14.

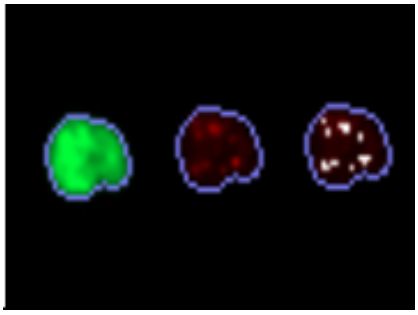

Figure 14. Example of the Gen 5 dual-mask analysis protocol. Masking the nuclei of a SG cell within the green channel (blue line) while masking the γ-H2AX foci of the same cell within the far-red channel (white line) demarcates the two key signals individually.

5.8. Zombie cell death assay

To determine the cell-killing efficacy of treatments, an automated image-based cell death assay was utilized. This cell death assay makes use of the Zombie UV dye (Biolegend, #423107), originally designed for flow-cytometry protocols. I repurposed and optimized this method for 2-D image-based analysis. The assay uses membrane permeabilization as a marker of apoptotic cell death and facilitates determination of the percentage of dead/dying cells (Zombie+) within a given cell population thereby allowing me to determine drug efficacy.

Cells were seeded (3500 cells/well) in 96-well imaging plates. The following day, drug treatments were applied according to experimental design (as outlined in Results), cells were washed (2 x 50uL PBS), fixed with 1% PFA (10 mins, RT), and incubated with 1:500 Zombie UV dye in PBS (15 mins, 37^{o}C). Lastly, the wells were washed (2 x 50uL PBS) and filled with 50uL of PBS to maintain moisture.

Images were acquired and processed in a similar was as the γ-H2AX dual-mask protocol. Primary masks were applied to the green/red fluorescent nuclei, and a secondary mask was applied to blue fluorescent emitted by Zombie UV dye surrounding the primary mask, if any. Zombie+ objects containing a nuclear mask (Green/Red) were considered to be a real cell, while Zombie+ objects without a nuclear mask were considered as debris. The number of Zombie+ cell (blue + green/red) was divided by the total number of cells in the well to calculate the percentage of dead cells in the cell population. Figure 15 outlines examples of Zombie +/- cell and the application of the masking system.

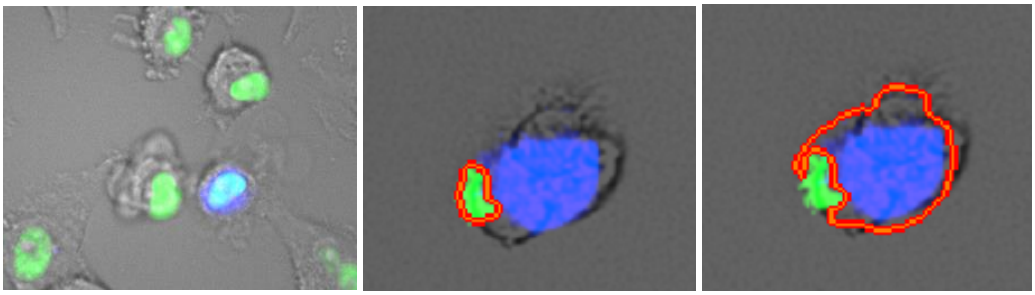

Figure 15. Images showed the merged image of Bright field, green and blue channel (Left), and Images demonstrated how the Gen 5 protocol recognized a Zombie + cell (Right) and the associated nuclei to ensure the accuracy of the experiment.

5.9. Cell migration assay

A cell invasion assay was optimized to measure cell motility amongst the SG and TRR lines. To create a cell-free zone in the middle of the well, I developed a unique method using 96-well imaging plates. A sterile solution of 3% low-melting point agarose in PBS was prepared, 11uL of agarose was dropped into the center of wells, followed by plate incubation for 15 mins at 4^{o}C. Cells were then seeded at a density of 3500 cell/well and incubated at 32.5^{o}C for 1.5 hours to allow attachment. After incubation, each agarose plug within each individual well was removed via vacuum suction to generate central cell-free space for migration, wells were washed with 50uL PBS twice to remove extra cells that were not attached, and 200uL of complete culture medium were added to each well.

Plates were then transferred to the BioSpa 8 incubator linked to the Cytation V-Gen 5 system and whole-well kinetic readings were acquired every 4 hours according to

the manufacturer instructions. Figure 14 outlines a well containing SG/TRR at the beginning (T0) and the end of experiment (T96).

The number of cells that invade into the central zone were masked (yellow mask, Figure 16) and analyzed to determine the rate of invasion.

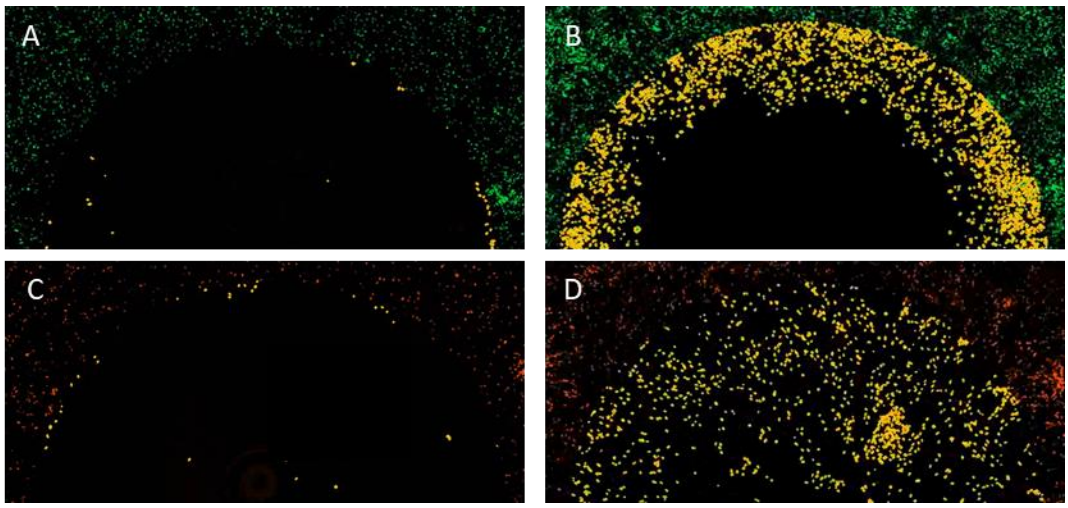

Figure 16. Cell migration assay. Images on the left show an initial image (at 0 h the view of corresponding to SG (B) and TRR (D) following 96 hrs incubation. The cells that migrate into the central cell-free zone were masked and selected for further analysis.

5.10. RNA extraction and Clariom D analysis

SG and TRR cells were seeded and grown in 10cm culture dishes (SARSTEDT, #6020611) and treated with TMZ or DMSO (Sigma, SHBJ7919) for 72 hours prior to harvest. Pure RNA from treated SG/TRR were isolated with QIAGEN RNeasy (# 74134), and stored in TBE buffer at -80^{o}C (Table 2). The Centre for Applied Genomics in The Hospital for Sick Children (Toronto, Canada) processed these samples whereby they underwent Claroim D analysis (Thermo Fisher) as per the

manufacturer's recommended protocols. This service provides comprehensive comparative transcriptome-wide analysis amongst RNA samples. Although we were focused on differentially-expressed gene candidates amongst these cell types, Clariom D assays enable rapid discovery of coding and long non-coding genes, exons, splice variants, and rare transcripts. Further details are provided in the "Supplementary appendices". The readout of the Clariom D assay was analyzed using the manufacturer's proprietary Transcriptome Analysis Console (TAC) software (Thermo Fisher). With the assistance of Mr. Mike Wakem (Advisor, Thermo Fisher), the data was analyzed according to the protocol associated with TAC software. Data was processed and presented in order of differential expression amongst selected treatment/cell type groups.

5.11. Protein expression analysis

The expression level of TMZ resistant-associated and DNA-damage-repair-associated proteins were determined via Western analysis. Pellets were harvested and lysed with Western blot lysis buffer (Table 2.) for 30 mins at 4^{o}C, the lysate were centrifuged at 13000rpm for 10 mins to remove cell debris[159]. Protein was quantified, 20ug were loaded into each well of a BIS-TRIS 4%-15% precast gel (Invitrogen), and run in running buffer (Table 2) at 150V for 65 mins. Proteins were transferred to nitrocellulose membrane in transfer buffer (Table 2) at 20V overnight at 4^{o}C.

The membrane was incubated with primary antibodies in 5% milk overnight at 4^{o}C, washed (3x 5 mins in TBST, table 2) and then with corresponding secondary

antibody for an hour in RT. Following the second wash (3x 5mins TBST), membrane was incubated in Clarity ECL solution (Bio-Rad) according to companies' instruction. Densitometry of immunoblot images were performed using Image J analysis software (NIH, US) in order to quantify the protein expression levels; data was normalized with the base-line level of untreated SG. Antibodies are listed in table 3.

Table 3. The source and catalog number of antibodies used in protein expression assay

Protein	Source	Cat. #	Host
Actin	CST	4968	Rabbit
Ape1	CST	4128	Rabbit
ATM	CST	2873	Rabbit
p-ATM (s1981)	CST	4526	Mouse
ATR	CST	2790	Rabbit
p-ATR(s428)	CST	2853	Rabbit
p-BRCA1	CST	9009	Rabbit
Ctip	CST	9201	Rabbit
LigaseI	SCB	G2910	Rabbit
LigaseIII	Abcam	ab185815	Rabbit
MDR-1	CST	12683	Rabbit
MGMT	CST	2739	Rabbit
MPG	Abcam	ab196553	Rabbit
Mre11	CST	4847	Rabbit
Nbs1	CST	3001	Rabbit
p53	CST	9282	Rabbit
Rad50	CST	3427	Rabbit

Protein	Source	Cat. #	Host
TopoI	Abcam	ab3825	Rabbit
Topolla	Cedarlane	A300-054A	Rabbit
Topollb	Cedarlane	A300-950A	Rabbit
TIF1b	CST	4124	Rabbit
p-TIF1b (s824)	CST	4127	Rabbit
Caspase 3	CST	9664	Rabbit
Claved Caspase 3	CST	9665	Rabbit
Caspase 7	CST	12827	Rabbit
Claved Caspase 7	CST	8438	Rabbit
Caspase 9	CST	9508	Rabbit
Claved Caspase 9	CST	7237	Rabbit
PARP	CST	9542	Rabbit
XRCC1			Rabbit
Anti-Rabbit IgG	CST	7074	Goat
Anti-Mouse IgG	CST	7075	Horse

5.12. Gene knock-down/ over-expression analysis

I sought to further delineate the function of specific proteins, that we identified via RNA and protein analysis, that may mediate TMZ resistance. Using a knockdown and over expression approach. For knock-down experiments, shRNAs (see table 4.) were expressed in target cells via lentiviral delivery. To generate the lentiviral particles, plasmid DNA of containing short-hairpin sequences corresponding to the gene target (in pLKO vector, Millipore-Sigma, CA) were co-transfected (XtremeGene,

Millipore-Sigma, CA), into 293LTV cells (Cell Biolab, US) with a lentiviral packaging mix (Millipore-Sigma, CA) containing vectors for VSV-G, KGP1-IR, and RTR-2 according to manufacturer's specifications. Following media replacement 16 hrs after transfections, cells were incubated for another 24 hours prior to collection of virus particle-containing medium. Three total media collections occurred (3 x 24 hrs) with viral media combined followed by filter-sterilization. Viral media was combined with fresh media (1:3 ratio) and transduced in corresponding U251 cells (parental and SG/TRR). Cells were incubated in viral medium for 48 hours to allow transduction followed by antibiotic selection for 3 passages (puromycin, 1ug/mL, ThermoFisher, CA). Knockdown success was confirmed via western analysis using validated antibodies corresponding to the targeted gene-of-interest (ie. XRCC1 and MGMT).

Table 4. Plasmid containing the shRNA or gene knock-down experiments, all plasmids were purchased from Sigma-Aldrich.

shXRCC1 Cat#	Target sequence
TRCN0000273633	TCCAGGGCAAGCACTTCTTTC
TRCN0000273634	CGATACGTCACAGCCTTCAAT
TRCN0000273635	AGTCAGAAGGACAGGACAATG
TRCN0000007913	GACCTAAATTGCCAGCTCCAA
shMGMT Cat#	
TRCN0000427322	GAGCAGGGTCTGCACGAAATA
TRCN0000413668	AGCCTGGCTGAATGCCTATTT
TRCN0000419534	TGAGCGACACACACGTGTAAC
TRCN0000427501	TAACGCTGCCCTTGCTCTATT
TRCN0000022364	GCTGTATTAAAGGAAGTGGCA

For overexpression, plasmids containing gene-specific cDNAs were transfected to the cell lines using Polyjet transfection reagent (SL1000688, FroggaBio), as per the

manufacturer's protocol. Transfected cells underwent antibiotic selection, depending on the plasmid's selection cassette, and stable over-expressing lines were established following selection and 3 cycles of cell passaging.

5.13. Data analysis and statistics

High-throughput data underwent initial data collection, processing and analysis via GEN5 software (Biotek). Subsequently, data were analyzed via MS Excel. Means of technical replicates were calculated and the mean of means from multiple experiments are presented in the figures, with error bars representing standard deviation of means. The data were analyzed by two-way analysis of variance (ANOVA), followed by post hoc Tukey's test or Bonferroni test (as specified in corresponding figure legends).

5.14. Combenefit

Combenefit is a data analysis software developed by the Cancer Research UK Cambridge Institute. This program allows for improved analysis, quantification and presentation of combined effect of drugs for synergy determination (Lowew, Bliss, and HAS) for *in vitro* systems. In general, this software first extracts single agent effects to generate dose-response curves as a matrix of % of the control. While referencing the single-agent curves, the dose-response surface of drug combination are generated, and the characteristics (Antagonstic, independent, synergy) are determined based on the selected synergy model [99].

6. Results

6.1. Development of cell-based assays & characterization of TMZ resistance

6.1.1. Cell growth under Temozolomide

Using the fluorescent reporter U251 lines (SG/TRR), a proliferation assay was performed by quantifying cell counts every 24 hours under increasing TMZ concentrations (Experimental design showed in figure 17A.).

As imaged in Figure 17B & C display mixed cell populations in one well of a 96-well plate at 72 hours with or without TMZ. The SG: TRR ratio was ~ 1: 1 in figure 17B (Control condition), which resemble the ratio with which the cells were initially seeded, thus indicating that that baseline (DMSO/control) proliferation rate of SG and TRR are similar. However, Figure 17C (200μM TMZ) shows that the TRR population predominates as few SG cells are present, suggesting that the TRR is able to resist and thrive in TMZ growth conditions compared to SG; they are surviving and proliferating at 200μM TMZ (2.9 - 6.7μM in human glioma tissue[160]) , in contrast to SG.

As shown in Figure 17D &E, the base-line proliferation rate indicates no difference between SG and TRR ($P>0.05$). In contrast, TMZ treated (100μM, 200μM and 400μM) SG cells displayed severe growth suppression. Although, dose-dependent growth suppression effects were also observed in TMZ-treated TRR, these effects were muted compared to SG, with TRR cells still showing overall growth throughout all TMZ treatment cohorts over the 96 hr period.

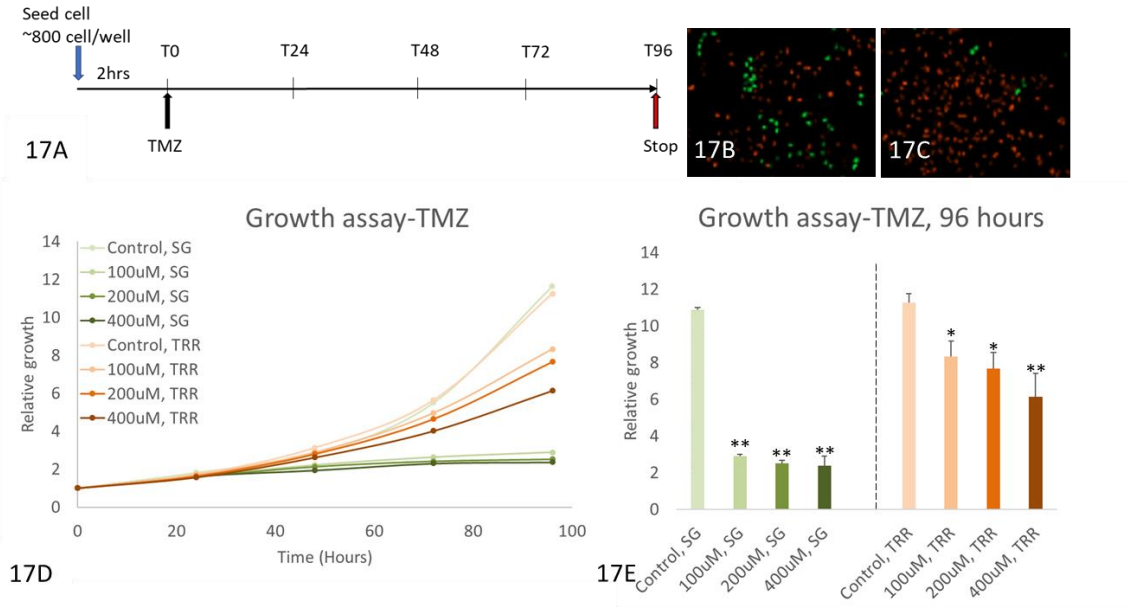

Figure 17. (A) Experimental design for proliferation assay. SG and TRR cells were mixed in a 1:1 ratio, with approximately 800 cells seeded per 96-well. Temozolomide treatment gradient (400µM, 200µM, 100µM and DMSO control) was applied, and cell counts were quantified via Cytation V every 24 hours for 5 days. (B & C) Merged images of the green and the red fluorescent channel of well under DMSO control (B) and 200µM TMZ (C) at 72 hours. (D) Line graph illustrating the relative growth of SG and TRR with TMZ. (E) Bar graph demonstrating the relative growth 96 hours after treatment (*=p<0.05, **=p<0.01, comparing to control SG, post hoc. Tukey's test after two-way ANOVA. N=4, n=48).

6.1.2. Alkaline Comet assay

The newly developed high throughput alkaline comet assay was utilized to determine DNA damage in cells following TMZ treatment after 1 hour (Figure 18A). In figure 18C, both SG and TRR display a dose-dependent increase in DNA damage, but generally, damage in TRR is significantly lower ($p<0.05$ for all 100µM, $p<0.01$ for 200µM and 400µM treatments.) when compared to SG. Figure 18C displays

representative individual comets in SG and TRR cells with different concentrations of TMZ. The area and the intensity of the comet tail is relatively lower in TRR, suggesting that a lower amount of DNA breakage/fragmentation in TRR relative to SG.

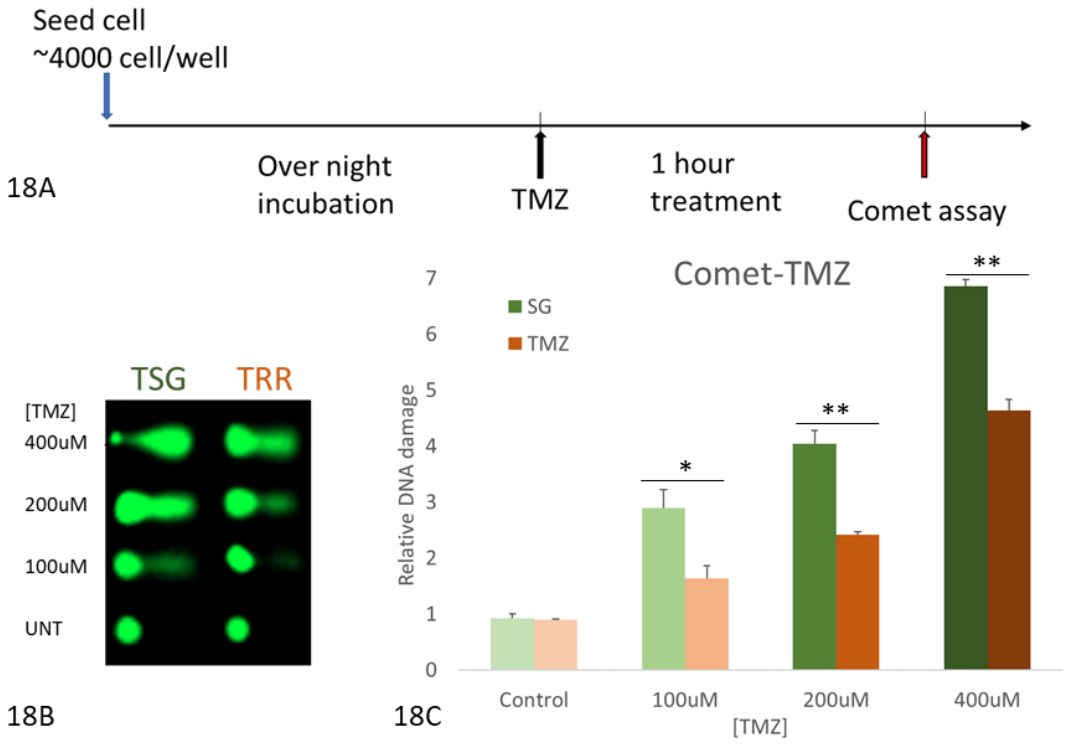

Figure 18. (A) Experimental design for analysis of relative DNA damage quantification via alkaline comet assay amongst SG and TRR cells following TMZ treatment. SG/TRR cells were seeded at ~4000 cells/well and incubated overnight, followed by treatment with TMZ (100µM, 200µM and 400µM) for an hour and harvesting for comet analysis. (B) Images of single cell comets of SG/TRR with increasing [TMZ]. (C) Bar graph displaying the relative mean DNA damage in U251 cells under TMZ treatment; values were normalized to untreated SG control and relative damage amongst SG and TRR following TMZ treatment were compared within the same [TMZ]. (*= p<0.05, **= p<0.01, post hoc. T-test with Bonferroni correction after two-way ANOVA. N=3, n=144).

6.1.3. γ-H2AX assay

As an alternative approach to detect DNA damage, the formation of γH2AX assay foci is detected via immunofluorescence (IF) using a specific anti-γH2AX antibody. This method detects individual γH2AX foci, where each foci in an indicator of individual DNA DSB lesions. This assay was used quantify the mean number of DNA double strand breaks per nucleus following TMZ treatment (Figure 19A). Figure. 19B illustrates examples of γH2AX foci within nuclei; there are more damage-induced foci in SG than TRR under the same [TMZ]. The readout and analysis of the γH2AX assays represented in the bar graphs (Figure 19); two analysis method were used, fraction of γH2AX+ cells (Figure 19C) and mean γH2AX foci/nuclei (Figure 19D). The fraction of γH2AX + cells demonstrate the proportion of cells that have mid- to high levels of DNA damage and generate more definitive data. In contrast, the mean γH2AX+ foci/nuclei measure is a more sensitive method to characterize low to medium DNA damage, which is important in identifying pharmacological potency and efficacy of drugs. Both analysis methods show congruence and suggest that the amount of DNA lesions are significantly higher in SG relative to TRR when treated with the same [TMZ] ($p<0.01$). Overall, the result of γH2AX assay data is consistent with the comet assay data showing that the TRR line resists TMZ-induced DNA damage.

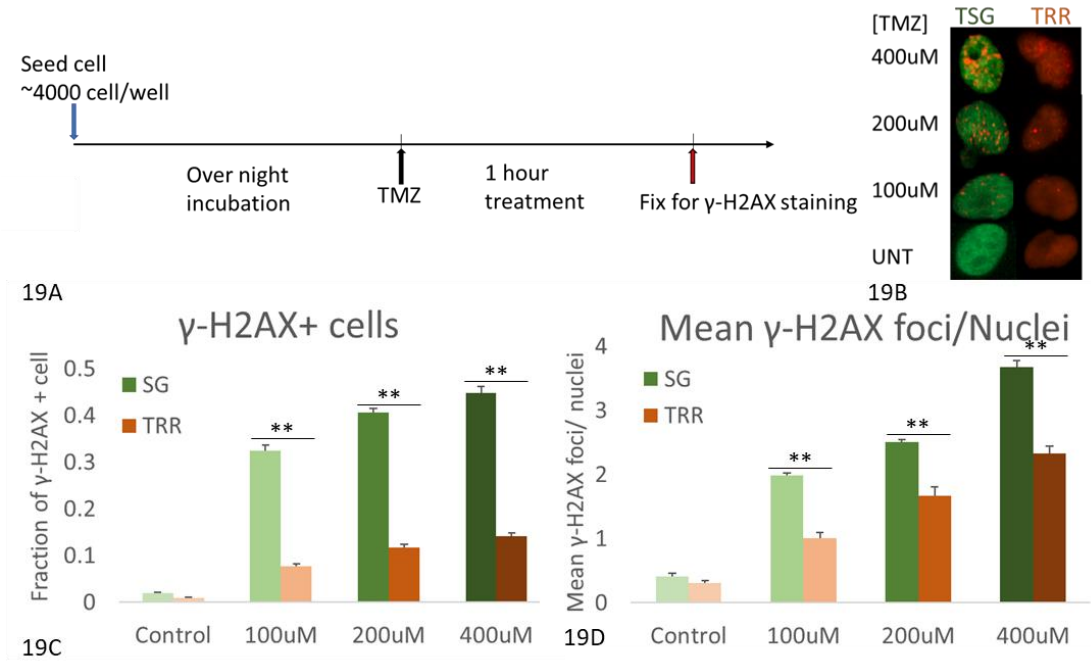

Figure 19. (A) Experimental design for γH2AX assay. SG/TRR cells were seeded at ~4000 cells/well and incubated overnight followed by TMZ treatment (100µM, 200µM and 400µM) for an hour, 4% paraformaldehyde-mediated fixation and immunostaining. (B) Images showing γH2AX foci (orange bars) stained via IF in nuclei of SG/TRR following TMZ. Bar graphs showing the relative number of γH2AX+ cells (3+ foci/nucleus) (C), and mean γH2AX foci per nuclei (D) following TMZ treatment. Comparisons were conducted between SG and TRR under the same treatment group; (= p<0.01, post hoc. T-test with Bonferroni correction after two-way ANOVA. N=3, n=36).**

6.1.4. Zombie cell death assay

Cell killing an important endpoint of therapeutics for effective cancer control. To track cell killing, the Zombie death assay was utilized to indicate late stage cell death and to quantify the percentage of dead cells within the population. The experimental design using two specific time points are showed below (Figure 20). While no significant change in cell death occurred following TMZ treatment for 48

hours, at 72 hours TMZ treatment SG cells displayed a significant dose-dependent increase in cell death compared to TRR with no apparent change in TRR cells. Combined with the DNA damage data, these findings confirm that the newly established fluorescently-labelled TRR line significantly resists TMZ-induced damage compared to drug-naïve SG cells.

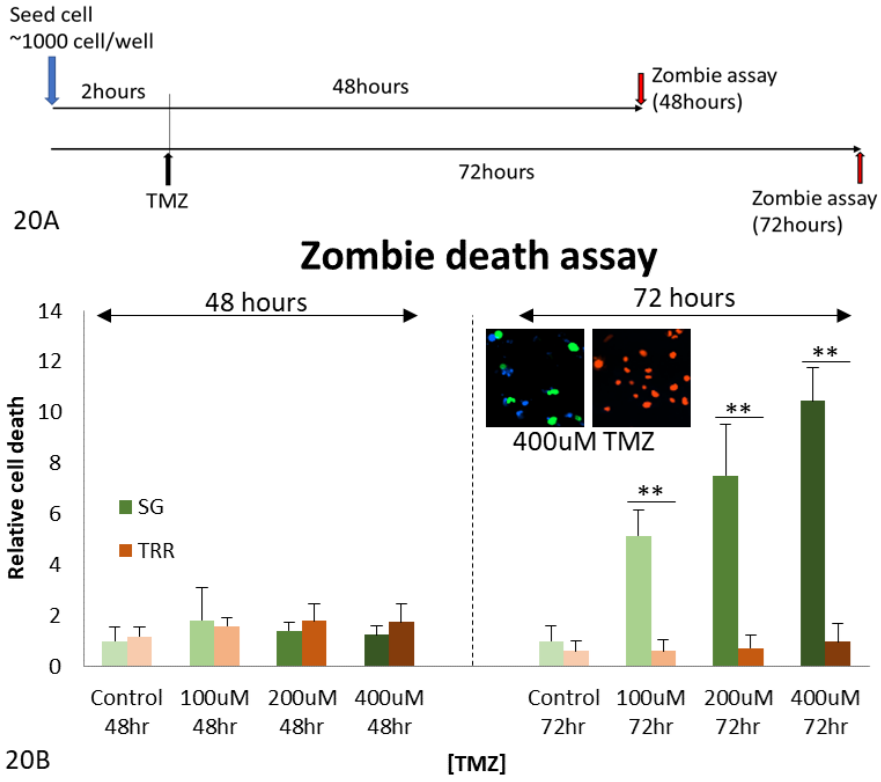

Figure 20. (A) Experimental design for the Zombie cell death assay. SG/TRR cells were seeded at ~1000 cell/well and incubated for 2 hours followed by treatment with TMZ (100µM, 200µM and 400 µM) for 48 hours and/or 72 hours prior to fixation and Zombie Dye staining. (B) Bar graphs indicating the relative fraction of dead cells resulting from TMZ treatment. Data were normalized to the untreated control. (= p< 0.01, post hoc. T-test with Bonferroni correction after two-way ANOVA. N=3, n=36). Inset images demonstrate a representative section of wells containing SG/TRR cells following a 72 hr treatment with 400µM TMZ.**

6.1.5. Cell migration assay

As GBM resistant clones are known to be highly motile and invasive throughout the cerebrum, infiltration of cancer cells further increased the difficulty to treat GBM. To address the mobility of the resistant clones a kinetic motility assay was designed to investigate migratory properties of the TRR line (Figure 21B). TRR demonstrated a more rapid initial migration rate, which showed over 7-fold enhanced motility within the first 4-24 hours with significantly higher TRR cell in the center compared to SG in the first 3 days ($p<0.01$). As cell densities increased within the central cell-free zone TRR migration slowed while SG caught up following 80 hours. These data indicate that TRR cells are highly motile and mimic the invasive properties of rGBM cells.

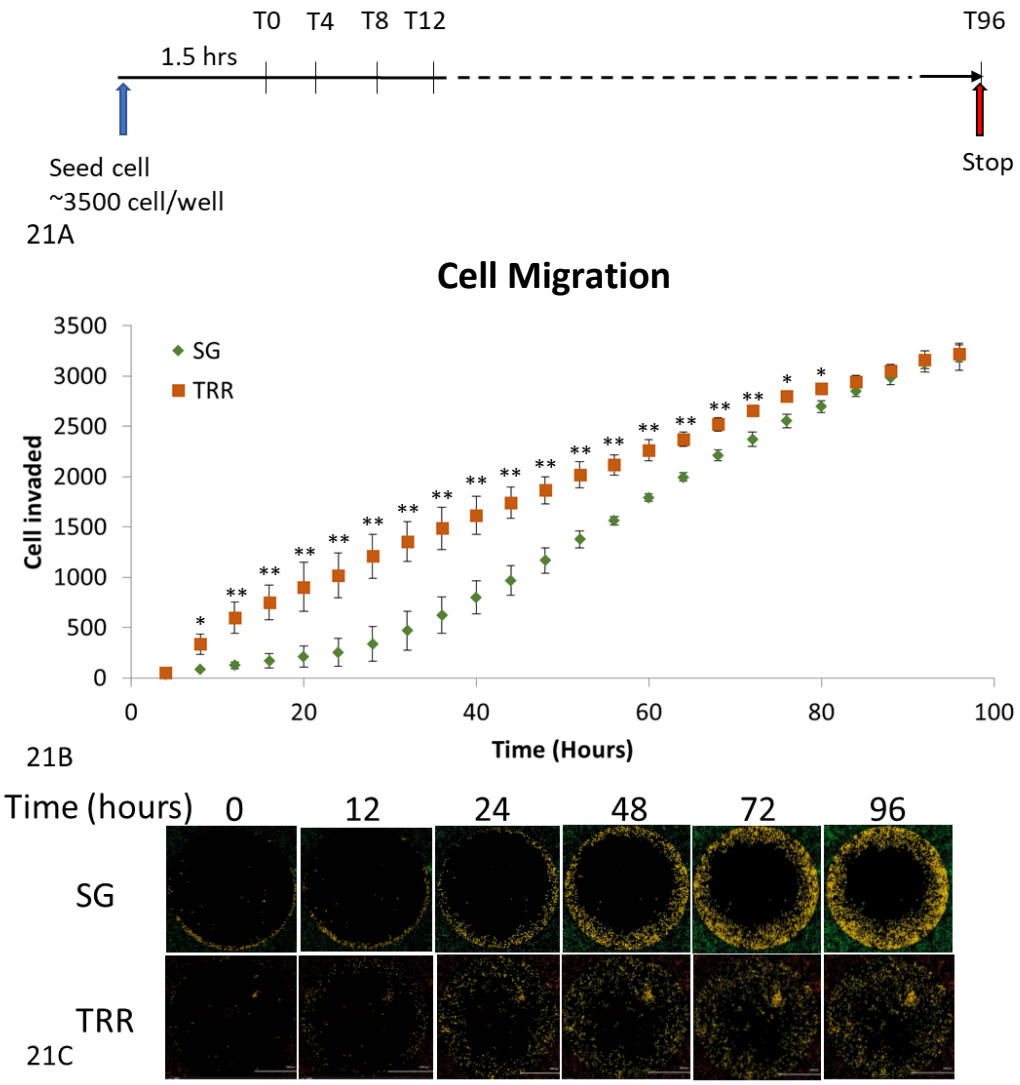

Figure 21. (A) Experimental design of the GBM cell migration assay. SG/TRR cells were seeded in specially-prepared 96-well plates (well centers coated with agarose beads) and allowed to settle for 1.5 hours. Following removal of agarose plugs (to expose a cell-free zone), cells were imaged every 4 hours and the number of cells that migrated into the center of the well were tracked and recorded. (B) Plot of the number of cells that migrated into the center zone over the 96 hours incubation period. (*= p< 0.05, **= p< 0.01, compared between SG and TRR at the same time-point, post hoc. T-test with Bonferroni correction after two-way ANOVA. N=3, n=24). (C) Whole-well image of SG and TRR demonstrating how cells were selected, at different timepoints from 0 to

96 hours throughout the experiment. TRR showed enhanced migration compared to SG.

6.2. Identification of pathways that contribute to resistance

6.2.1. Expression of O^6-methylguanine-DNA methyltransferase (MGMT).

Epigenetic regulation of *MGMT* is a common occurrence in rGBM [57]. In this light, relative MGMT expression in the SG/TRR model system was compared between SG and TRR using western analysis. Although the baseline MGMT expression level is low (1.03-fold) in SG (T0), the baseline expression (T0) of MGMT is markedly higher in TRR and increases with TMZ treatment.

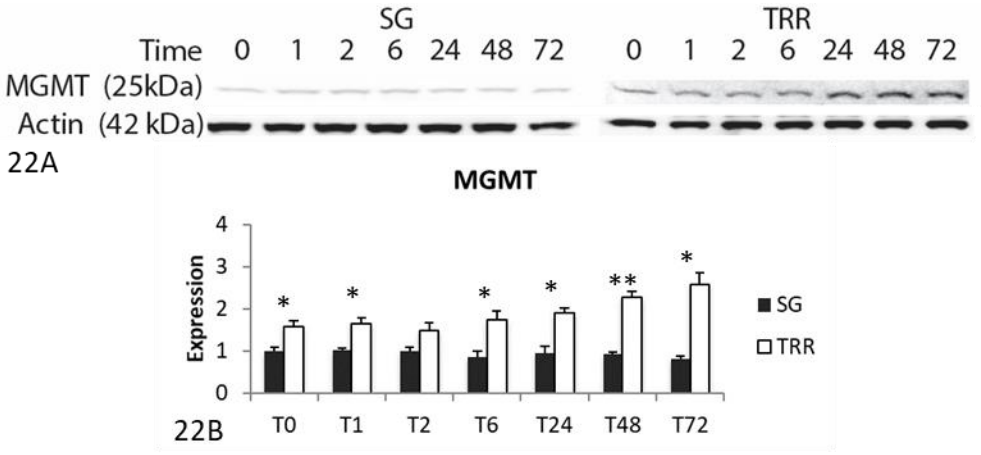

Figure 22. (A) Western blot showing levels of MGMT protein in SG and TRR following TMZ treatment, results suggested MGMT expression increased in response to TMZ during the treatment course. Signals were quantified via densitometry, normalized with the expression of actin, and represented in a bar graph (B). (n=3, *=p<0.05, **=p< 0.01. Compared between SG and TRR at the same time point, post hoc. T-test with Bonferroni's correction after two-way ANOVA.)

6.2.2. Differentially-expressed DNA double-stranded break repair genes amongst SG and TRR lines

To further elucidate molecular pathways that may be altered in TRR compared to SG, I utilized a differential gene expression analysis technique: microarray analysis. Clariom D Microarray analysis (Table 5), of SG and TRR lines (with and without TMZ treatment) identified a number of differentially-expressed RNAs corresponding to genes that encoding proteins involved in the DNA double-stranded break repair pathway. In addition to basal differences, following TMZ treatment, the RNA expression level of several important regulatory genes involved in DSB sensing and repair are implicated, including Mre11, Rad50, BRCA1, BRCA2 and XRCC2. These data provide insight as to the molecular mechanisms underlying TMZ resistance and drug responses in the TRR cell model.

Table 5. Claroim D readout of DSBR proteins in SG/TRR in difference condition; groups that were pretreated with TMZ were marked with (T)

SG vs TRR		SG vs SG(T)		TRR vs TRR(T)		SG(T) vs TRR(T)	
Gene Symbol	Fold Change	Gene Symbol	Fold Change	Gene Symbol	Fold Change	Gene Symbol	Fold Change
RAD51B	3.04	BRCA2	26.42	XRCC2	13.62	MRE11A	2.12
RAD54B	1.85	XRCC2	16.06	BRCA2	8.69	RAD51B	2.11
RAD21; MIR3610	1.81	BRCA1	9.44	BRCA1	8.66	XRCC4	1.71
RAD54L	1.62	FEN1	5.8	RAD50	4.04	DMC1	1.63
RAD52	1.47	GEN1	5.42	PRKDC	3.37	RAD54L	1.59
MRE11A	1.46	RAD51C	4.66	GEN1	3.08	XRCC6	1.53
BRCA2	1.32	XRCC3	3.91	RAD54B; FSBP	2.78	RAD51B	-1.34
RAD51	-1.34	RAD50	3.55	RAD51C	2.77	RAD51D	-1.38
XRCC2	-1.41	RAD54B; FSBP	3.5	DMC1	2.55	RAD51C	-1.46
RAD54L	-1.46	RAD54L	3.24	FEN1	2.39	RAD21	-1.59
XRCC3	-1.52	RAD51B	2.91	MRE11A	2.3	RAD54B	-1.62
XRCC6	-1.59	RAD51	2.41	RAD51B	2.18	XRCC2	-1.66
BRCA1	-1.7	RAD52	2.39	XRCC4	2.17	GEN1	-1.78
PRKDC	-1.84	PRKDC	2.23	XRCC3	1.87	RAD50	-1.82
RAD50	-2.07	LIG4	2.11	RAD54L	1.82	BRCA1	-1.85
RAD54B; FSBP	-2.16	RAD51D	1.68	LIG4	1.64	BRCA2	-2.3
		MRE11A	1.58	RAD54L	1.37	FEN1	-2.34
		DMC1	1.44	RAD52	-1.48	RAD52	-2.4
		RAD54L	1.4	RAD51	-1.78	RAD54L	-2.61
		RAD54B	1.33	RAD21	-1.95	RAD54B; FSBP	-2.72
		XRCC6	-2.24	RAD54B	-2.25	XRCC3	-3.19
						RAD51	-5.75

To validate microarray findings, Western analysis was undertaken, particularly to determine whether differential RNA expression led to actual changes in protein expression. The expression of MRN complex (Mre11, Rad50 and Nibrin), ATM (and p-ATM), TIF1 β (and p-TIF1 β) were specifically examined (Figure 23). The baseline expression of Rad 50 was significantly higher in SG (Figure 23B), agreeing with the Clariom D analysis; however, with TMZ treatment, the expression level of Rad50 increased in TRR significantly higher than observed in SG.

Phosphorylation of ATM is a marker for activated DSBR, In SG, the p-ATM signal was observed to increase significantly higher, suggesting that an intact DSBR pathway and its activation in SG following TMZ treatment (Figure 23A &C). However, p-ATM expression in TRR remained unchanged, indicating a lack of ATM phosphorylation or DSBR induction. Furthermore, the baseline ATM level was markedly lower in TRR (Figure 23D).Similarly, activation (phosphorylation) of TIF1β is a primary downstream event arising from ATM activation. My data shows higher baseline levels of TIF1b expression in TRR compared to SG. Furthermore, SG demonstrates normal damage/TMZ-induced induction of the p-TIF1β signal, whereas this signal is maintained at a high level in TRR. These results suggest that in TRR, there is perpetual baseline phosphorylation/activation of TIF1β independent of the ATM activating signal; thus, persistent induction of damage-independent DSBR pathways. Conversely, SG retains damage-dependent ATM-mediated DSBR signaling.

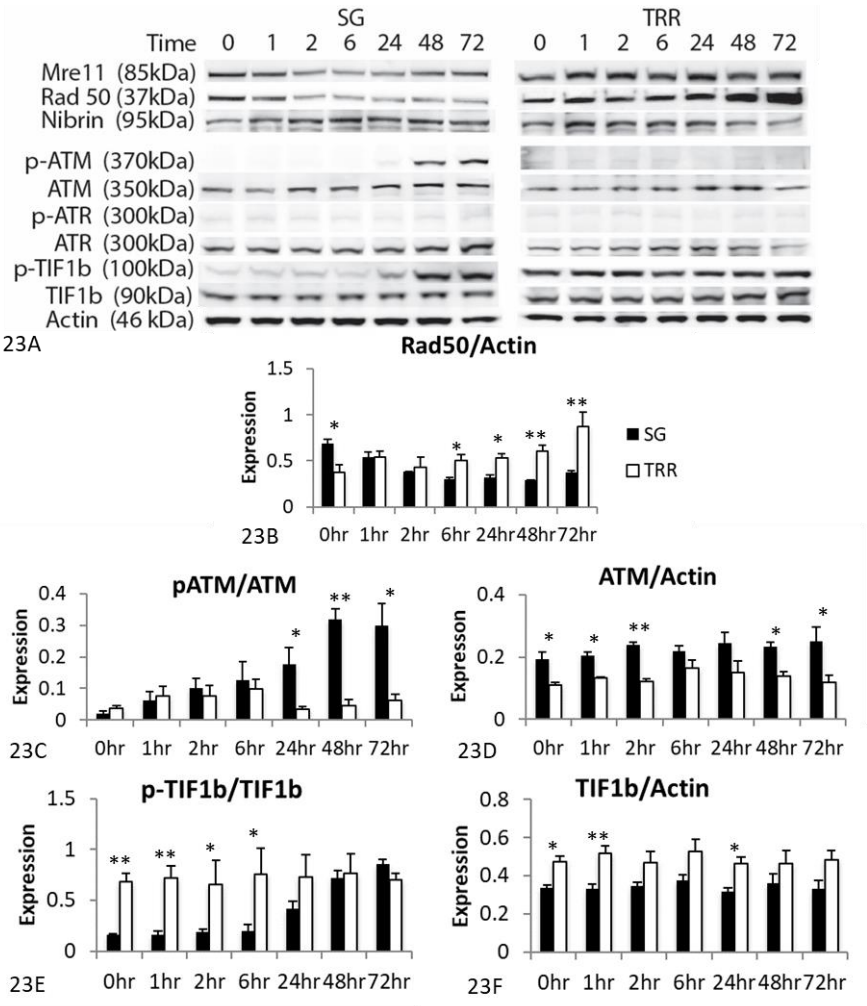

Figure 23. (A) Western analysis of select DSBR protein members in comparison to microarray data (as obtained in Table 4). (B-F) Expression level of key proteins regulating DNA double-stranded break repair (Rad50, ATM, and TIF1β) in SG and TRR following TMZ treatment (0, 1,2, 6,24,48,72 hours), result showed that there is a lack of ATM activation in TRR, while the phosphorylation of TIF1β in TRR is continuous in contrast to the induction activation in SG. Blot signals were quantified; signals of phosphorylated proteins were normalized with the expression of the corresponding pan-protein, while the pan-proteins were normalized against actin, and illustrated via bar graph. (n=3, *=p<0.05, **=p< 0.01. Compared between SG and TRR at the same time point, post hoc. T-test with Bonferroni's correction after two-way ANOVA.)

6.2.3. Expression of base excision repair (BER) pathway-related gene products

In addition to double stranded break repair, DNA single stranded break repair (SSBR) pathways feature prominently in the in the transcriptomic screen. Base excision repair (BER) is one arm of the SSBR and several of these pathway-members were found to be altered in the TRR line (see table 5.). Base excision repair pathway proteins, such as apurinic endonucleases (APE), Endonuclease VIII-like glycosylases (NEIL), poly-ADP ribose polymerases (PARP), X-ray repair cross-complementing protein 1 (XRCC1), DNA polymeraseβ (POLβ) and DNA ligase were amongst the most differentially-regulated BER proteins, comparing SG and TRR.

Table 6. Clariom D analysis indicating the differential expression of BER pathway-members in SG/TRR. Treatment groups that underwent pretreatment with TMZ are marked with (T)

SG vs TRR		SG vs SG(T)		TRR vs TRR(T)		SG(T) vs TRR(T)	
Gene Symbol	Fold Change	Gene Symbol	Fold Change	Gene Symbol	Fold Change	Gene Symbol	Fold Change
NEIL3	1.88	NEIL3	5.01	NEIL3	2.11	APEX1	1.56
APEX2	1.64	PARP2	2.36	MBD4	1.87	APEX2	1.31
APLF	1.59	TDG	2.11	NTHL1	1.45	PARP1	-1.3
APLF	1.47	APLF	2.03	PARP2	1.44	PARP3	-1.31
TDG	1.31	MBD4	1.85	POLB	1.42	POLB	-1.34
POLB	-1.39	APEX2	1.5	LIG3	-1.36	NEIL2	-1.4
APEX2	-1.39	POLB	1.37	NEIL1	-1.38	MBD4	-1.52
APEX1	-1.52	XRCC1	1.33	MPG	-1.4	NEIL1	-1.52
NEIL2	-1.54	OGG1	1.31	APEX1	-1.48	PARP2	-1.54
MBD4	-1.54	LIG3	-1.56	XRCC1	-1.55	APEX2	-1.68
NTHL1	-1.7	APEX1	-3.49	TDG	-1.91	XRCC1	-1.75
UNG	-1.81			SMUG1	-2.09	UNG	-1.83
						SMUG1	-2.23
						TDG	-3.07

Expression level of BER proteins were determined via Western analysis. Data suggested that the protein expression level of MPG in TRR increased significantly following 72 hours of TMZ treatment. TRR also displayed higher baseline

expression of Ape1, whereby an increase in protein expression was observed throughout the TMZ treatment course. Expression of XRCC1 was also found to be markedly up-regulated following 72 hours of TMZ as was expression of Ligase III, whose protein stability depends on expression of and its association with XRCC1. These data indicate that select BER proteins (ie. Xrcc1 and Lig 3) show plastic expression under different timepoints of the experiment.

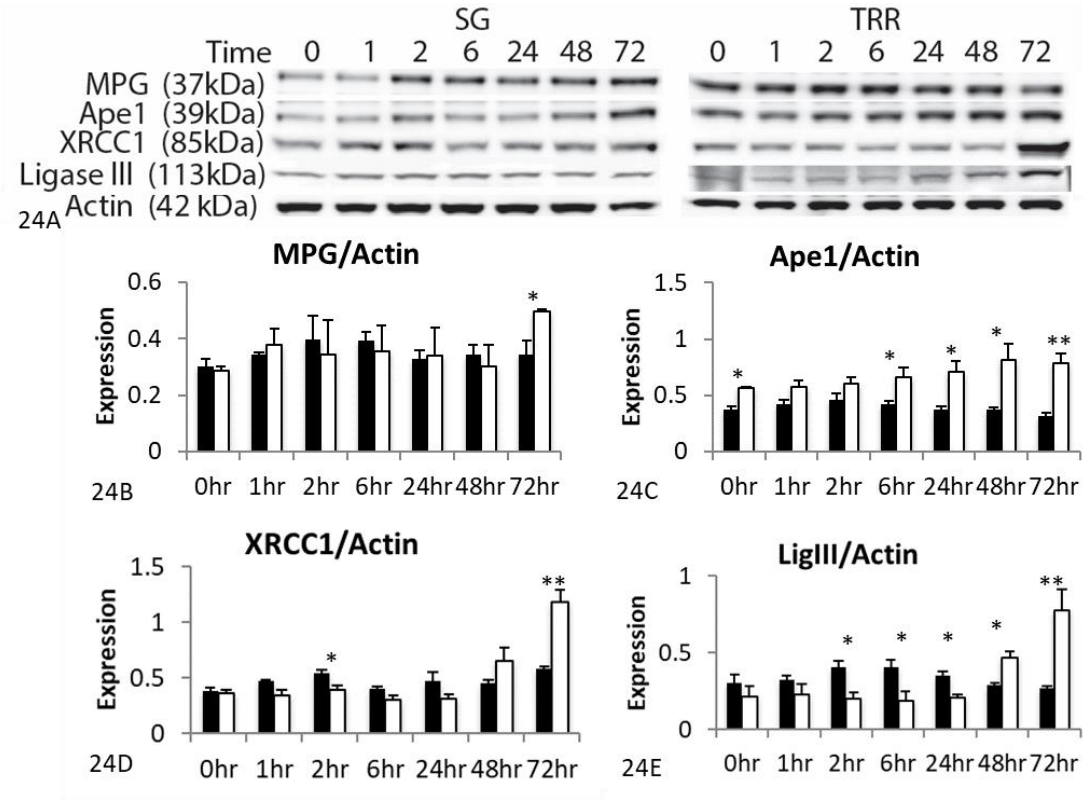

Figure 24. (A) Western analysis of base excision repair pathway proteins (MPG, Ape1, XRCC1 and DNA ligase III). Relative protein expression signals were quantified and normalized to actin (n=3, *=p<0.05, **=p< 0.01. Compared between SG and TRR at the same time point, post hoc. T-test with Bonferroni's correction after two-way ANOVA.). A marked increase in expression of MPG, Xrcc1 and LigIII was noted in the TMZ-treated TRR (72 hrs) compared to SG. Ape1 display enhanced baseline expression in TRR which increases with TMZ treatment.

6.3. Contribution of modified pathways in TMZ resistance

6.3.1. O^6-methylguanine-DNA methyltransferase (MGMT)

In a majority of clinical GBM cases, MGMT expression largely associates with TMZ resistance. MGMT enzymatically neutralizes TMZ-mediated methylation. To assess the relative contribution of MGMT to the TMZ-resistance in TRR, MGMT expression was knocked-down (up to ~50%) via lentiviral-mediated transduction of MGMT-specific shRNAs (figure 25B). *shMGMT*-expressing cells were assayed via comet assay to determine the resultant DNA damage repair profile. DNA damage repair analysis revealed no significant differences between SG and individual *shMGMT*-expressing TRR. However, analysis of co-expressed pooled shRNAs against MGMT in TRR accumulated more DNA damage when compared to TRR infected with scrambled controlled (*shSCM*). Overall, these data suggest that MGMT factors into TMZ resistance, however; the muted yet significant reduction through knockdown studies suggests additional targets, such as BER, may mediate TMZ resistance.

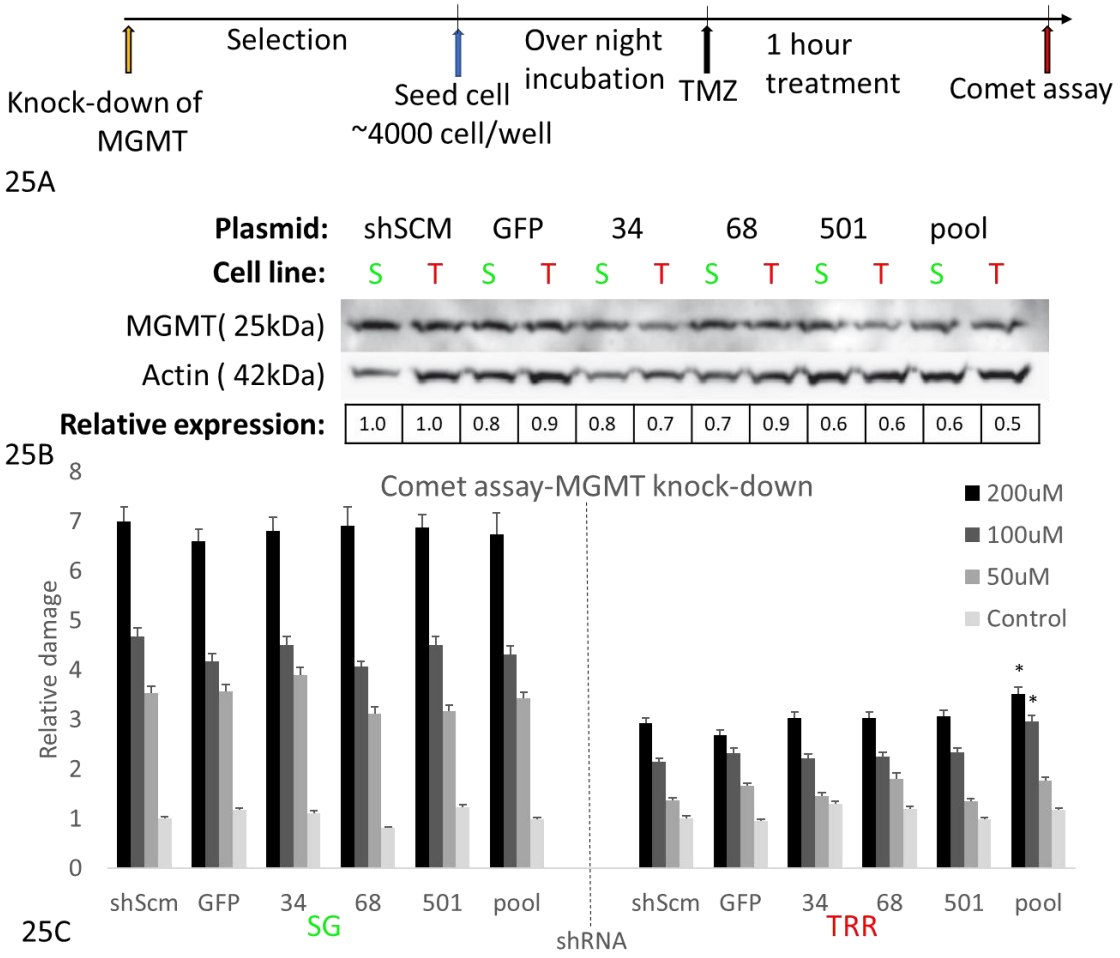

Figure 25. (A) Experimental design of MGMT knock-down assay with the shRNA-mediated RNAi technique. SG/TRR cells were infected with virus containing shRNA against MGMT followed by puromycin selection. (B) Protein expression analysis of MGMT in SG/TRR transduced with different shRNA(s); residual MGMT signals were normalized against MGMT expressed in SG expressing scrambled control (shScm). Cells were seeded and incubated overnight prior to TMZ treatment (1 hour). (C) The relative DNA damage of cell lines following treatment with different [TMZ]. (* =p<0.05, compared to SG/TRR infected with shScm plasmid and treated with the same [TMZ]. post hoc. T-test with Bonferroni correction after two-way ANOVA. N=3, n=18).

6.3.2. XRCC1-mediated base excision repair

Base excision repair is a commonly modified DNA damage repair pathway in cancer [95,161,162]. Clariom D transcriptomic analysis and Western analysis demonstrates that BER pathway is upregulated in TRR, particularly following TMZ treatment. When TRR was treated with TMZ for 72 hours, the expression of XRCC1 and Ligase III were further enhanced, likely enhancing BER activity. Indeed, XRCC1/LigIII are central to the BER response. To characterize the function of XRCC1 in rGBM, several experiments approaches were used to determine its role in mediating chemoresistance.

6.3.2.1. Enhanced XRCC1 expression in TRR with TMZ pretreatment

Western analysis of XRCC1 demonstrated a TMZ-induced enhancement of protein expression following 72 hours treatment, specifically in the TRR line and not the SG lines. This data indicates that the TMZ-resistant line may inherently possess plasticity to respond to and resolve *de novo* DNA damage. Clinically, the implication of this finding may be significant as it may explain why rGBM can resist follow-up first line (TMZ, IR) and second-line therapy (Topoisomerase-1 inhibitors, other DSB-inducers). Furthermore, it highlights the prominence of Xrcc1/BER in mediating this resistance in light of the continued focus strictly on MGMT expression status. However, as XRCC1 over-expression does not occur until 72 hrs post TMZ treatment, when TMZ has peak activity in these cells, we sought to determine whether XRCC1 upregulation was responsible for enhancing repair of other break-types. TRR cells were first pretreated with 200μM TMZ to achieve enhanced expression of XRCC1.

Pre-treatment with DMSO served as a control. Cells were then harvested, re-plated and underwent treatment with H_2O_2 (25μM) to mimic oxidative damage (single strand breaks), or with Etoposide (2μM, a Topoisomerase-2 inhibitor), to induce both single and double stranded breaks. Cellular response to this XRCC1 stimulation and drug post-treatment was assayed via a modified proteinase-K comet assay. This assay accounts for protein-linked DNA breaks which commonly occurs in Topoisomerase-mediated DNA breaks, such as those induced by Etoposide. This comparative analysis revealed that T72R (TRR cells pretreated with TMZ for 72 hours) as compared to T0R (mock pretreatment), accumulated significantly less DNA damage, suggesting that TMZ pretreatment with concomitant XRCC1 over-expression serves to enhance TRR repair. T72R cells displayed higher repair activity towards DNA SSBs induced by H_2O_2; T72R accumulated less damage when compared against similarly-treated T0R, suggesting again, TMZ pretreatment enhanced DNA damage repair. Similar results were obtained with Etoposide, suggesting a generalized enhanced DNA repair activity associated with DNA damage-induced XRCC1 expression in resistant GBM cells, but not drug-naïve GBM cells.

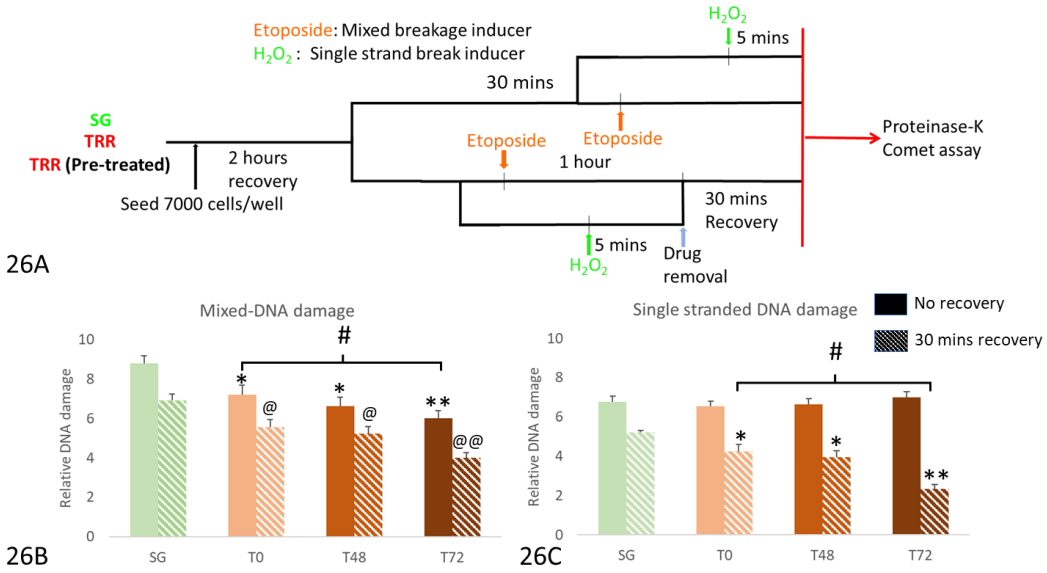

Figure 26. (A) Proteinase-K comet assay to determine SG/TRR drug-treatment sensitivity following TMZ pretreatment and concomitant XRCC1 stimulation. (B) Mean relative damage in cells induced following Etoposide treatment (Mixed-DNA damage), with/without recovery. (* =p<0.05, ** =p<0.01, compared to SG without recovery. post hoc. Tukey's test after two-way ANOVA. N=3, n=27. @=p<0.05, @@ =p<0.01, compared to SG with recovery. post hoc. Tukey's test after two-way ANOVA. N=3, n=27. # =p<0.05, in contrast to TRR without pretreatment. post hoc. Tukey's test after two-way ANOVA. N=3, n=27). (C) Mean relative damage in cells induced following H_2O_2 treatment (single-stranded DNA damage), with/without recovery. (* =p<0.05, ** =p<0.01, compared to SG with recovery. post hoc. Tukey's test after two-way ANOVA. N=3, n=27. # =p<0.05, in contrast to TRR without pretreatment. post hoc. Tukey's test after two-way ANOVA. N=3, n=27).

6.3.2.2. Over-expression of XRCC1 in SG

Since enhancement of XRCC1 expression via TMZ pretreatment stimulated DNA repair activity and subsequent cellular drug resistance, to ensure that the enhancement of XRCC1 is the key factor to DNA damage resistance, XRCC1 was artificially over-expressed in SG through transfection with an XRCC1-YFP expression construct. Western analysis of transfectants showed ~2-fold overexpression was achieved in SG cells (Figure 27B). Etoposide treatment of SG/XRCC1-YFP and TRR cells displayed significantly lower DNA damage relative to SG/YFP controls. Similarly, H_2O_2 treatment followed by 30 mins of recovery, revealed that both SG/ XRCC1-YFP and TRR cells displayed significantly lower DNA damage relative to SG/YFP controls. As all cells displayed equal DNA damage immediately following H_2O_2 treatment, the residual DNA damage differences following 30 mins recovery indicate accelerated DNA repair activity occurred in treatment groups with enhanced XRCC1 expression (SG+XRCC1/YFP and TRR). In summary, these data indicate that over-expressing XRCC1 in SG can phenocopy the enhanced DNA damage repair activity associated with TRR.

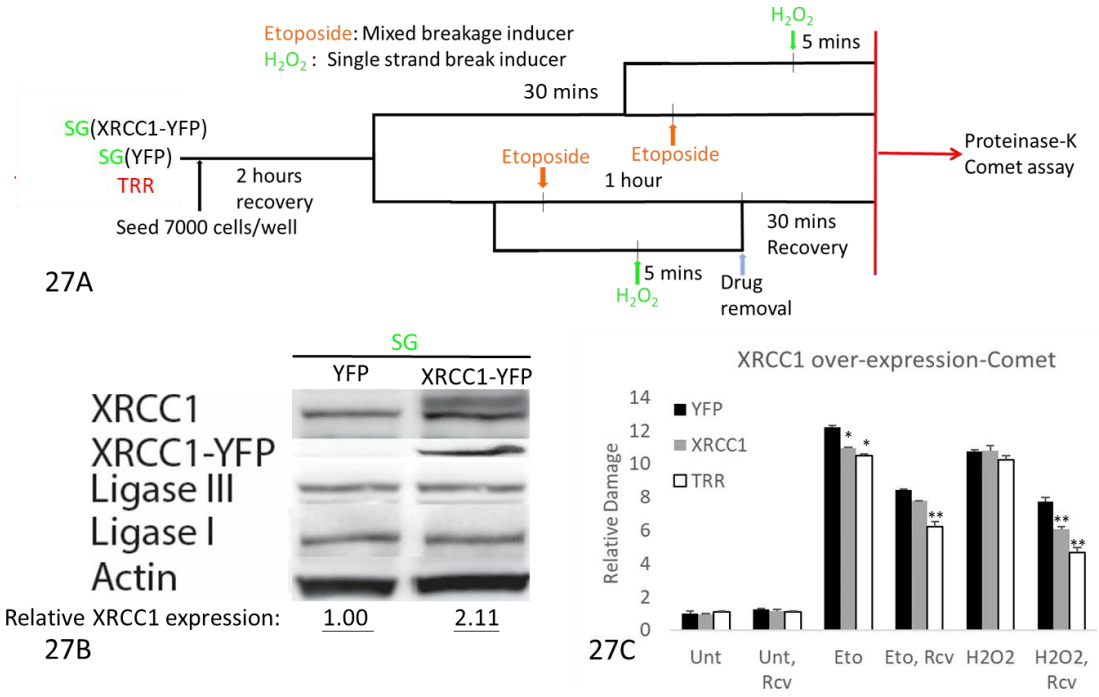

Figure 27. (A) Proteinase-K comet assay to compare TRR DNA repair activity with SG cells with XRCC1 over-expression. (B) Western analysis confirming over-expression of XRCC1 and other associated proteins in SG transfected with the XRCC1-YFP expression construct (YFP empty vector served as control). (C) Mean relative DNA damage in cell lines treated with DNA damaging agents. (* =p<0.05, ** =p<0.01, compared to SG(YFP). post hoc. T-test after two-way ANOVA. N=3, n=18).

6.3.2.3. Knock-down of XRCC1 in SG & TRR

Since enhanced XRCC1 expression promotes DNA repair in TRR cells, the converse experiment was performed to determine whether TRR-associated XRCC1/BER-mediated DNA repair activity could be reversed to resemble repair rates ascribed to SG. RNA interference was employed to knock-down XRCC1 expression in SG and TRR, and DNA damage was examined following treatment with DNA damaging

agents via Proteinase-K comet assay (figure 28), cell growth assay (figure 29A-D) cell death assay (figure 29E).

The knock-down efficiency of the *shXRCC1* in SG and TRR was >60% (Figure 28B). This level of knockdown is not surprising as XRCC1 is considered an essential gene [132]. Furthermore, Ligase III levels were concomitantly reduced in the shXRCC1 cells. DNA damage repair assays were used to assess whether TRR could be re-sensitized to TMZ via XRCC1 suppression. Indeed, TRR/shXRCC1 cells displayed reduced DNA damage repair activity following Etoposide- and peroxide-induced DNA damage compared to TRR/shSCM controls (figure 28D). Furthermore, TRR/shXRCC1 cells pre-treated with TMZ (a treatment which normally induces XRCC1 expression) incurred damage levels similarly to pretreated SG/shSCM and SG/shXRCC1 following subsequent treatment with Etoposide or peroxide (figure 28F), indicating that reduced expression of XRCC1 was a determining factor in mediating TRR resistance to DNA damaging chemotherapeutics, including DNA alkylation (TMZ), SSBs (peroxide) and DSBs (Etoposide).

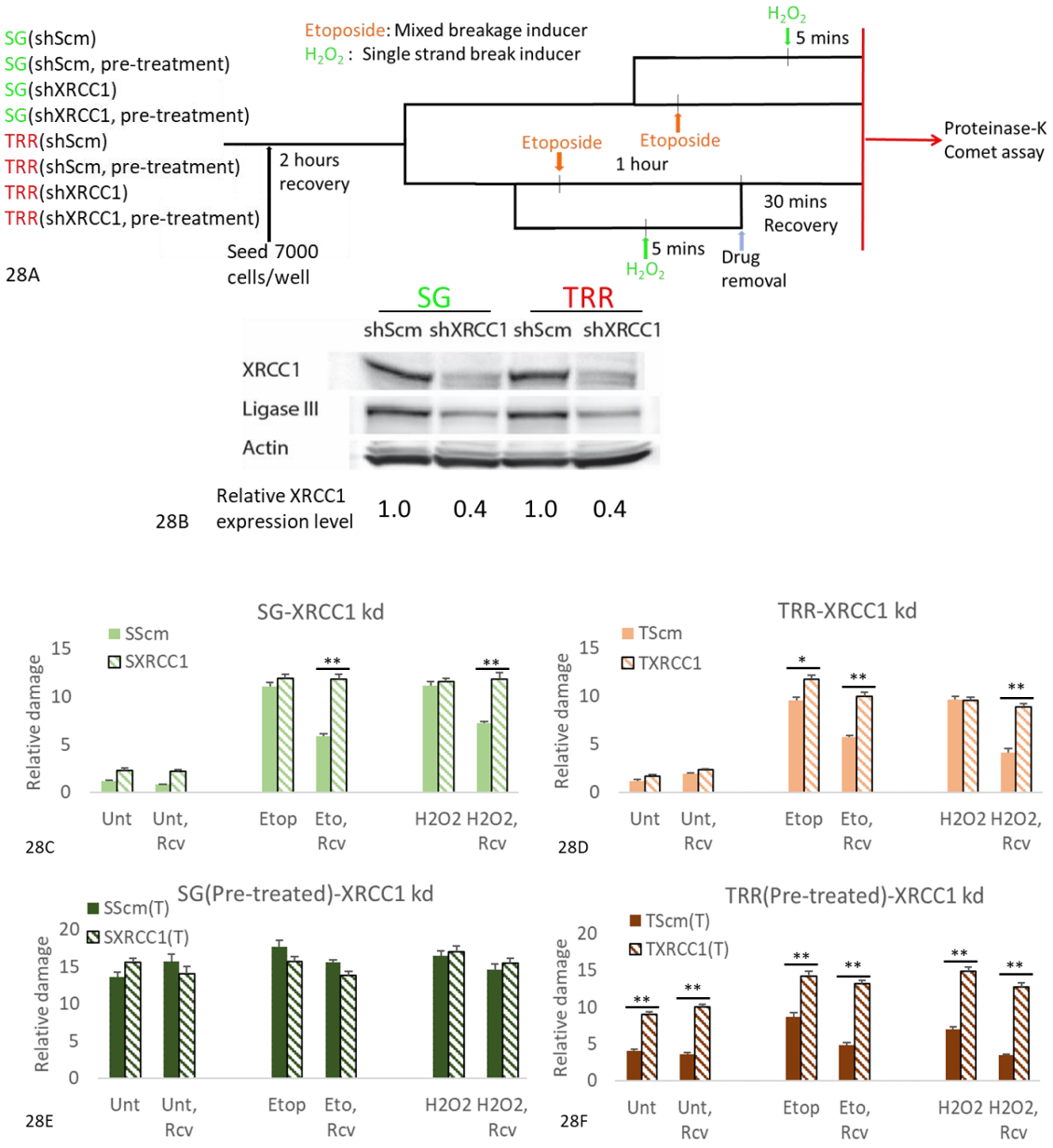

Figure 28. (A) Proteinase-K comet assay on SG and TRR cells following XRCC1 knockdown. (B) Western analysis indicating XRCC1 and Ligase III expression in SG & TRR cells following shXRCC1 transduction. (C-F) Proteinase-K comet assay results showing the mean relative DNA damage in cell lines treated with DNA damage agents. (* =p<0.05, ** =p<0.01, compared within treatment groups. post hoc. T-test with Bonferroni's correction after two-way ANOVA. N=3, n=18).

The overall cellular consequence of reduced expression of XRCC1 and subsequent re-sensitization of TRR cells to chemotherapeutic agents was assessed via cellular growth assays. These data showed that XRCC1 reduction resulted in reduced cell growth in both mock-treated and drug-treated groups. When comparing the growth rate between the shXRCC1 cells to their shSCM counterpart, a TMZ dose-dependent decrease in growth was identified in TRR (figure 29D), indicating that XRCC1 is a determining factor in mediating TRR resistance to TMZ.

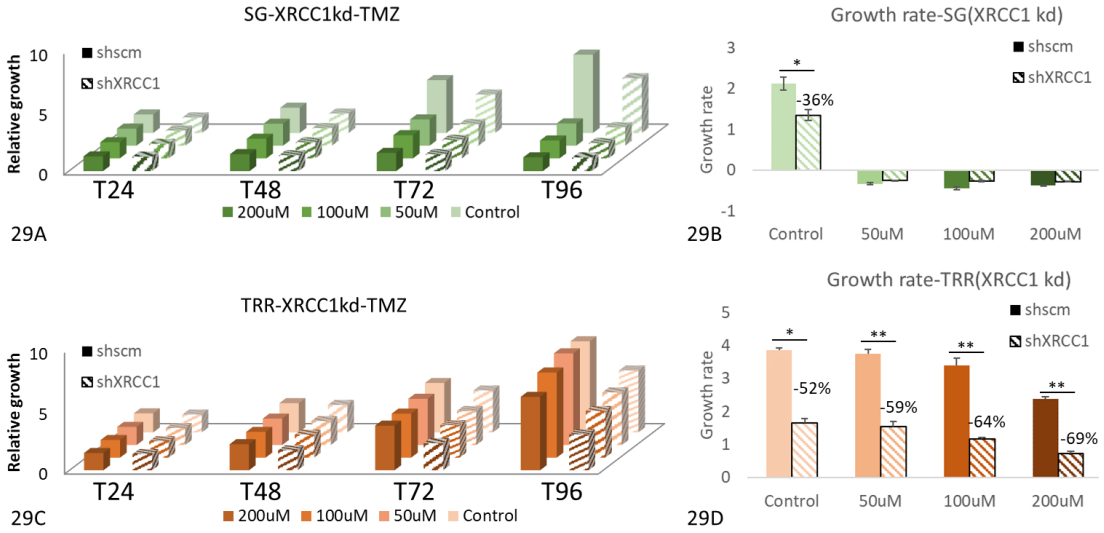

Figure 29. Growth assay on shXRCC1 expressing SG(A) &TRR (C) cells. Cells underwent TMZ treatment for 96 hours, and cell readings were taken every 24 hours. Readouts were normalized with the base line reading (T0). (B &D) Growth rate calculated from 72 to 96 hours; the rates were compared between same treatment groups (* =p<0.05, ** =p<0.01, post hoc. T-test with Bonferroni's correction after two-way ANOVA. N=3, n=18), and the % differences were graphically represented.

6.4. Re-sensitizing rGBM to TMZ by inhibiting Base excision repair

At the apex of the BER response is PARP (refer to figure 5 in INTRODUCTION), whose function is to sense SSBs and signal the XRCC1-mediated repair response. XRCC1 is a scaffolding protein without discernable enzymatic targets; however, clinical PARP inhibitors are already used in a variety of therapies. Therefore, TRR cells were treated with PARP inhibitors (PARPi) to compare against TRR/shXRCC1 in order to determine whether a clinically-relevant pharmacological agent can suppress BER activity and resolve TMZ resistance in rGBM (TRR) cells. TRR/shXRCC1 cells were compared to TRR cell treated with Pamiparib, a small molecule inhibitor of PARP with GBM-relevant ability to cross the blood-brain-barrier [136]. PARPi treatment in TRR was found to significantly re-sensitize TRR cells to TMZ and enhance TMZ-mediated cell death, similarly to TRR/shXRCC1 (Figure 30). These data indicate that, based on the TRR cell model, BER inhibition in general is a viable modality to restoring TMZ sensitivity and enhancing cell death to counteract rGBM.

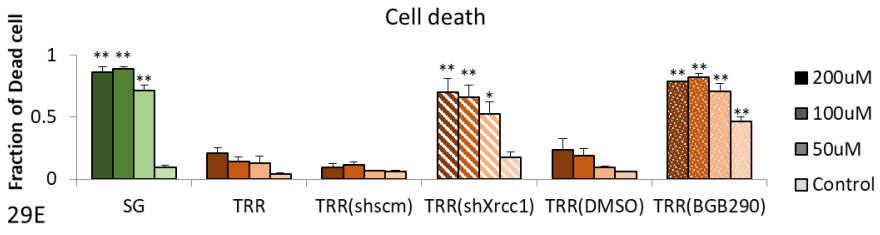

Figure 30. Death assay comparing SG and TRR following 72 hrs TMZ/PARPi treatment. (* =p<0.05, ** =p<0.01, post hoc. Tukey's test after two-way ANOVA. N=3, n=12), XRCC1 knocked-down in TRR restored TMZ sensitivity, cell deaths were observed, application of Pamiparib also mimicked that phenotype.

My identification of BER being transcriptionally and translationally- regulated in TRR combined with the PARPi data suggest a novel treatment modality to counteract rGBM. XRCC1 is a central protein in the BER response. My findings that TRR cells can acutely enhance XRCC1 expression in the face of DNA damaging chemotherapy in order to evade the cell killing effects of this treatment is an elegant example of the plasticity that rGBM may possess to adapt to a hostile microenvironment and survive.

Poly ADP-ribose polymerase (PARP) is essential for BER[114,133,163]. PARP inhibition is an effective way to inhibit BER; however, there are a great number of types of PARP inhbitors that have been developed, including calatylic inhibitors and PARP trappers (Figure 30)

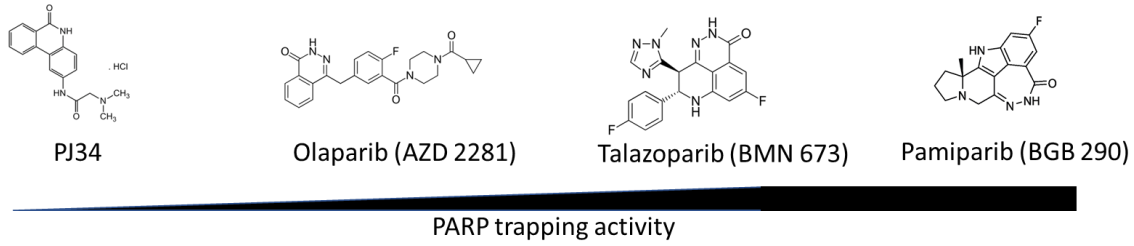

Figure 31. Small molecule inhibitors for Poly ADP-ribose polymerase. PJ34 is a PARP inhibitor with limited PARP trapping activity, Olaparib is an intermediate trapper, Talazoparib is a potent PARP trapper and Pamiparib (BGB290) is a potent PARP trapper that is able to pass across the Blood-brain barrier[136].

To determine whether specific classes of PARP inhibitors/trappers are more amenable to TMZ resensitization in TRR, these agents were co-treated and

compared with TMZ in TRR cells. The efficacy of the combined treatment was investigated using cell-based synergy assays, including cell growth, DNA damage and cell death.

6.4.1. PJ34 vs TMZ

6.4.1.1. Cell growth assay

To examine the PJ34-TMZ co-treatment, a kinetic growth rate analysis was undertaken where cells were measured **every 24 hours for 5 days,** and the value of multiple dose combinations at different time points were collected and plotted into a 3-D graph (figure 32A & C). The relative growth at **96 hours** was used to generate Combenefit graphs to determine synergy (Figure 32B &D).

The relative growth through the whole treatment course suggested that 100μM and 200μM of TMZ was able to suppress growth in SG (Figure 32A). PJ34 treatment (1μM, 10μM) showed cooperativity with TMZ and showed further growth suppression; results that correspond with Combenefit data (Figure 32B), where at higher PJ34 concentrations, increasing synergy was noted.

In TRR (Figure 32C), TMZ concentrations of 200μM demonstrated growth suppression; however, in combination with PJ34 (10μM), lower TMZ concentrations were able to significantly suppress TRR. Combenefit analysis (Figure 32D) corresponded with this data and showed synergy between increasing [TMZ] and [PJ34].

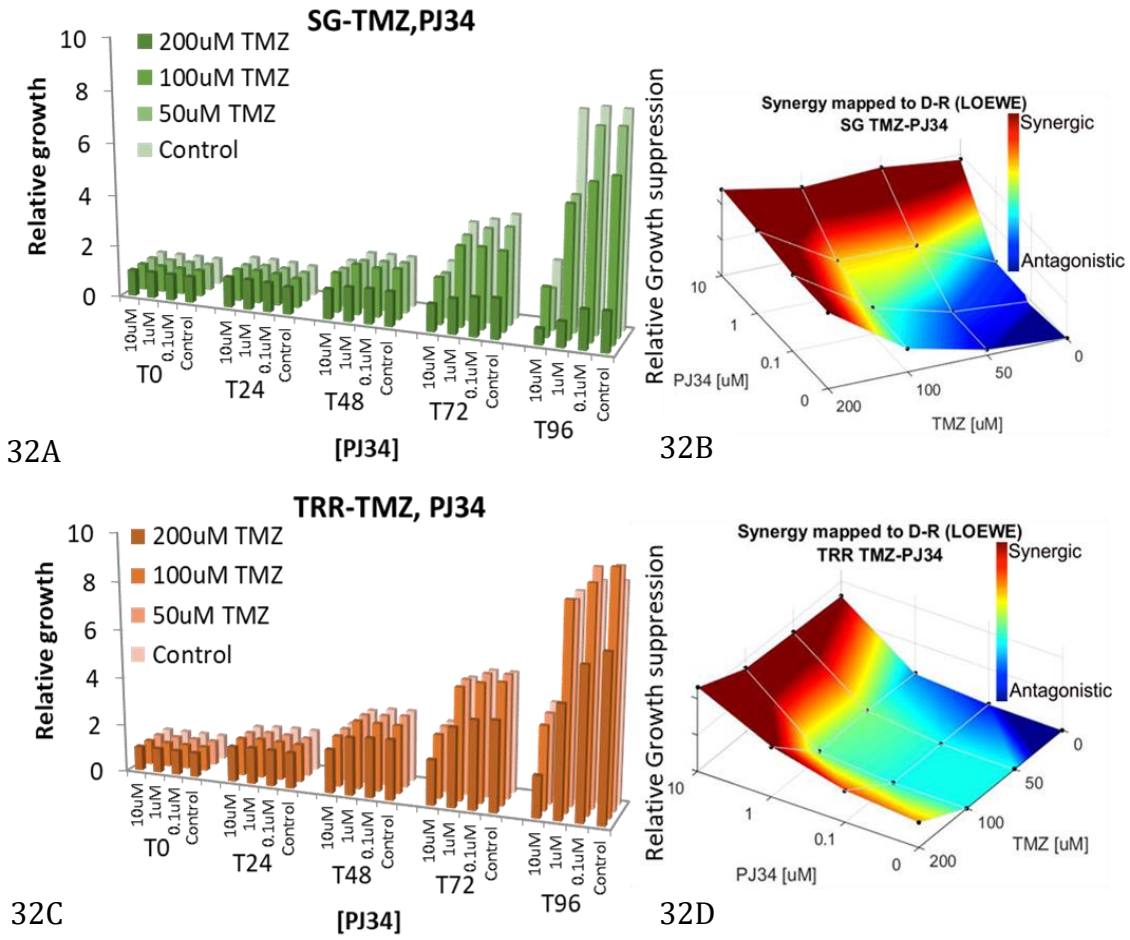

Figure 32. Growth assay (N=3, n=9) investigating the effect of PARP inhibition to sensitize TRR cells to TMZ. Relative growth rate of treatment groups at different time points for SG (A) and TRR (C). Relative growth suppression demonstrated via Combenefit analysis; synergism of TMZ with PJ34 in SG (B) and TRR(D) are represented in 3-D heat maps, Combenefit analysis suggested that PJ34 cooperates with TMZ at high PJ34 concentrations.

6.4.1.2. DNA damage assays

To address the capability of PJ34 to enhance TMZ-induced DNA damage, alkaline comet assay (figure 33A-D) and γH2AX analysis (figure 33E-H) were used to quantify DNA damage. Cells were pretreated with PJ34 for 30 mins followed by

TMZ treatment for **1 hour**, and the ensuing DNA damage was quantified. Alkaline comet analysis indicated that while PJ34 is able to synergistically enhance TMZ-induced damage in SG (Figure 33A &B), TRR cells do not show such synergy with PJ34 during TMZ co-treatment (Figure 33C & D). Similar to comet data, the γH2AX analysis show that PJ34 enhances TMZ-induced damage in SG at higher concentrations (Figure 33F), whereas PJ34 had little effect on enhancing TMZ damage in TRR (figure 33H).

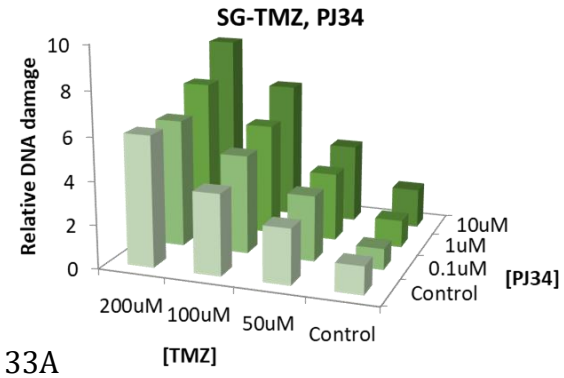

33A

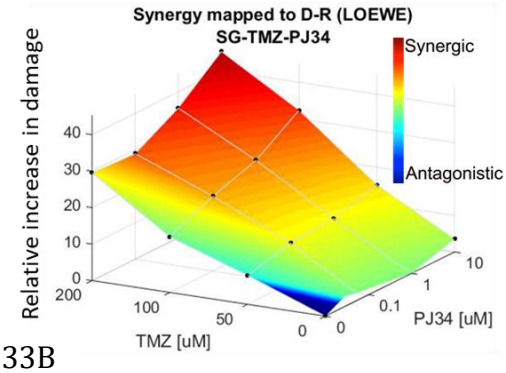

33B

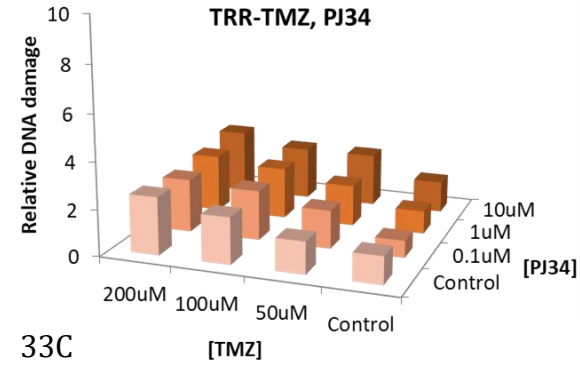

33C

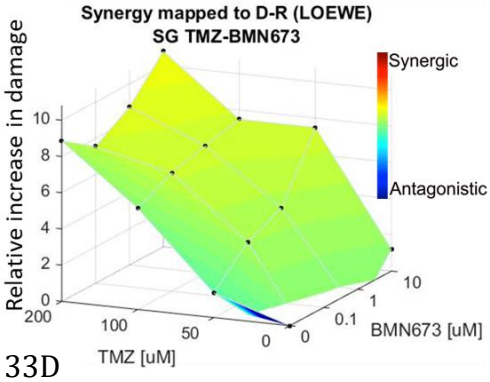

33D

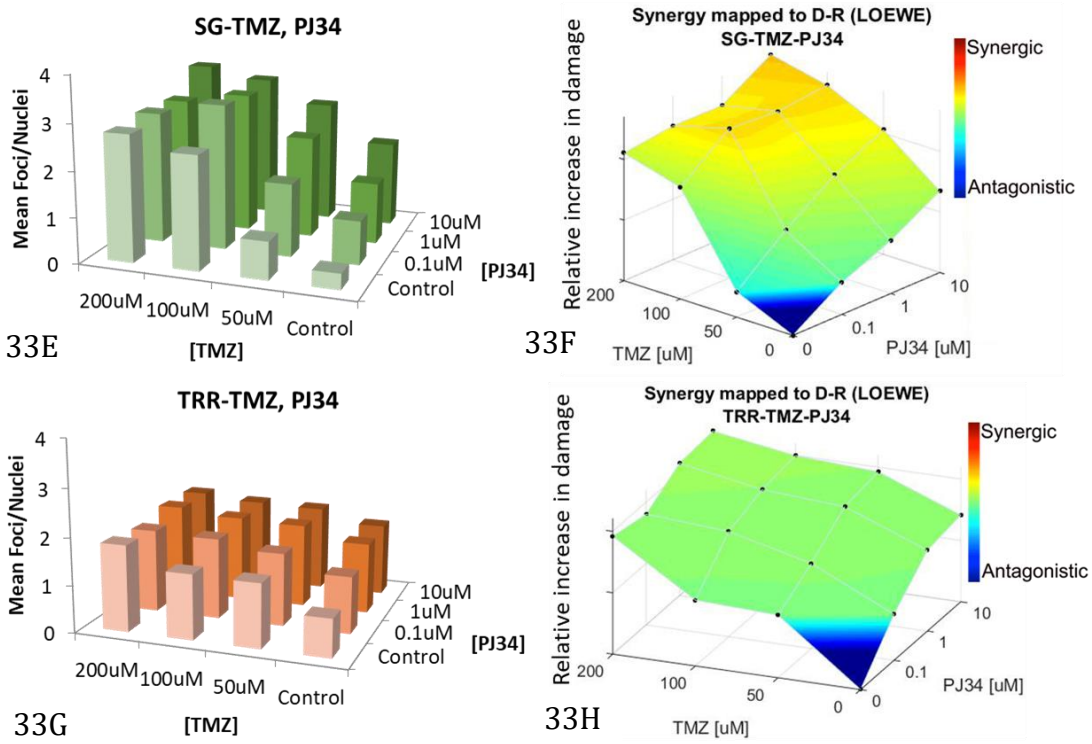

Figure 33. Comet analysis (N=3, n=9) of SG (A) and TRR (C) following co-treatment with TMZ and PJ34. Relative increase in DNA damage in SG (B) and TRR (D) were demonstrated via Combenefit analysis to illustrate cooperativity of co-treatments. DNA lesion quantification of SG (E) and TRR (G) via γH2AX analysis (N=3, n=9) represented in a 3-D bar graph format; cooperativity in SG (F) and TRR (H) were analyzed via Combenefit, results suggested PJ34 showed noticeable synergic effect with TMZ in SG, but not in TRR.

6.4.1.3. Cell death assay

The capability of PJ34 to enhance cell killing of TMZ in SG/TRR was studied via the Zombie cell death assay; cells were treated with combinations of drugs and incubated for **72 hours**. The fraction of Zombie+ cells in SG (figure 34A) and TRR (Figure 34C) are represented in the 3-D bar graph, and cooperativity was assessed

via Combenefit analysis (figure 34B & D). PJ34 at 1μM and 10μM sensitized SG cells to TMZ-induced cell death (Figure 34B). However, TRR cells displayed a relatively weak, but slightly synergistic increase in TMZ-induced cell death at higher [PJ34] (Figure 34D).

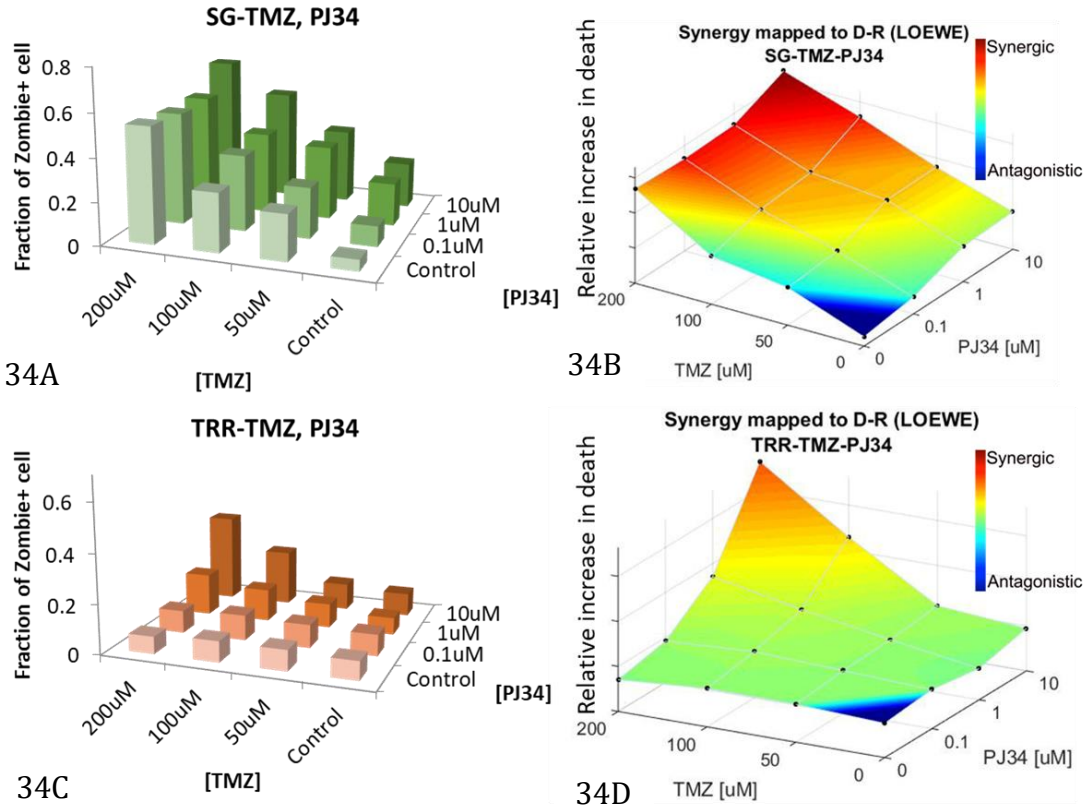

Figure 34. 3-D bar graph showing the fraction of dead cell (Zombie+) in SG (A) and TRR (C) under different combinations of TMZ and PJ34. Relative increase in fraction of dead cell in SG (B) and TRR (D) were analyzed via Combenefit and represented by 3-D heat map (N=3, n=9). Synergic effect is stronger in SG when TMZ combined with PJ34, while only weak synergy is observed in TRR at high concentration.

6.4.2. Olaparib vs TMZ

6.4.2.1. Cell growth assay

Like the conditions above, cell growth with TMZ and Olaparib (Olap) co-treatment was measured over a 5-day treatment period, with readings were taken every 24 hours and normalized to time 0. Relative growth suppression was calculated and underwent Combenefit analysis to generate 3-D heat maps.

In the both SG ad TRR, Olap by itself reduced cell growth (Figure 35A & B), while co-treatment of TMZ with Olap demonstrated synergistic growth suppression. Interestingly, Olap was able to overcome TRR resistance to TMZ (50μM and 100μM, Figure 35C). TMZ co-treatment with Olap was strongly synergistic in TRR, indicating that Olap can re-sensitize TRR to TMZ, even at individual TMZ doses that do not normally affect TRR.

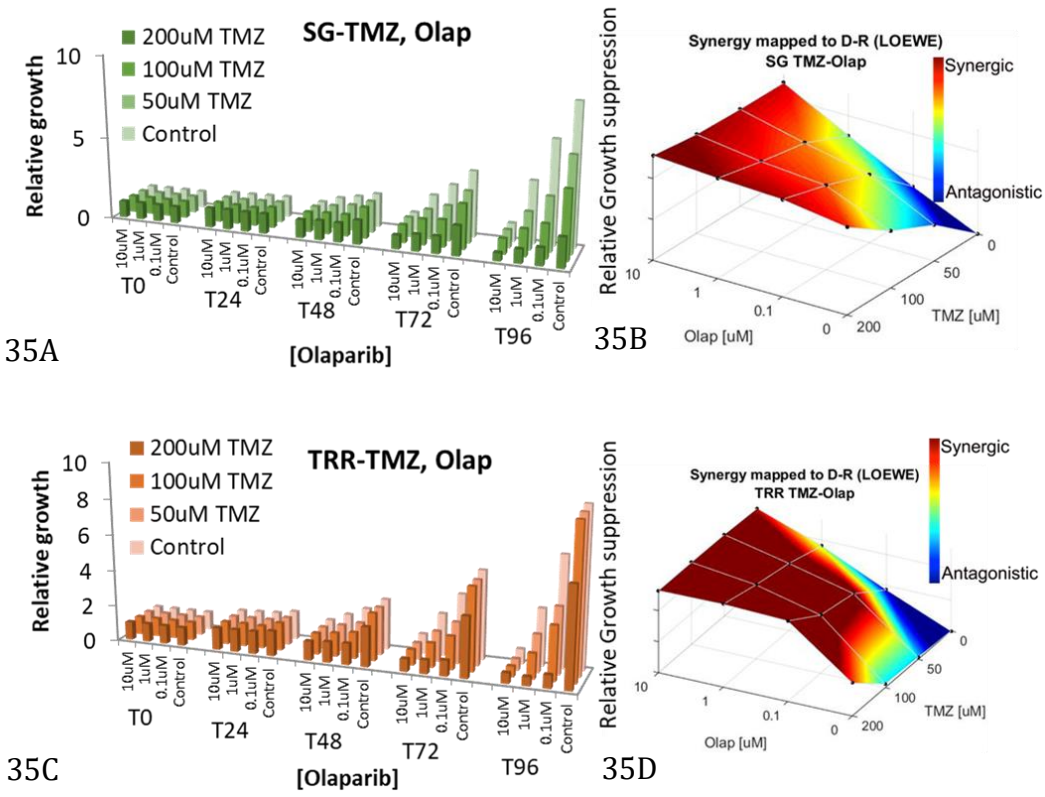

Figure 35. Relative growth of SG (A) and TRR (C) following co-treatment with TMZ and Olap. Relative growth suppression of SG (B) and TRR (D) were analyzed via Combenefit to demonstrate drug synergism (N=3, n=9), Synergic analysis suggested that, TMZ-Olap treatment is synergy in SG, where the combined treatment provide a strong cooperative effect in TRR, due to the basal resistance against TMZ alone.

6.4.2.2. DNA damage assay

DNA damage analysis, via comet and γ-H2AX assays, demonstrated that Olap itself enhanced DNA damage in GBM cells at high Olap concentrations. Co-treatment of Olap with TMZ showed synergistic enhancement of cellular DNA damage in both SG and TRR, even at low TMZ concentrations. Alkaline comet analysis revealed that

Olap was able to increase TMZ sensitivity by promoting TMZ-induced DNA damage (Figure 36A) in SG (Figure 36B) and TRR (Figure 36D) a synergistic manner. Similarly, γH2AX analysis concurred with comet data, where Olap sensitized SG and TRR to TMZ (Figure 36E, G). TMZ-Olap showed widespread synergy in SG (Figure 36F) and at high concentrations of TMZ/Olap in TRR (Figure 36G).

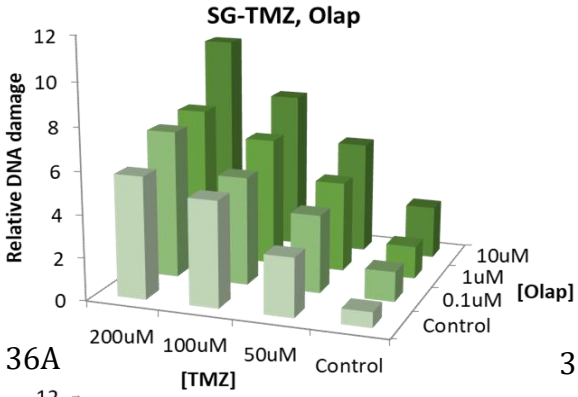

36A

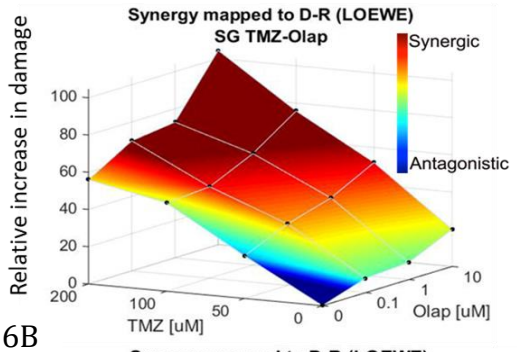

36B

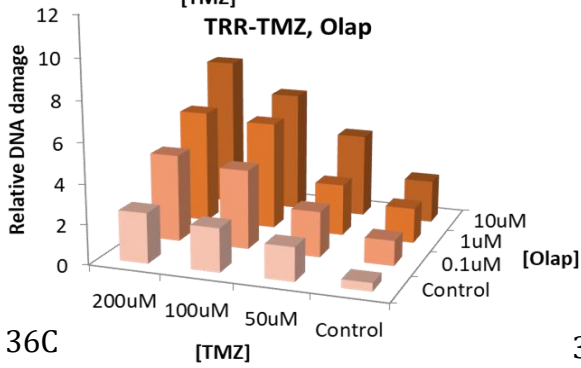

36C

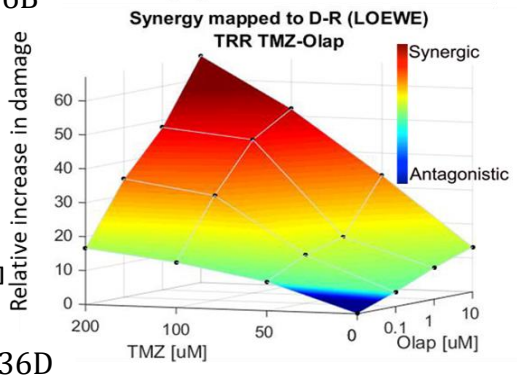

36D

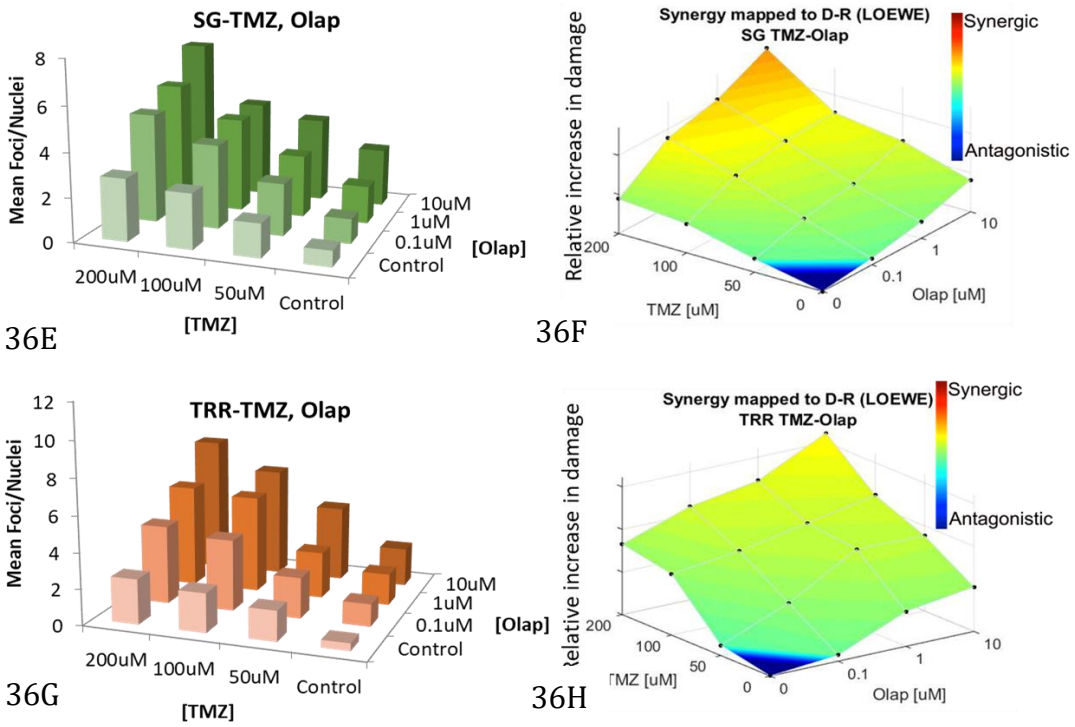

Figure 36. Comet analysis (N=3, n=9) of SG (A) and TRR (C) combinatorial co-treatment (TMZ+ Olap) expressed in relative DNA damage. Relative increase in damage of SG (B) and TRR (D) was demonstrated with Combenefit analysis to illustrate cooperative effects. DNA damage quantification of SG (E) and TRR (G) with γH2AX foci assay (N=3, n=9) is represented in the bar graph, while cooperative in SG (F) and TRR (H) was analyzed via Combenefit, synergic increases of DNA damage were observed both in SG and TRR.

6.4.2.3. Cell death assay

Cell death analysis was performed to characterize the cellular effect of enhanced DNA damage arising from TMZ/Olap co-treatment. Cells were treated with TMZ and/or Olap for 72 hours prior to fixation and Zombie dye application to mark and quantify cell death events.

Treatment of Olap alone at 1μM and 10μM enhanced cell death (Figure 37A &C). When combined with TMZ, Olap further promoted cell killing in SG, with

synergy noted at 1μM and 10μM (Figure 37B). Co-treatment with TMZ and Olap combination (1μM and 10μM) in TRR resulted in higher cell death events were (Figure 37C), in a synergistic manner following Combenefit analysis (Figure 37D), These data, combined with DNA damage data, indicate that Olaparib can re-sensitize TRR to TMZ-induced DNA damage and cell death.

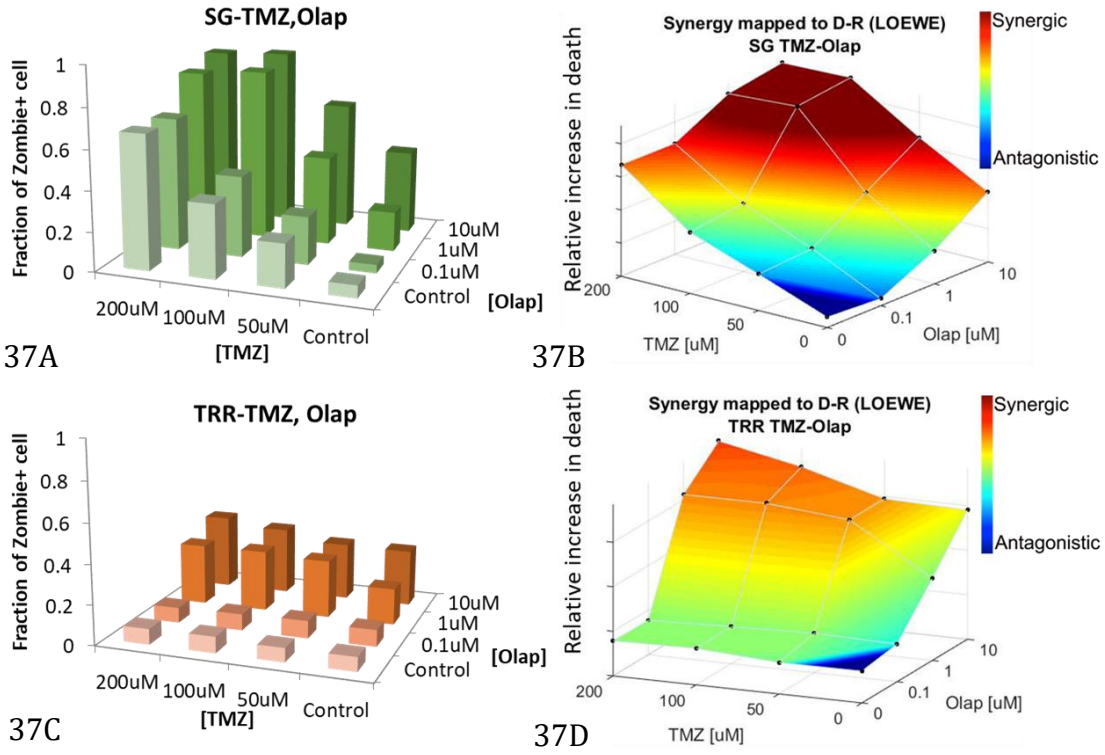

Figure 37. 3-D bar graph showing the fraction of dead cells (Zombie+) in SG (A) and TRR (C) following co-treatment with TMZ with Olap. Relative increase in the fraction of dead cells in SG (B) and TRR (D) was analyzed via Combenefit analysis and represented in the 3-D heat map (N=3, n=9), data suggested that Olaparib strongly promoted the efficacy of TMZ in both SG and TRR, Olaparib re-sensitized TRR toward TMZ induced cell death.

6.4.3. Talazoparib vs TMZ

6.4.3.1. Growth assay

Talazoparib is a highly potent PARP inhibitor [138,164], but also possesses PARP trapping properties [137]. Growth assay was performed, with serial dilution of TMZ and Talazoparib. Cell counts were taken every 24-hour over a 96-hour interval, and the readings were normalized with the T0 reading of the same well, to calculate relative growth.

Talazoparib alone demonstrated strong growth inhibition in both SG (Figure 38A) and TRR (Figure 38C). Combined with TMZ, Talazoparib induced even more significant growth effects. In addition to the cooperative enhancement of TMZ efficacy in SG, Talazoparib showed pronounced synergy with TMZ in TRR and appeared to reverse TMZ resistance in TRR.

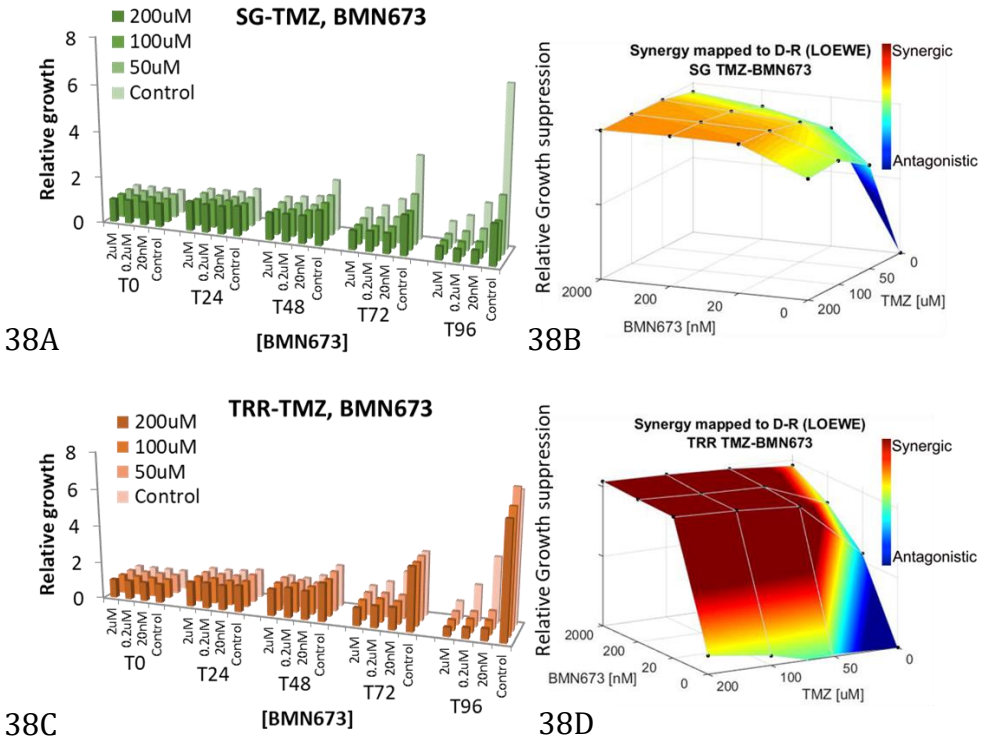

Figure 38. Relative growth of SG (A) and TRR (C) under combined treatment of TMZ and Talazoparib (BMN673). Relative growth suppression demonstrated via Combenefit analysis; synergism of TMZ with Talazoparib in SG (B) and TRR (D) was analyzed with Combenefit, and 3-D heat maps were plotted to demonstrate synergism (N=3, n=9), results showed that Talazoparib enhanced TMZ-induced death in both SG and TRR, where the degree of synergy is higher in TRR due to its resistant nature against TMZ.

6.4.3.2. DNA damage assays

Alkaline comet and γH2AX assays were used to investigate the combined effect of Talazoparib with TMZ to induce DNA damage in TRR. Cells were pretreated with Talazoparib for 30 mins prior application of TMZ. Both comet and γH2AX data agree; Talazoparib alone is genotoxic to these GBM cells. When co-treated with TMZ (20nM, 200nM and 2μM), Talazoparib further increased the accumulation of TMZ-induced

damage in SG (Figure 39A & B) while Talazoparib enhanced TMZ-induced DNA damage in TRR with significant synergy (Figure 39C & D).

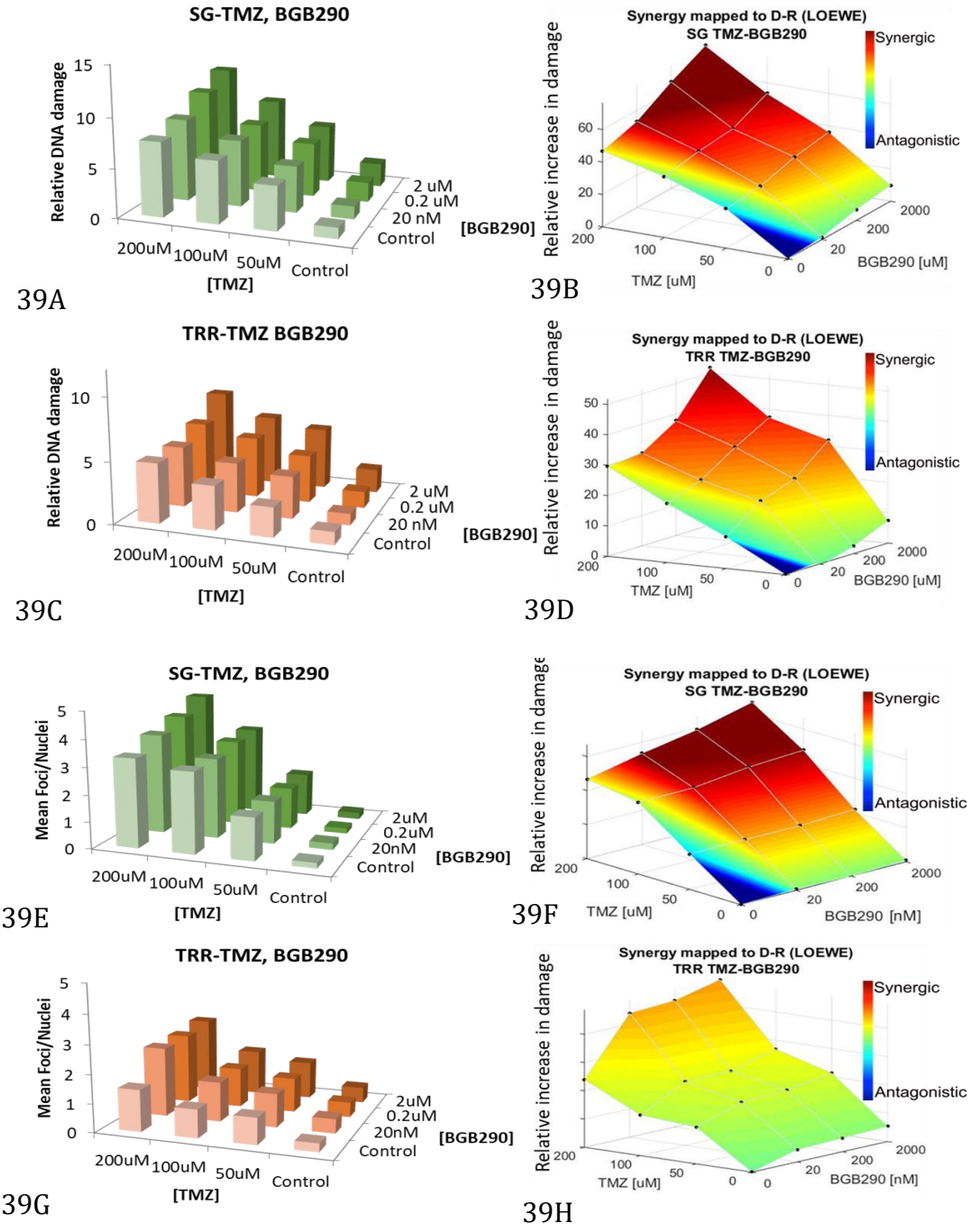

Figure 39. Comet analysis (N=3, n=9) pf SG (A) and TRR (C) following co-treatment with TMZ+Talazoparib. Relative increase in DNA damage in SG (B) and TRR (D) was demonstrated via Combenefit analysis to illustrate

cooperativity. DNA damage quantification of SG (E) and TRR (G) via γH2AX foci analysis (N=3, n=9) is represented in the 3-D bar graph, while cooperativity in SG (F) and TRR (H) where is shown via Combenefit analysis, Talazoparib synergistically enhanced TMZ induced DNA damage/lesion, where the synergic effects were stronger in SG in contrast to TRR.

6.4.3.3. Cell death assay

The Zombie death assay was performed to determine the cellular consequence of enhanced DNA damage arising from co-treatment of TMZ with Talazoparib . Cells were co-treated with TMZ & Talazoparib and the fraction of dead cells were measured at 72 hours post-treatment (Figure 40A & C), and the relative increase in cell death was measured and analyzed with Combenefit (Figure 40B & D).
Single agent treatment with Talazoparib demonstrated a dose-dependent increase in cell death. With co-treatment with TMZ, significant synergy with Talazoparib was identified in both SG (Figure 40B) and TRR (Figure 40D) with combined treatment nearly ablating SG cells. These data are consistent with growth and DNA damage assays. These data show that Talazoparib can reverse the TMZ-resistance observed in TRR and restore TMZ sensitivity in TRR to a similar extent as TMZ-treated SG (alone).

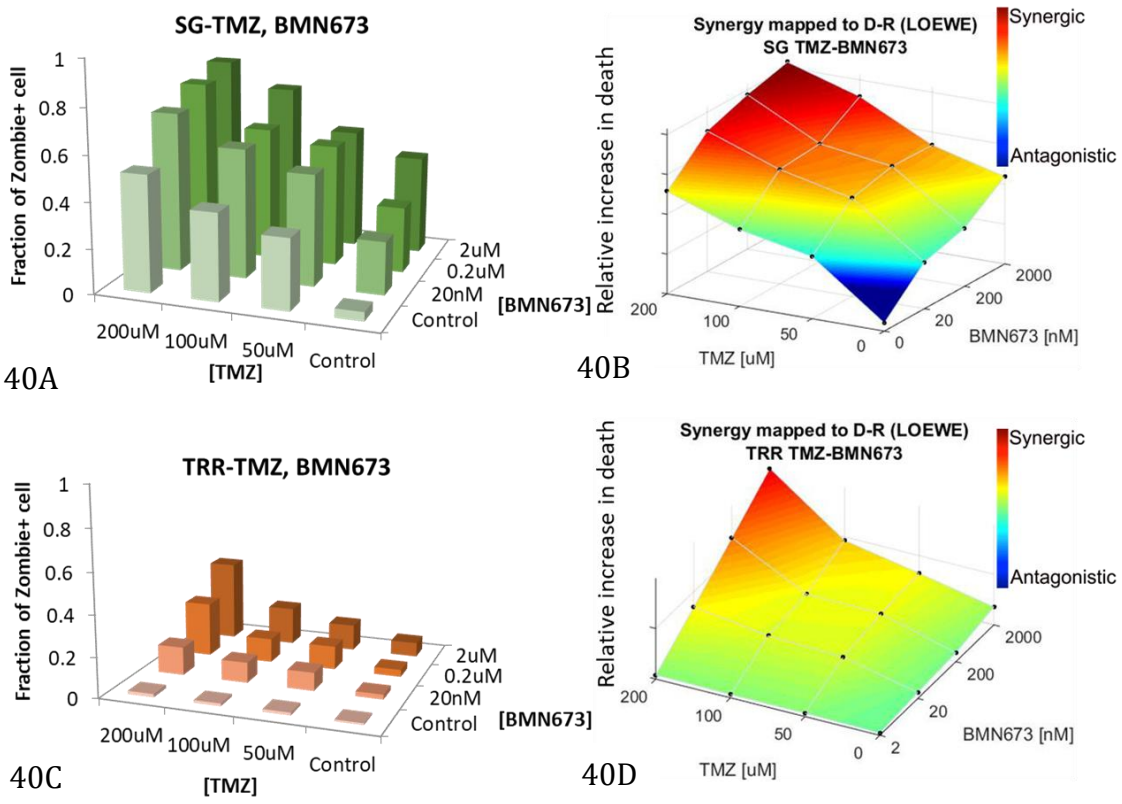

Figure 40. Fraction of dead cells (Zombie+) in SG (A) and TRR (C) following co-treatment with TMZ and Talazoparib. Relative increase in fraction of dead cell in SG (B) and TRR (D) were analyzed via Combenefit analysis and showed in 3-D heat map (N=3, n=9), Talazoparib synergizes with TMZ in SG to induce more cell death, whereas TRR was re-sensitized to TMZ with Talazoparib resulting in successful cell killing.

6.4.4. Pamiparib vs TMZ

6.4.4.1. Cell growth assay

Pamiparib is a derivative of Talazoparib, which the unique ability to pass-through the blood-brain barrier; potentially having significant impact in the clinical management of rGBM. The anti-rGBM properties of Pamiparib as a co-treatment with TMZ were investigated. Like Talazoparib, significant growth suppression was

observed in cells treated with Pamiparib alone. This was enhanced when cells were combined with TMZ, as Pamiparib enhanced growth suppression in both SG (Figure 41A & B) and TRR (Figure 41C & D). In TRR, co-treatment with Pamiparib significantly re-sensitized cells to TMZ, and synergistically reduced growth (figure 41D).

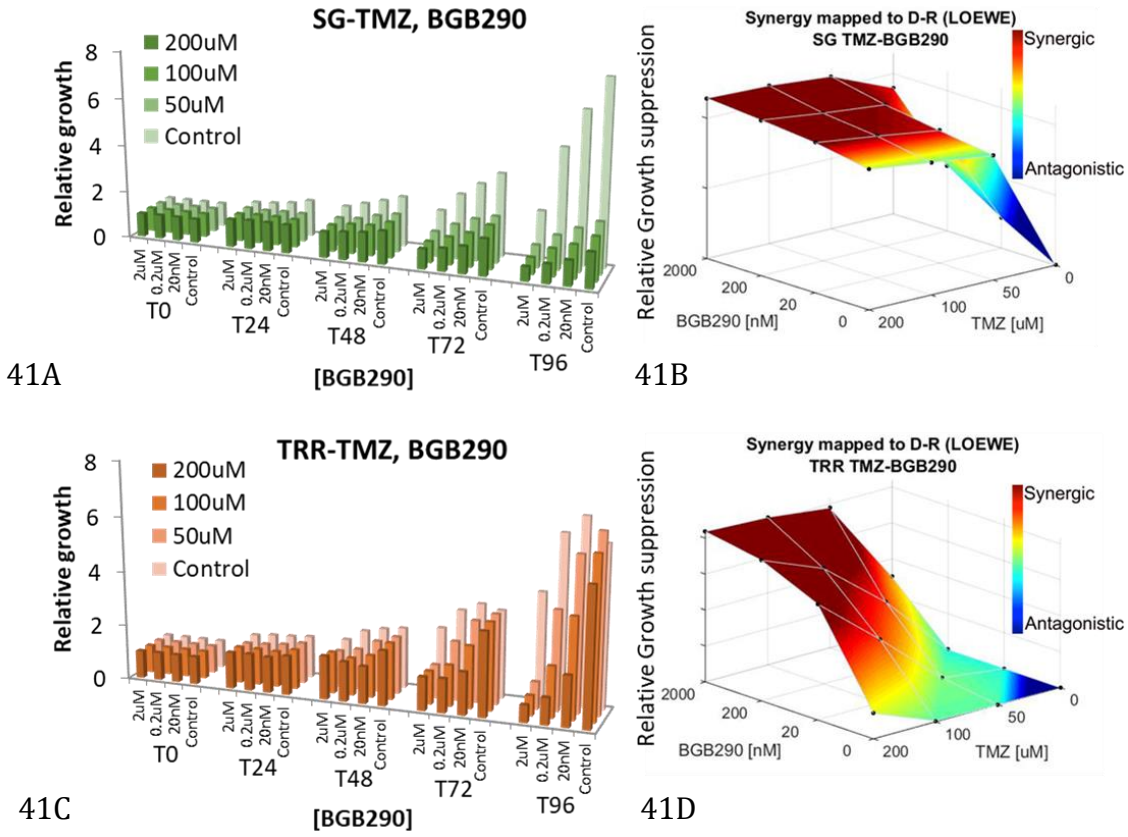

Figure 41. Relative growth of SG (A) and TRR (C) following co-treatment with TMZ and Pamiparib (BGB290) for 96 hours. Relative growth suppression of SG (B) and TRR (D) was analyzed via Combenefit analysis and represented in the 3-D heat maps to show synergy (N=3, n=9), Strong synergy were observed in SG and TRR, were synergic effects started at lower drug concentrations in SG than in TRR.

6.4.4.2. DNA damage assays

DNA damage analysis was used to evaluate DNA damage accumulation of TRR cells following co-treatment with Pamiparib and TMZ. Cells were pretreated with Pamiparib for 30 mins prior to co-application of TMZ. Pamiparib demonstrated similar characteristics as Talazoparib, inducing DNA damage by itself, and when co-applied with TMZ at any tested concentration (Figure 42). TMZ-induced DNA damage was further enhanced in the presence of Pamiparib in a dose dependent manner with significant synergy observed at [BGB290]>200nM in both SG and TRR.

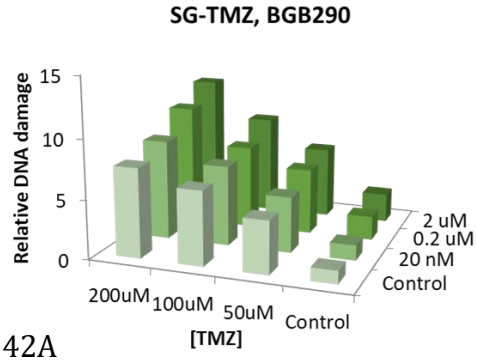

42A

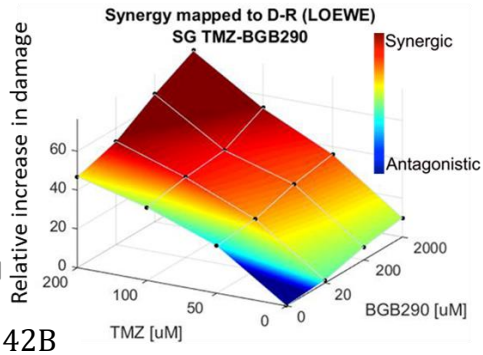

42B

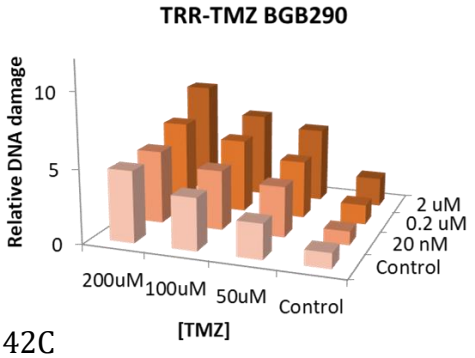

42C

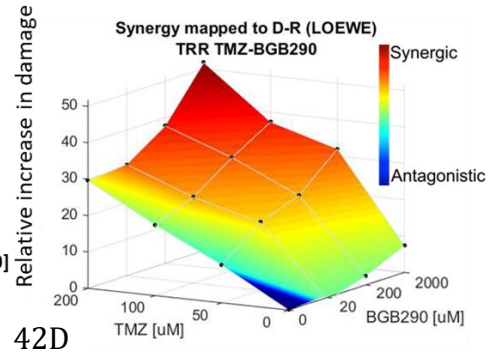

42D

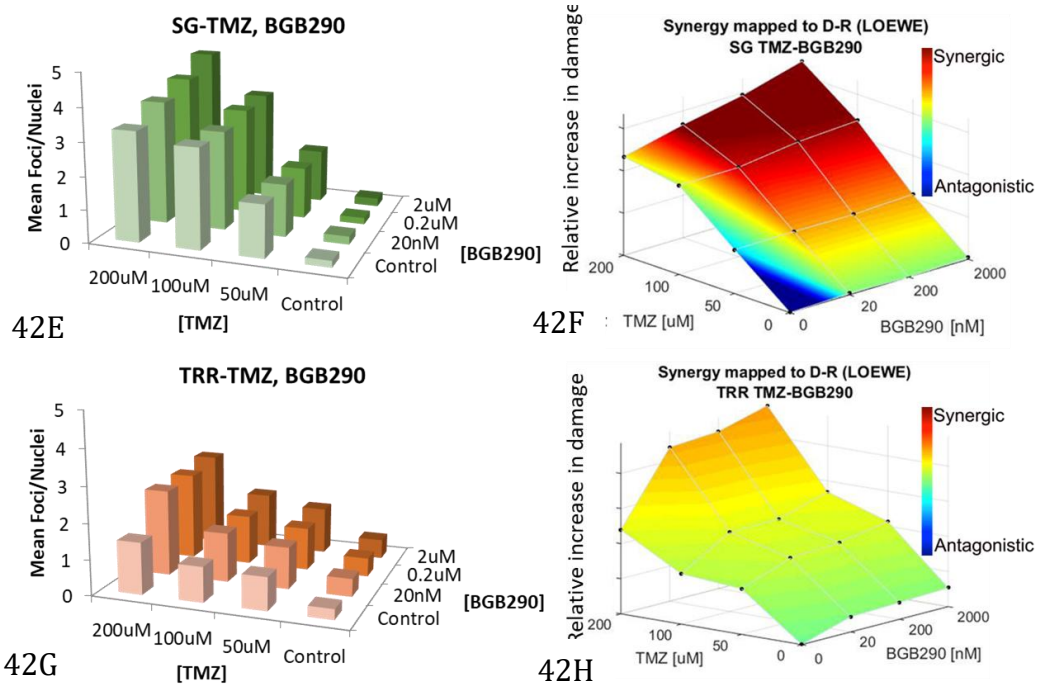

Figure 42. Comet analysis (N=3, n=9) of SG (A) and TRR (C) following co-treatment with TMZ+ Pamiparib. Relative increase in damage of SG (B) and TRR (D) were demonstrated via Combenefit analysis to quantify cellular cooperativity. DNA damage analysis of SG (E) and TRR (G) using γ-H2AX foci analysis (N=3, n=9) is represented in the 3-D bar graph, while cooperative in SG (F) and TRR (H) was measured via Combenefit analysis. Pamiparib synergistically enhanced DNA damage/lesion in SG and TRR. Although synergic effects were stronger in SG in contrast to TRR, synergistic cell death in TRR/rGBM is important considering the lack of TMZ (alone) sensitivity.

6.4.4.3. Cell death assay

The ability of Pamiparib to re-sensitize TRR, and ultimately rGBM, was tested using a death assay. Cells were treated with TMZ and Pamiparib for 72 hrs, and the fraction of dead cell in the population was recorded. Pamiparib, functioning as a potent PARPi with PARP trapping activity, successfully enhanced TMZ-induced cell

death in SG, while demonstrating TMZ re-sensitization in TRR when co-treated with TMZ in a synergistic manner.

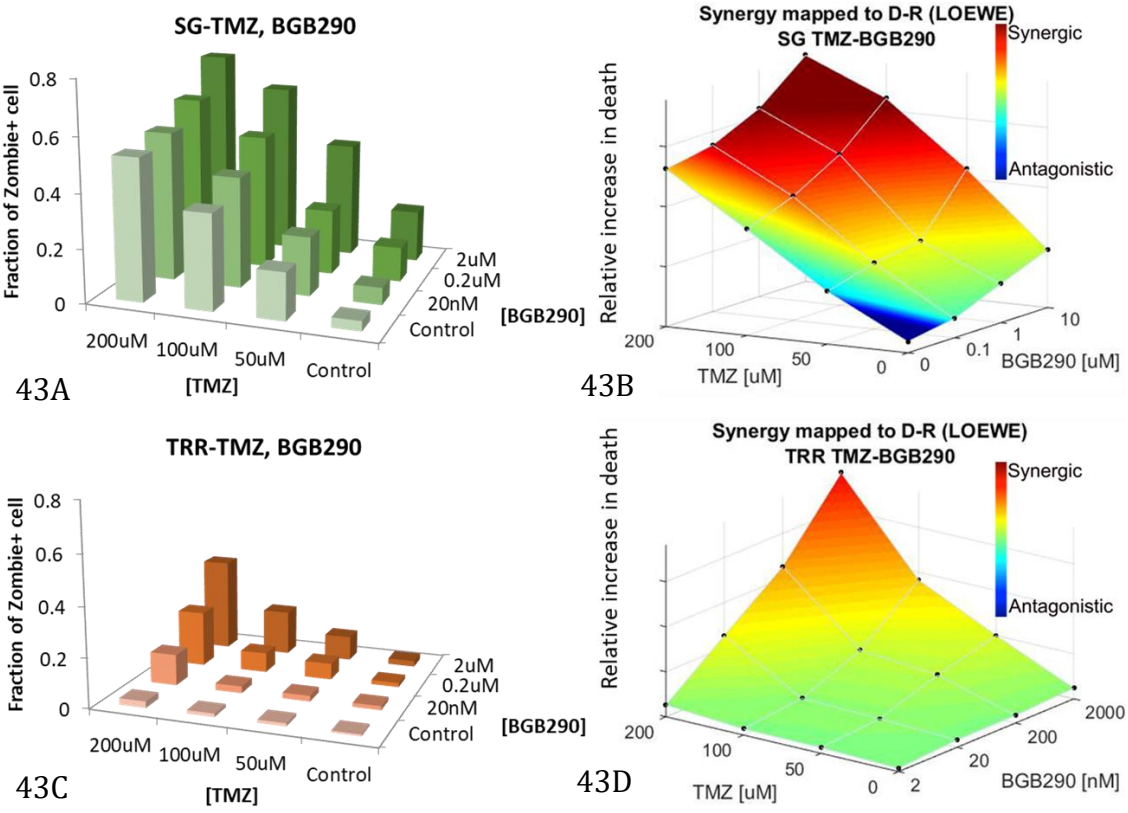

Figure 43. Fraction of dead cells (Zombie+) in SG (A) and TRR (C) following co-treatment with TMZ and Pamiparib. Relative increase in fraction of dead cells in SG (B) and TRR (D) were analyzed via Combenefit analysis and represented in a 3-D heat map (N=3, n=9), application of Pamiparib as co-treatment re-sensitized TRR, and incidents of TMZ-induced cell death increased with drug concentration.

6.4.5. Efficacy of PARPi/t to re-sensitize rGBM

To summarize the efficacy of PARP inhibitors /trappers to re-sensitize rGBM against TMZ, result of the growth assays of all 4 PARPi/t were integrated to conclude and compare the effect of inhibitors (Figure 44).

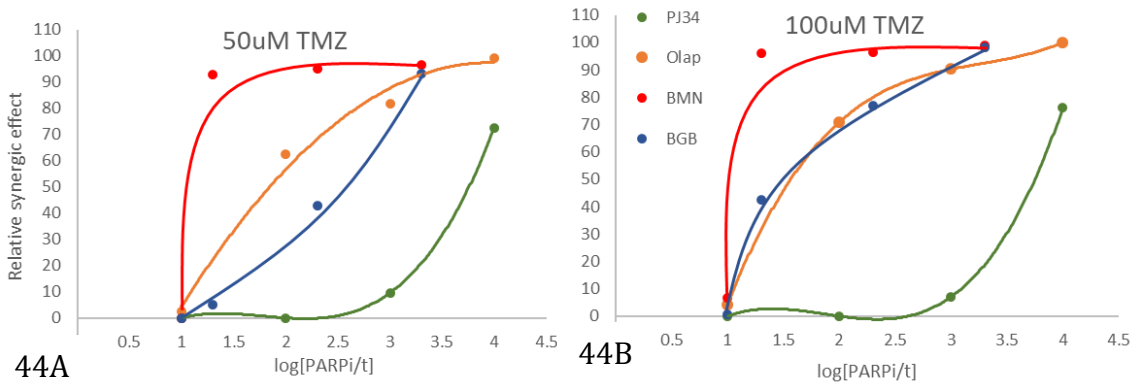

Figure 44. Relative re-sensitization of PARP inhibitors/trappers to TRR under 50μM (A) and 100μM (B) of TMZ. Relationship between relative synergic effect and logarithm of [PARPi/t] were showed, Talazoparib (BMN) showed the strongest re-sensitization effect, followed by, Olaparib (Olap), Pamiparib (BGB, blood-brain barrier penetrating), and PJ34 is the weakest among all inhibitors used in this experiment.

The above graph demonstrated the capability of each PARPi/t to induce re-sensitization effect to TRR toward TMZ, Talazoparib is the most potent, in terms of re-sensitization effect; Pamiparib and Olaparib also demonstrated effect of re-sensitization, while PJ34 only re-sensitize TRR under high concentration.

6.5. Potential role of XRCC1 in cell migration

TRR was shown to be more mobile in terms of cell migration in previous validation experiments, to investigate the potential role of XRCC1 mediating cancer migration, experiments were performed to study the effect of XRCC1 knock-down and PARP trapper to cell migration in TRR. SG, TRR (shSCM), TRR(XRCC1) and TRR(shSCM) treated with 2μM of Pamiparib were seeded into migration plate with empty central zone, and experiment were perform with/without the present of 200μM of TMZ.

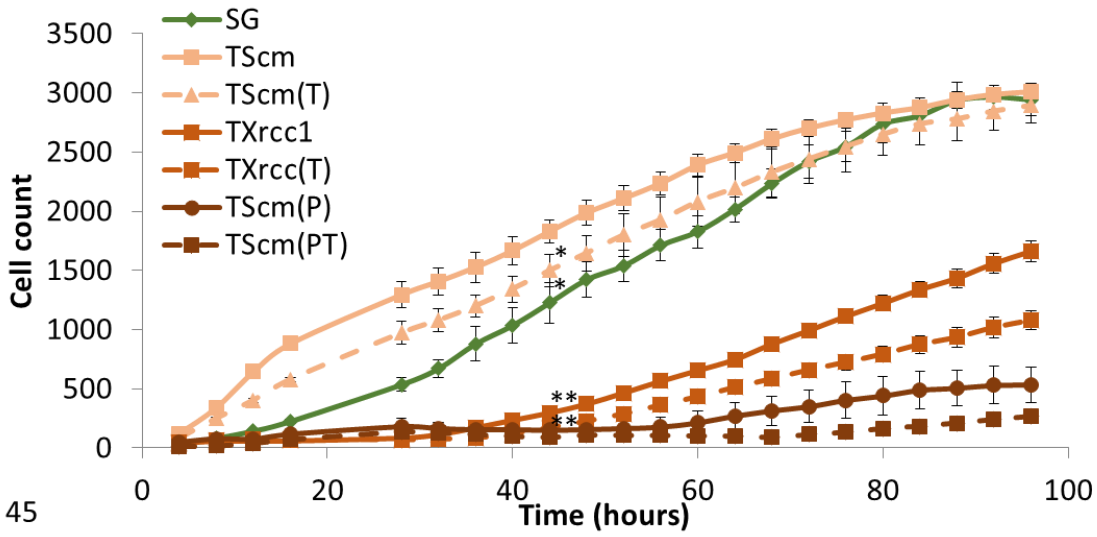

Figure 45. Quantification of the number of migrating fluorescent GBM cells; migration into the central cell-free zone. Kinetic quantification of cell migration of SG, TRR, TRR-shSCM (TScm), TRR-shXRCC1 (TXRCC1) with/without Pamiparib (P) and TMZ (T) at different timepoints. In all cases, TRR cells, without Pamiparib/shXrcc1, showed enhanced migration which was superseded by PARPt /i treatment or application of shXRCC1. Statistical analysis was performed with the 48-hours timepoint. (*= p<0.05, **=p<0.01, Post hoc. T-test with Bonferroni's correction after two-way ANOVA.)

Results suggested that there were correlation between XRCC1 and cell migration in TRR. XRCC1 knock-down in TRR significantly reduced the number of cells migrated into the central zone, application of TMZ further reduce the migration. Application of Pamiparib in TRR (shSCM) also showed reduction of migration, where application of TMZ enhanced the reduction at 48 hours.

6.6. Transformation of SG/TRR to 3-D cultures and validations

To determine the applicability of the newly-derived 2-D SG/TRR model to the 3-D setting, SG/TRR lines were cultured in ultra-low attachment plates which resulted in 3-D spheroids formation. TMZ-Pamiparib treatments were applied to these 3-D SG/TRR spheroids and Western analyses was performed to characterize these 3-D fluorescent cell lines.

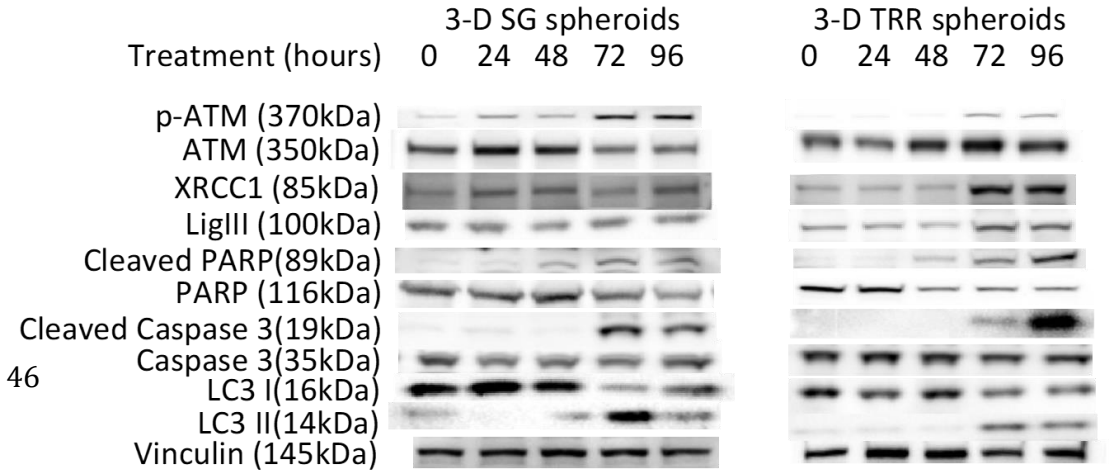

46

Figure 46. Preliminary Western blot results of 3-D SG/TRR showing expression level of ATM, p-ATM, XRCC1, LigIII, Cleaved/whole PARP, Cleaved/whole Caspase 3, and LC3 I/II. 3-D spheorids were treated with 200μM TMZ and 2μM of Pamiparib for 0, 24, 48, 72, 96 hours. These data show intact DNA damage repair responses (p-ATM), cell death events (PARP and Caspase), and autophagy (LC3 II). Similar to the 2-D TRR response, XRCC1/LigIII expression was also stimulated at 72 hours.

Results showed that there was activation of ATM through phosphorylation in both SG (throughout 96 hours of treatment) and TRR (At 72 and 96 hours), which indicates severe DNA damage. There was a trend of XRCC1/LigIII upregulation in

TRR after 72 hours, which agrees with the results seen in 2-D TRR. Cleavage of PARP and Caspase 3 indicated cell death events occurred in both 3-D SG and TRR under TMZ/Pamiparib after 72 hours of treatment, and the expression of LC3II suggested initiation of autophagic activities.

6.7. Preliminary studies on patient derived tumorsphere model

To determine the applicability of the TRR-based findings in a clinical cell model, I extended my analysis to 3-D BTIC cells that originated from a treatment naïve GBM patient (BTIC 241, 972) and a GBM patient following TMZ+IR treatment who underwent re-surgery to remove the recurring tumour (BTIC 935). Expression of XRCC1 was found to be higher in post-treatment patient cells (Figure 47), which agrees with the observations in the 2-D and 3-D SG/TRR models developed in the lab. More importantly, cleavage of PARP and Caspase 3 indicated that combination treatment of 200μM TMZ and 2μM of Pamiparib was able to initiate cell death events, which agrees with the results seen in 2-D and 3-D SG/TRR model. This preliminary analysis using relevant clinical samples recapitulates my U251 cell-based data; thus, providing initial biochemical validation of my new model system, particularly with regards to molecular events that follow TMZ treatment in patient cells.

Figure 47. Expression level of XRCC1, LigIII, Cleaved/whole PARP and Cleaved/whole Caspase 3 in BTIC tumorspheres. BTIC tumorspheoroids were treated with 200µM TMZ and 2µM of Pamiparib for 0, ,24, 48, 72, 96 hours. The expression level in drug naïve cells (BTIC 935) and post-treatment cells (BTIC 241, 972) were showed. Expression levels of XRCC1 were higher in post-treatment BTIC models (BTIC 241 and 972), where combination treatment of TMZ-Pamiparib induced cell death signaling pathways (PARP and Caspase cleavage) in all BTIC models.

7. Discussion

7.1. Development and characterization of a tractable TMZ-resistant model of GBM

In this research project, the drug-sensitive U251 GBM cell line underwent continuous TMZ treatment to mimic sustained chemotherapy. Isolation and expansion of drug-resistant outgrowing cells led to successful development of an *in vitro* 2-D model modeling resistant GBM (rGBM). The goal of this project was to develop and characterize a bona fide 2-D cell model with which to perform high-content screening and identify novel anti-rGBM therapeutics [165,166]. U251 cells were transfected with a red and green nuclear fluorescent reporter. The red fluorescent line underwent sustained treatment with TMZ for 3 weeks to select outgrowing

TMZ-resistant clones, whereas the mock-treated green nuclear fluorescent line represented the drug-naïve/sensitive line. By utilizing a two-colour fluorescent reporter system, this novel cell-based screening system is amenable to highly accurate, trackable kinetic analyses for screening, hit-validation and characterization.

Resistance toward the only standard-of-care approved chemotherapeutic, Temozolomide (TMZ), was validated via a multitude of assays while also identifying novel gene targets for future analysis. Through the high throughput image-based assays developed in the lab, the resistant TRR (TMZ resistant red fluorescent line) showed similar characteristics to treatment-resistant 3-D BTIC, which have been previously been demonstrated to display higher tolerance against growth suppression [167,168], DNA damage [169–171], and cell death [172,173] induced by TMZ.

One of the most commonly studied mechanism of resistance is the epigenetic regulation of MGMT [29,45,113]. Thus, in my study, the RNA and protein expression of MGMT, and its' contribution toward TMZ resistance in my newly developed cell model was investigated. My data suggested that RNA expression of MGMT was not notably affected following TMZ resistance (baseline TRR vs SG); however, TMZ treatment of the TRR line resulted in MGMT protein expression levels increasing significantly. In terms of functionality, a 50% knock-down of MGMT expression was did not affect TMZ resistance, suggesting that either gene dosing effects may be at play or that MGMT is not a major factor for TMZ resistance in this cell model. However, an important finding from this data is the expressional modification of MGMT in response to TMZ. While I did not analyze MGMT promoter methylation or

upstream epigenetic changes in my TRR line following acute TMZ treatment, clinical characterization of MGMT promoter methylation often occurs months following initial TMZ treatment following resection of the primary brain tumour and concomitant recurrence (often following re-surgery or post-mortem rGBM analysis) [113,115,174]. My data suggests that MGMT epigenetic changes may be much more plastic than previously thought and that MGMT-mediated resistance may occur very early on in the treatment course thus directly impacting the immediate emergence of outgrowing resistance clones that drive formation of rGBM[45,54,79].

Modulation of DNA damage repair activity and mechanisms are frequently reported in resistant GBM [78,79,82,90,96]. The molecular regulation of DNA single-stranded and double-stranded break repair pathway genes were investigated via Clariom D microarray-based transcriptomic analysis. My findings reiterated yet further defined the DNA damage repair pathways that are markedly regulated in TRR, including both DNA double-stranded break repair and single-stranded break repair. Comparative Clariom D screens on SG & TRR suggested that a numerous of DNA double-stranded break repair (DSBR) signaling gene were regulated, including Mre11, Rad51, DNA-PK (PRKDC), BRCA1 and 2. Subsequent investigation of DSBR protein expression and signaling showed that ATM and TIF1β phosphorylation were modified in TRR. ATM is activated via phosphorylation at the S1981 site and is responsible for initiation of DSBR [96,108]. With discernable DNA damage induced by TMZ, ATM phosphorylation was suppressed in TRR, suggesting alterations in mechanisms underlying ATM phosphorylation (ie. Mre11, Rad51) may contribute to this resistant model. However, TIF1β (Kap1) was shown to be perpetually activated

in TRR. TIF1β, is a central downstream signaling/effector protein of the ATM signaling pathway [175,176], which is responsible for signaling and activation of DNA repair. Therefore, my findings suggest that the downstream effector pathway of ATM phosphorylation remains active, bypassing the apparent ATM suppression, resulting in a hyperactive DNA DSBR response. Previous work has identified additional proteins that can facilitate Kap1 phosphorylation, such as CCAR2/DBE1 and MAGE-C2[175,176]. Enhanced signaling or protein-interactions between TIF1β and these proteins might be responsible for mediating enhanced TIF1β phosphorylation (p-TIF1β) seen in TRR.

Remarkably, the modification in base-excision repair was implicated in this study. The expression level of BER associated proteins, including Ape1, PARP1, XRCC1, and Ligase III, were all potentially to be transcriptionally and/or translationally-upregulated. In addition to heightened baseline levels of these BER proteins, XRCC1/Ligase III expression were found to be further enhanced following 72 hours of TMZ treatment in TRR; providing a possible mechanism of cell death resistance observed in TRR compared to SG.

7.2. Role of base-excision repair in rGBM development and progression

Base-excision repair is a common and highly active innate single-stranded break repair mechanism, responsible for the removal of endogenous and exogenous DNA damage [162]. A number of studies have linked BER deficiency to carcinogenesis, as malfunctioning DNA repair activity is responsible for the accumulation of DNA

damage-induced mutations, genomic instability [177]. In addition, defective BER is also causative in cancer progression, metastasis and therapeutic resistance [178].

To characterize the role of XRCC1-mediated BER and its potential hyperactivity in rGBM, I performed a multitude of studies comparing SG and TRR. XRCC1/LigIII (X1/L3) expression was enhanced in TRR with TMZ, followed by DNA damage analysis. Subsequent XRCC1 overexpression and concomitant DNA repair analysis confirmed that TMZ-mediated X1/L3-induction was indeed responsible for enhanced DNA repair activity and promoting resistance toward alkylating agent-induced DNA damage. Furthermore, I found that TMZ-mediated X1/L3 induction also mediates resistance to other DNA damage break-types (ie. Topoisomerase and oxidative); thus, providing additional molecular insight as to the lack of success of second-line therapeutics used to treat rGBM [71]. As an alternative approach, XRCC1 was knocked down using an RNA interference technique. Similarly, my data showed that a reduction of XRCC1 levels reduced cell growth and DNA repair activity resulting in enhanced cell death. Together, these two experiments again, showing that XRCC1 plays a critical role in DNA damage resistance and repair, which contribute greatly in TMZ resistance [117,163]. Furthermore, it points to XRCC1/BER as a potential therapeutic target to counteract rGBM.

7.3. Re-sensitization of TRR via inhibition of PARP-dependent BER pathway

In light of the importance of XRCC1-mediated BER in rGBM, BER has previously been shown to be an important therapeutic target in multiple cancer types[161]. XRCC1 is a scaffolding protein, lacking enzymatic activity itself per se, and multimerizes a large multi-protein repair complex to the breaksite. Therefore, I

looked to its upstream activator, PARP, whereby a number of clinically-relevant inhibitors have already been develop for use to inhibit BER. Most PARP inhibitors are typically used to generate synergistic lethality in cancers that have DNA repair defects [128]. However, in my study, I used PARP inhibitors as a way to reduce XRCC1-mediated BER hyperactivity as clinically-relevant therapeutic co-treatment to re-sensitize rGBM to TMZ. A multitude of assays including growth rate analysis, DNA damage repair and cell death analysis of SG/TRR under different combinations of TMZ and PARPi/PARPt were undertaken. My data showed that PARPi/PARPt, as a co-treatment with TMZ, did parallel the XRCC1 knockdown experiments indicating this agent as a viable co-operative treatment with TMZ and enhance its efficacy against TRR/rGBM.

Generally, most PARP inhibitors have varying PARPi/PAPRt activity ; however, I found that those agents with higher PARPt activities were more potent than PARPi, in suppressing TRR cell growth, enhancing TMZ-mediated damage and induction of cell death. PARP trappers, such as Talazoparib [138,164] and Pamiparib [136], can stabilize PARP-DNA complexes, thus inducing lethal DNA lesions when they collide with replication machinery during DNA replication [139,141,179]. These arrest the cell cycle and ensuing unrepaired DNA DSBs induce cell death. Talazoparib and Pamiparib demonstrated strong synergistic activity with TMZ due to effective inhibition of XRCC1-mediated BER. In contrast, PJ34, an inhibitor for PARP with low PARP trapping activity [180,181], showed only additive effects at higher drug concentrations when co-treated with TMZ. Olaparib, a PARPi shown with some trapping activity

[179,182], showed stronger additive-synergic effects relative to PJ34, but less than that of Talazoparib and Pamiparib.

In the context of GBM, a brain tumour with protection by the blood-brain barrier which can restrict drug entry into CNS tissue, identifying an agent with capability to penetrate this selective membrane is essential. In this light, our findings with Pamiparib are promising using my rGBM model. While Pamiparib is currently undergoing clinical trials in a variety of tumours, including GBM [136], further mechanistic analysis to validate the therapeutic value of Pamiparib to rGBM should be undertaken.

7.4. XRCC1 as a potential biomarker

In addition to having diagnostic risk factor value for cancer development[177], my data and other recent studies show that changes in XRCC1-mediated BER may underpin the development and progression of GBM, opening the door for its potential use as biomarker, particularly for onset of rGBM [183]. Baseline expression changes in XRCC1 were observed in the TRR/rGBM model developed in this study, supporting the use of XRCC1 as a progression marker in TMZ-resistant GBM. Further clinical evidence to support this sub-hypothesis was my finding that XRCC1 expression was higher in the treatment-resistant patient-driven 3-D GBM BTIC line compared to similarly-derived drug-naïve BTICs; in agreement with my 2-D culture model data (TRR vs SG).

8. Future directions

8.1. Investigating the mechanism of cross-resistance towards secondary therapeutics

This project has identified that one of the mechanisms of TMZ resistance in GBM is an enhancement in DNA single-stranded break repair, which resolves TMZ-induced damage, thus allowing cancer cell survival. However, following resistance, other DNA damaging agents, such as Topoisomerase poisons, are often used as a second-line therapeutic to counteract rGBM, with little success [72,73]. Similarly, I find that TRR can resist Topoisomerase and oxidative DNA damage, indicative of acquired cross-resistance to other DNA damaging agents. As replicative stress can convert single-stranded breaks (ie. from TMZ) into double-stranded breaks, the lack of apparent toxicity suggests that rGBM cells have acquired enhanced DNA DSBR activity, which may or may not be XRCC1-dependent. The TRR model now enables a unique way to study this cross-resistance mechanism. Despite TRR having not undergone prior exposure to other DNA damaging agents (e.g. Etoposide), cross-resistance prevails. To improve therapeutic outcome of GBM patients, the cross-resistance of rGBM to other anti-GBM agents should be studied using the new model system to determine mechanistic insight of cross-resistance.

8.2. Intratumoral heterogeneity

Intratumoral heterogeneity (ITH) is increasingly becoming recognized as an important factor complicating anti-GBM strategy [53,54,184], One of the limitations in my current rGBM model system is that, the mechanisms of resistance in the TRR cell

line originated from a clonal expansion from a population that survives TMZ selection. Theoretically, the genetic considerations of the resistance line are common in TRR, as the contribution of intratumorally heterogeneity might be under-estimated in this study. As mentioned in section 3.3., Multiple clones were harvested and stored, although only one clone was fully analyzed, the analysis of additional clones may be useful. Clariom D analysis will provide the molecular snapshot of expression with which to compare all clones while select key experiments can be repeated in using these additional clones to determine if ITH amongst these clones varies the results. One important future study is to evaluate the therapeutic efficacy of TMZ-Pamiparib with these additional clones, to further understand the therapeutic value of PARPi/PARPt as co-treatment during ITH.

8.3. Translation to patient-driven models and other clinical models

To investigate the potential of using PARP inhibitors (PARPt) in GBM treatment, a combination therapy approach to evaluate the effect of TMZ-Pamiparib will be tested in an expanded set of GBM patient-derived 3-D BTICs. Particularly interesting is our access to patient-matched BTICs wherein cells are derived from individual GBM patients who have undergone surgery to remove both the primary and subsequent resistant tumour (following re-surgery). My preliminary experiments with the sensitive (treatment naïve) and resistant (post-treatment) patient derived BTIC models confirms an increase in XRCC1 expression with resistance, supporting my assertion that BER activity is likely enhanced in the patient-derived rGBM BTIC model. Therefore, as a follow-up, Pamiparib co-treatment with TMZ should be

studied to determine the potential to re-sensitize post-treatment BTIC cells toward chemotherapy. Furthermore, Pamiparib could also be co-treated with second line therapies (ie. Topoisomerase inhibitors and other alkylators) to determine whether PARP inhibition can overcome cross-resistance. These data will require follow-up in pre-clinical models, such as mouse xenograft models typically used to characterize BTICs *in vivo*. This model should be used to further validate the outcome of TMZ-Pamiparib combined treatment, and its ability to improve anti-rGBM treatments.

8.4. High-content screening of SG vs TRR

The ultimate goal of establishing my fluorescent rGBM cell line was to establish a model with which to perform drug-screening to identify novel agents to counteract rGBM. While my efforts to validate this system through molecular analysis unexpectedly led to novel actionable biological findings (XRCC1) and subsequently illuminated a drug target (Pamiparib), this model is now ready for realizing that goal. A "low-hanging fruit" approach is to screen compounds within the FDA-approved drug library for anti-rGBM capability. The advantage of this approach is the fact that FDA-approved compounds already have known pharmacological and clinical data with which any findings can be immediately applied to a rGBM patient setting with little to no administrative/regulatory delays via off-label and compassionate use grounds. Furthermore, patient-matched BTICs can be used for either hit validation or undergo personalized medicine screening using this library in order to identify compounds that can act on each individual's rGBM. Furthermore, the motile nature of my TRR cells relative to SG can also be used to screen agents

that may negate or suppress this motility. High-content screening that integrates scratch assays is especially amenable to our analysis methods. Through cell masking and tracking, controlled "scratches" in each well of the 96-well plate could be monitored and FDA-approved drugs that reduce migration into the scratch could represent novel agents that reduce the invasive properties of rGBM cells. 3-D patient BTICs could be used to validate these findings. Finally, my lab has some success in transforming the U251-based 2-D SG and TRR cells into 3-D tumorspheres by varying the media, plastic-ware and trophic factors to grow these cells. The generation of a fluorescent 3-D model version of primary and resistant GBM would be major breakthrough in screening for clinically-relevant agents and for validation studies. Co-culture of SG and TRR would allow for a plethora of clinically-relevant readouts that inform growth, migration, invasion and cell killing properties of rGBM that would also be amenable to drug-screening.

9. Significance of study

This project delivers a novel, tractable 2-D cell model with distinguishable TMZ sensitive and resistant lines; resistance against TMZ was validated and characterized. The majority of previous rGBM studies, while utilizing clinical samples derived from patients with GBM recurrence [42,52,54], lack mechanistic insight as to treatment resistance nor are the amenable for drug screening and development studies. My validation data supported by preliminary clinically-relevant BTIC data, provides for newfound capability for this cell screening model to

monitor acute changes resulting from TMZ treatment in a kinetic, sensitive, reproducible manner. TMZ-induced increase expression of MGMT following 96 hours treatment, and the stimulated enhancement of XRCC1 expression following 72 hour treatment were good example of short-term induced responses, that are not observable in GBM patients until well into the onset of rGBM. Furthermore, these data reveal the plasticity of these signaling systems and point to their induction early into the treatment regimen and their potential importance in mediating outgrowth of resistant clones.

The critical role of XRCC1-mediated base-excision repair is especially compelling in mediation of TMZ resistance and was further investigated. My findings suggest that XRCC1 can respond to acute TMZ-induced damage and significantly contributes to enhanced DNA damage tolerance and single-stranded break repair activity in rGBM, a finding that is remains underappreciated in the GBM research field. Consequently, this finding reveals PARP inhibitors as a potential therapeutic to counteract rGBM, an agent already in clinical use in a variety of other malignancies. My data compares a variety of PARP inhibitor types, generally, application of PARPi synergistically enhanced TMZ efficacies, where effects were usually stronger in SG, but a co-treatment of TMZ and PARPi/t re-sensitize the resistant TRR model toward TMZ, and showed reduction in growth, improvements in DNA damage/lesion induction, and enhanced cell-killing effects, which ultimately could promote therapeutic outcomes of patients against rGBM. My data also identifies those with PARP-trapping ability as being particularly effective, specifically Pamiparib, which can cross the BBB, being especially topical. Furthermore, for the first time, I also link

enhanced XRCC1/BER-mediated damage with cell motility, suggesting that the highly invasive nature of rGBM is intrinsically linked to enhanced DNA damage repair capacity.

In the greater schema, my project highlights the potential of XRCC1 as a biomarker for tumour progression and novel treatment target. Furthermore, through a variety of validation experiments and comparative analysis with patient-derived lines, this new tractable cell-based model represents an ideal system with which to screen and identify novel anti-rGBM agents.

A central goal for chemotherapy is the induction of DNA damage. Although many cellular mechanisms exist to counteract therapy (ie. transporter changes, tumour microenvironment, vascularization, hypoxia, etc…), I find that rGBM achieves its resistance is via changes in the DNA damage repair profile of the tumour. It is estimated that over 90% of tumours incur mutations on 1 or more DNA damage repair genes; therefore, alternations in DNA repair, especially in the context of onset of resistance is common. The findings of this study may serve as a model for other disease sites, including other CNS and non-CNS tumour types. A similar approach may be undertaken to identify other DNA repair modifiers that may mediate resistance and a pathway analysis that illuminates known small molecule inhibitors/activators can be used to modulate the target DNA repair activity in order to achieve effective drug re-sensitization.

10. References

1. Reifenberger, G., Blümcke, I., Pietsch, T. &Paulus, W. Pathology and Classification of Tumors of the Nervous System. in *Oncology of CNS Tumors* 3–75 (Springer Berlin Heidelberg, 2010). doi:10.1007/978-3-642-02874-8_1
2. Louis, D. N. *et al.* The 2016 World Health Organization Classification of Tumors of the Central Nervous System: a summary. *Acta Neuropathologica* **131**, 803–820 (2016).
3. Sild, M. &Ruthazer, E. S. Radial glia: Progenitor, pathway, and partner. *Neuroscientist* **17**, 288–302 (2011).
4. Schwartzbaum, J. A., Fisher, J. L., Aldape, K. D. &Wrensch, M. Epidemiology and molecular pathology of glioma. *Nature Clinical Practice Neurology* **2**, 494–503 (2006).
5. Komori, T. Pathology and Genetics of Diffuse Gliomas in Adults. *Neurol. Med. Chir. (Tokyo).* **55**, 28–37 (2014).
6. Robles Irizarry, L., Hambardzumyan, D., Nakano, I., Gladson, C. L. &Ahluwalia, M. S. Therapeutic targeting of VEGF in the treatment of glioblastoma. *Expert Opin. Ther. Targets* **16**, 973–984 (2012).
7. Prayson, R. A. Histologic Classification of High-Grade Gliomas. in *High-Grade Gliomas* 3–35 (2007). doi:10.1007/978-1-59745-185-7_1
8. Furnari, F. B. *et al.* Malignant astrocytic glioma: Genetics, biology, and paths to treatment. *Genes and Development* **21**, 2683–2710 (2007).
9. Liberski, P. P. &Kordek, R. Ultrastructural pathology of glial brain tumors revisited: A review. *Ultrastructural Pathology* **21**, 1–31 (1997).
10. Rock, K. *et al.* A clinical review of treatment outcomes in glioblastoma multiforme - The validation in a non-trial population of the results of a randomised Phase III clinical trial: Has a more radical approach improved survival? *Br. J. Radiol.* **85**, 729–733 (2012).
11. Bougnaud, S. *et al.* Molecular crosstalk between tumour and brain parenchyma instructs histopathological features in glioblastoma. *Oncotarget* **7**, 31955–31971 (2016).
12. Chaichana, K. L. *et al.* The efficacy of carmustine wafers for older patients with glioblastoma multiforme: prolonging survival. *Neurol. Res.* **33**, 759–764 (2011).
13. Walker, E.V *et al.* Malignant primary brain and other central nervous system tumors diagnosed in Canada from 2009 to 2013. *Neuro. Oncol.* **21**, 360–369 (2019).
14. Urhie, O. *et al.* Glioblastoma Survival Outcomes at a Tertiary Hospital in Appalachia: Factors Impacting the Survival of Patients Following Implementation of the Stupp Protocol. *World Neurosurg.* **115**, e59–e66 (2018).

15. Chandra, A. *et al.* Insurance type impacts the economic burden and survival of patients with newly diagnosed glioblastoma. *J. Neurosurg.* 1–11 (2019). doi:10.3171/2019.3.jns182629
16. Kimmell, K., Sanchez, D. &Marko, N. Cost effectiveness analysis of Glioblastoma multiforme therapeuties. *Neuro. Oncol.* **16**, v181–v181 (2014).
17. Thakkar, J. P. *et al.* Epidemiologic and molecular prognostic review of glioblastoma. *Cancer Epidemiology Biomarkers and Prevention* **23**, 1985–1996 (2014).
18. Hodges, L. C., Smith, J. L., Garret, A. &Tate, S. Prevalence of glioblastoma multiforme in subjects with prior therapeutic radiation. *J. Neurosci. Nurs.* **24**, 79–83 (1992).
19. Ostrom, Q. T. *et al.* CBTRUS statistical report: Primary brain and central nervous system tumors diagnosed in the United States in 2007–2011. *Neuro. Oncol.* **16**, iv1–iv63 (2014).
20. Brennan, C. W. *et al.* The somatic genomic landscape of glioblastoma. *Cell* **155**, 462 (2013).
21. Sonoda, Y., Shibahara, I., Saito, R., Kumabe, T. &Tominaga, T. The Role of IDH1 and IDH2 Mutations in Malignant Gliomas. in *Tumors of the Central Nervous System, Volume 2* **2**, 47–52 (Springer Netherlands, 2011).
22. Y. P. Lam, E. di Tomaso, H.-K. Ng, P. Expression of p19 INK4d, CDK4, CDK6 in glioblastoma multiforme. *Br. J. Neurosurg.* **14**, 28–32 (2002).
23. Zhang, W. *et al.* Whole-genome microRNA expression profiling identifies a 5-microRNA signature as a prognostic biomarker in Chinese patients with primary glioblastoma multiforme. *Cancer* **119**, 814–824 (2013).
24. Shibahara, I. *et al.* New insights into glioma classification based on isocitrate dehydrogenase 1 and 2 gene status. in *Brain Tumor Pathology* **28**, 203–208 (2011).
25. Liu, X. &Ling, Z. Q. Role of isocitrate dehydrogenase 1/2 (IDH 1/2) gene mutations in human tumors. *Histology and Histopathology* **30**, 1155–1160 (2015).
26. Dang, L., Jin, S. &Su, S. M. IDH mutations in glioma and acute myeloid leukemia. *Trends in Molecular Medicine* **16**, 387–397 (2010).
27. Holland, E. C. Glioblastoma multiforme: The terminator. *Proc. Natl. Acad. Sci.* **97**, 6242–6244 (2000).
28. Grahovac, G., Tomac, D., Lambasa, S., Zoric, A. &Habek, M. Cerebellar glioblastomas: Pathophysiology, clinical presentation and management. *Acta Neurochirurgica* **151**, 653–657 (2009).
29. Ramalho-Carvalho, J. *et al.* Altered Expression of MGMT in High-Grade Gliomas Results from the Combined Effect of Epigenetic and Genetic Aberrations. *PLoS One* **8**, (2013).
30. Goplen, D. *et al.* αB-crystallin is elevated in highly infiltrative apoptosis-resistant glioblastoma cells. *Am. J. Pathol.* **177**, 1618–1628 (2010).
31. Hajri, R., Dunet, V. &O.Prior, J. Glioblastoma Multiforme Recurrence. *Radiology* **280**, 326–327 (2016).

32. Sharma, V. *et al.* Toroidal-spiral particles for codelivery of anti-VEGFR-2 antibody and irinotecan: A potential implant to hinder recurrence of glioblastoma multiforme. *Biomacromolecules* **15**, 756–762 (2014).
33. Chamberlain, M. C. Radiographic patterns of relapse in glioblastoma. *J. Neurooncol.* **101**, 319–323 (2011).
34. Gao, Q., Lei, T. &Ye, F. Therapeutic targeting of EGFR-activated metabolic pathways in glioblastoma. *Expert Opin. Investig. Drugs* **22**, 1023–1040 (2013).
35. Wee, P. &Wang, Z. Epidermal growth factor receptor cell proliferation signaling pathways. *Cancers* **9**, 1–45 (2017).
36. Gan, H. K., Cvrljevic, A. N. &Johns, T. G. The epidermal growth factor receptor variant III (EGFRvIII): Where wild things are altered. in *FEBS Journal* **280**, 5350–5370 (2013).
37. Dubrow, R. *et al.* Time trends in glioblastoma multiforme survival: The role of temozolomide. *Neuro. Oncol.* **15**, 1750–1761 (2013).
38. Ohka, F., Natsume, A. &Wakabayashi, T. Current trends in targeted therapies for glioblastoma multiforme. *Neurology Research International* **2012**, (2012).
39. Stupp, R., Mason, W. P. &van denBent, M. J. Radiotherapy plus Concomitant and Adjuvant Temozolomide for Glioblastoma. *Oncol. Times* **27**, 15–16 (2005).
40. Mason, W. P. *et al.* Canadian recommendations for the treatment of glioblastoma multiforme. *Current Oncology* **14**, 110–117 (2007).
41. Kim, T. G. *et al.* Immunological factors relating to the antitumor effect of temozolomide chemoimmunotherapy in a murine glioma model. *Clin. Vaccine Immunol.* **17**, 143–153 (2010).
42. Koul, D. PTEN Signaling pathways in glioblastoma PTEN signaling pathways in glioblastoma. *Cancer Biol. Ther.* **7**, 1321–1325 (2008).
43. Paff, M., Alexandru-Abrams, D., Hsu, F. P. K. &Bota, D. A. The evolution of the EGFRvIII (rindopepimut) immunotherapy for glioblastoma multiforme patients. *Hum. Vaccines Immunother.* **10**, 3322–3331 (2014).
44. Shiraishi, S. *et al.* Influence of p53 mutations on prognosis of patients with glioblastoma. *Cancer* **95**, 249–257 (2002).
45. Perazzoli, G. *et al.* Temozolomide resistance in glioblastoma cell lines: Implication of MGMT, MMR, P-glycoprotein and CD133 expression. *PLoS One* **10**, 1–24 (2015).
46. Barciszewska, A. M., Gurda, D., Głodowicz, P., Nowak, S. &Naskręt-Barciszewska, M. Z. A new epigenetic mechanism of temozolomide action in glioma cells. *PLoS One* **10**, (2015).
47. Perazzoli, G. *et al.* Temozolomide resistance in glioblastoma cell lines: Implication of MGMT, MMR, P-glycoprotein and CD133 expression. *PLoS One* **10**, 1–23 (2015).
48. Hanif, F., Malhi, S. M., Perveen, K., Simjee, S. U. &Muzaffar, K. Glioblastoma multiforme: A review of its epidemiology and pathogenesis through clinical presentation and treatment. *Asian Pacific J. Cancer Prev.* **18**, 3–9 (2017).
49. Kitange, G. J. *et al.* Induction of MGMT expression is associated with temozolomide resistance in glioblastoma xenografts. *Neuro. Oncol.* **11**, 281–291 (2009).

50. Chadt, J., Sykora, D., Nilsson, R. &Vodicka, P. Monitoring of dimethyl sulphate-induced N3-methyladenine, N7-methylguanine and O6-methylguanine DNA adducts using reversed-phase high performance liquid chromatography and mass spectrometry. *J. Chromatogr. B Anal. Technol. Biomed. Life Sci.* **867**, 43–48 (2008).
51. Lee, S. Y. Temozolomide resistance in glioblastoma multiforme. *Genes Dis.* **3**, 198–210 (2016).
52. Farias-Eisner, G. *et al.* Glioblastoma biomarkers from bench to bedside: Advances and challenges. *British Journal of Neurosurgery* **26**, 189–194 (2012).
53. Szerlip, N. J. *et al.* Intratumoral heterogeneity of receptor tyrosine kinases EGFR and PDGFRA amplification in glioblastoma defines subpopulations with distinct growth factor response. *Proc. Natl. Acad. Sci.* **109**, 3041–3046 (2012).
54. Qazi, M. A. *et al.* Intratumoral heterogeneity: Pathways to treatment resistance and relapse in human glioblastoma. *Ann. Oncol.* **28**, 1448–1456 (2017).
55. MacLeod, G. *et al.* Genome-Wide CRISPR-Cas9 Screens Expose Genetic Vulnerabilities and Mechanisms of Temozolomide Sensitivity in Glioblastoma Stem Cells. *Cell Rep.* **27**, 971-986.e9 (2019).
56. Stommel, J. *et al.* Coactivation of receptor tyrosine tumor cells to targeted therapies. *Science (80-.).* **318**, 287–90 (2007).
57. Chen, C., Xu, T., Lu, Y., Chen, J. &Wu, S. The efficacy of temozolomide for recurrent glioblastoma multiforme. *European Journal of Neurology* **20**, 223–230 (2013).
58. Baumann, M., Krause, M. &Hill, R. Exploring the role of cancer stem cells in radioresistance. *Nature Reviews Cancer* **8**, 545–554 (2008).
59. Pang, L. Y. &Argyle, D. J. The evolving cancer stem cell paradigm: Implications in veterinary oncology. *Veterinary Journal* **205**, 154–160 (2015).
60. Hamisch, C. *et al.* Impact of treatment on survival of patients with secondary glioblastoma. *J. Neurooncol.* **133**, 309–313 (2017).
61. Gessler, F. *et al.* Secondary Glioblastoma: Molecular and Clinical Factors That Affect Outcome After Malignant Progression of a Lower Grade Tumor. *World Neurosurg.* **102**, 49–55 (2017).
62. Sherriff, J. *et al.* Patterns of relapse in glioblastoma multiforme following concomitant chemoradiotherapy with temozolomide. *Br. J. Radiol.* **86**, 1–10 (2013).
63. L., C. *et al.* Glioblastoma recurrence patterns near neural stem cell regions. *Radiother. Oncol.* **116**, 294–300 (2015).
64. Goodwin, C. R. *et al.* Extraneural Glioblastoma Multiforme Vertebral Metastasis. *World Neurosurgery* **89**, 578-582.e3 (2016).
65. Granados, A. M., Zuñiga, N., Ospina, C. &Merchancano, L. Secondary glioblastoma with abdominal metastasis: Case report. *Radiol. Case Reports* **13**, 347–351 (2018).
66. Zhen, L., Yufeng, C., Zhenyu, S. &Lei, X. Multiple extracranial metastases from secondary glioblastoma multiforme: a case report and review of the literature. *J. Neurooncol.* **97**, 451–457 (2010).

67. Ohgaki, H. &Kleihues, P. The definition of primary and secondary glioblastoma. *Clinical Cancer Research* **19**, 764–772 (2013).
68. Maity, A., Pore, N., Haas-Kogan, D. A. &O'Rourke, D. M. PTEN mutation cooperates with EGFR activation in human glioblastoma cells to increase VEGF mRNA levels by transactivating an element in the proximal promoter. *Int. J. Radiat. Oncol.* **51**, 101–102 (2001).
69. Madhusudan, S., Abbotts, R. &Thompson, N. DNA repair in cancer: emerging targets for personalized therapy. *Cancer Manag. Res.* **6**, 77 (2014).
70. Roy, S., Lahiri, D., Maji, T. &Biswas, J. Recurrent Glioblastoma: Where we stand. *South Asian J. Cancer* **4**, 163 (2016).
71. Reardon, D. A. Therapeutic Advances in the Treatment of Glioblastoma: Rationale and Potential Role of Targeted Agents. *Oncologist* **11**, 152–164 (2006).
72. Andaloussi-Saghir, K. *et al.* Secondary gliosarcoma after the treatment of primary glioblastoma multiforme. *N. Am. J. Med. Sci.* **3**, 527–530 (2011).
73. Krolicki, L. *et al.* Prolonged survival in secondary glioblastoma following local injection of targeted alpha therapy with 213Bi-substance P analogue. *Eur. J. Nucl. Med. Mol. Imaging* **45**, 1636–1644 (2018).
74. Dumitru, C. A., Sandalcioglu, I. E. &Karsak, M. Cannabinoids in Glioblastoma Therapy: New Applications for Old Drugs. *Front. Mol. Neurosci.* **11**, 1–7 (2018).
75. Russo, C. *et al.* Low doses of widely consumed cannabinoids (cannabidiol and cannabidivarin) cause DNA damage and chromosomal aberrations in human-derived cells. *Arch. Toxicol.* **93**, 179–188 (2019).
76. Duchamp, O. *et al.* Magnetic resonance imaging study of carmustin and sorafenib antitumor efficacy evaluation in orthotopic human glioblastoma models xenografted in nude rats. *Eur. J. Cancer Suppl.* **6**, 109 (2008).
77. Shapira-Furman, T. *et al.* Biodegradable wafers releasing Temozolomide and Carmustine for the treatment of brain cancer. *J. Control. Release* **295**, 93–101 (2019).
78. Annovazzi, L. *et al.* The DNA damage/repair cascade in glioblastoma cell lines after chemotherapeutic agent treatment. *Int. J. Oncol.* **46**, 2299–2308 (2015).
79. Ramirez, Y. P., Weatherbee, J. L., Wheelhouse, R. T. &Ross, A. H. Glioblastoma multiforme therapy and mechanisms of resistance. *Pharmaceuticals* **6**, 1475–1506 (2013).
80. Jiang, L. *et al.* Genetic Evidence for Genotoxic Effect of Entecavir, an Anti-Hepatitis B Virus Nucleotide Analog. *PLoS One* **11**, e0147440 (2016).
81. Curtin, N. J. Inhibiting the DNA damage response as a therapeutic manoeuvre in cancer. *Br. J. Pharmacol.* **169**, 1745–1765 (2013).
82. Annovazzi, L. *et al.* The DNA damage/repair cascade in glioblastoma cell lines after chemotherapeutic agent treatment. *Int. J. Oncol.* **46**, 2299–2308 (2015).
83. Yin, S. &VanMeir, E. G. p53 Pathway Alterations in Brain Tumors. in *CNS Cancer* 283–314 (Humana Press, 2009). doi:10.1007/978-1-60327-553-8_14
84. McKinnon, Peter, J. DNA repair deficiency and neurological disease. *Nat. Rev. Neurosci.* **10**, 100–112 (2009).

85. D'Rozario, R. S. G. &Sansom, M. S. P. Helix dynamics in a membrane transport protein: comparative simulations of the glycerol-3-phosphate transporter and its constituent helices. *Mol. Membr. Biol.* **25**, 571–83 (2008).
86. JOVČEVSKA, I., KOČEVAR, N. &KOMEL, R. Glioma and glioblastoma - how much do we (not) know? *Mol. Clin. Oncol.* **1**, 935–941 (2013).
87. Shimizu, I., Yoshida, Y., Suda, M. &Minamino, T. DNA damage response and metabolic disease. *Cell Metabolism* **20**, 967–977 (2014).
88. Kubota, E. *et al.* Low ATM protein expression and depletion of p53 correlates with olaparib sensitivity in gastric cancer cell lines. *Cell Cycle* **13**, 2129–2137 (2014).
89. Rouse, J. &Jackson, S. P. Interfaces between the detection, signaling, and repair of DNA damage. *Science* **297**, 547–551 (2002).
90. Ito, M. *et al.* Early Chk1 Phosphorylation Is Driven by Temozolomide-Induced, DNA Double Strand Break- and Mismatch Repair-Independent DNA Damage. *PLoS One* **8**, 1–12 (2013).
91. Song, J. Y., Lim, J. W., Kim, H., Morio, T. &Kim, K. H. Oxidative stress induces nuclear loss of DNA repair proteins Ku70 and Ku80 and apoptosis in pancreatic acinar AR42J cells. *J. Biol. Chem.* **278**, 36676–36687 (2003).
92. You, Z. &Bailis, J. M. DNA damage and decisions: CtIP coordinates DNA repair and cell cycle checkpoints. *Trends in Cell Biology* **20**, 402–409 (2010).
93. Bennardo, N., Cheng, A., Huang, N. &Stark, J. M. Alternative-NHEJ is a mechanistically distinct pathway of mammalian chromosome break repair. *PLoS Genet.* **4**, (2008).
94. Zhao, W. *et al.* BRCA1-BARD1 promotes RAD51-mediated homologous DNA pairing. *Nature* **550**, (2017).
95. Liu, L., Taverna, P., Whitacre, C. M., Chatterjee, S. &Gerson, S. L. Pharmacologic disruption of base excision repair sensitizes mismatch repair-deficient and -proficient colon cancer cells to methylating agents. *Clin. Cancer Res.* **5**, 2908–2917 (1999).
96. Durocher, D. DNA Damage Sensing and Signaling. in *The DNA Damage Response: Implications on Cancer Formation and Treatment* 1–449 (2009). doi:10.1007/978-90-481-2561-6
97. Dar, I. &Barzilai, A. Cellular Responses to Oxidative Stress. in *The DNA Damage Response: Implications on Cancer Formation and Treatment* 1–449 (2009). doi:10.1007/978-90-481-2561-6
98. Guerra, B., Iwabuchi, K. &Issinger, O. G. Protein kinase CK2 is required for the recruitment of 53BP1 to sites of DNA double-strand break induced by radiomimetic drugs. *Cancer Lett.* **345**, 115–123 (2014).
99. Agnihotri, S. *et al.* ATM Regulates 3-Methylpurine-DNA Glycosylase and Promotes Therapeutic Resistance to Alkylating Agents. *Cancer Discov.* **4**, 1198–1213 (2014).
100. Tomicic, M. T. *et al.* Apoptosis induced by temozolomide and nimustine in glioblastoma cells is supported by JNK/c-Jun-mediated induction of the BH3-only protein BIM. *Oncotarget* **6**, 33755–33768 (2015).
101. Davis, A. J. &Chen, D. J. DNA double strand break repair via non-homologous end-joining. *Transl Cancer Res* **2**, 130–143 (2013).

102. Barnum, K. J. &Connell, M. J. O. Cell Cycle Regulation by Checkpoints. in *Nippon Ronen Igakkai Zasshi. Japanese Journal of Geriatrics* **35**, 713–716 (2011).
103. Modrich, P. Mismatch Repair in Replication Fidelity, Genetic Recombination, and Cancer Biology. *Annu. Rev. Biochem.* **65**, 101–133 (1996).
104. Guarné, A. The Functions of MutL in Mismatch Repair. in *Progress in Molecular Biology and Translational Science* **110**, 41–70 (2012).
105. Lebedeva, N. A., Rechkunova, N. I. &Lavrik, O. I. The new base excision repair pathway in mammals mediated by tyrosyl-DNA-phosphodiesterase 1. *Biopolym. Cell* **28**, 202–206 (2012).
106. Peña-Diaz, J. &Jiricny, J. Mammalian mismatch repair: Error-free or error-prone? *Trends in Biochemical Sciences* **37**, 206–214 (2012).
107. Swartzlander, D. B., Bauer, N. C., Corbett, A. H. &Doetsch, P. W. Regulation of base excision repair in eukaryotes by dynamic localization strategies. in *Progress in Molecular Biology and Translational Science* **110**, 93–121 (Elsevier Inc., 2012).
108. Tsai, W.Bin, Chung, Y. M., Takahashi, Y., Xu, Z. &Hu, M. C. T. Functional interaction between FOXO3a and ATM regulates DNA damage response. *Nat. Cell Biol.* **10**, 460–467 (2008).
109. Kuo, L. J. &Yang, L.-X. Gamma-H2AX - a novel biomarker for DNA double-strand breaks. *In Vivo* **22**, 305–9 (2008).
110. Das, B. B. *et al.* Optimal function of the DNA repair enzyme TDP1 requires its phosphorylation by ATM and/or DNA-PK. *EMBO J.* **28**, 3667–3680 (2009).
111. Sánchez-Pérez, I. DNA repair inhibitors in cancer treatment. *Clin. Transl. Oncol.* **8**, 642–646 (2006).
112. Amunugama, R. &Fishel, R. Homologous recombination in eukaryotes. in *Progress in Molecular Biology and Translational Science* **110**, 155–206 (Elsevier Inc., 2012).
113. Hsu, C. Y., Ho, H. L., Lin, S. C., Ho, T. D. H. &Ho, D. M. T. The MGMT promoter single-nucleotide polymorphism rs1625649 had prognostic impact on patients with MGMT methylated glioblastoma. *PLoS One* **12**, 1–10 (2017).
114. Zhang, J., F.G. Stevens, M. &D. Bradshaw, T. Temozolomide: Mechanisms of Action, Repair and Resistance. *Curr. Mol. Pharmacol.* **5**, 102–114 (2012).
115. Blanc, J. L. *et al.* Correlation of clinical features and methylation status of MGMT gene promoter in glioblastomas. *J. Neurooncol.* **68**, 275–283 (2004).
116. Rolhion, C. *et al.* O6-methylguanine-DNA methyltransferase gene (MGMT) expression in human glioblastomas in relation to patient characteristics and p53 accumulation. *Int. J. Cancer* **84**, 416–420 (1999).
117. Bandey, I., Chiou, S. H., Huang, A. P., Tsai, J. C. &Tu, P. H. Progranulin promotes Temozolomide resistance of glioblastoma by orchestrating DNA repair and tumor stemness. *Oncogene* **34**, 1853–1864 (2014).
118. Chalah, A. &Khosravi-Far, R. The Mitochondrial Death Pathway. in *Programmed Cell Death in Cancer Progression and Therapy* **615**, 25–45 (2008).
119. Shen, S. *et al.* Association and dissociation of autophagy, apoptosis and necrosis by systematic chemical study. *Oncogene* **30**, 4544–4556 (2011).
120. Zilfou, J. T., Spector, M. S. &Lowe, S. W. Slugging it out: Fine tuning the p52-PUMA Death Connection. *Cell* **123**, 543–545 (2005).

121. Melino, G. *et al.* p75 Induces Apoptosis via PUMA Transactivation and Bax Mitochondrial Translocation. *J. Biol. Chem.* **279**, 8076–8083 (2004).
122. Salvesen, G. S. &Riedl, S. J. Caspase mechanisms. *Advances in Experimental Medicine and Biology* **615**, 13–23 (2008).
123. Scavone, C. Acute neuronal injury: the role of excitotoxic programmed cell death mechanisms. *Brazilian J. Pharm. Sci.* **46**, 823–823 (2011).
124. Chulu, J. L. C. *et al.* Apoptosis induction by avian reovirus through p53 and mitochondria-mediated pathway. *Biochem. Biophys. Res. Commun.* **356**, 529–535 (2007).
125. Simon, H. U., Haj-Yehia, A. &Levi-Schaffer, F. Role of reactive oxygen species (ROS) in apoptosis induction. *Apoptosis* **5**, 415–8 (2000).
126. Rulten, S. L., Dantzer, F. &Caldecott, K. W. The Role of PARPs in DNA Strand Break Repair. in *PARP Inhibitors for Cancer Therapy* **169**, 47–78 (2015).
127. Canan, S. S. Structure Based Design of PARP Inhibitors. in *PARP Inhibitors for Cancer Therapy* 205–221 (2015). doi:10.1007/978-3-319-14151-0_8
128. Ha, K. *et al.* Histone deacetylase inhibitor treatment induces 'BRCAness' and synergistic lethality with PARP inhibitor and cisplatin against human triple negative breast cancer cells. *Oncotarget* **5**, 5637–5650 (2014).
129. Cardillo, T. M. *et al.* Synthetic lethality exploitation by an anti-trop-2-SN-38 antibody-drug conjugate, IMMU-132, plus PARP inhibitors in BRCA1/2-wild-type triple-negative breast cancer. *Clin. Cancer Res.* **23**, 3405–3415 (2017).
130. Höglund, A., Strömvall, K., Li, Y., Forshell, L. P. &Nilsson, J. A. Chk2 deficiency in Myc overexpressing lymphoma cells elicits a synergistic lethal response in combination with PARP inhibition. *Cell Cycle* **10**, 3598–3607 (2011).
131. Geng, L., Huehls, A. M., Wagner, J. M., Huntoon, C. J. &Karnitz, L. M. Checkpoint signaling, base excision repair, and PARP promote survival of colon cancer cells treated with 5-fluorodeoxyuridine but not 5-fluorouracil. *PLoS One* **6**, 1–10 (2011).
132. Schreiber, V. *et al.* Poly(ADP-ribose) polymerase-2 (PARP-2) is required for efficient base excision DNA repair in association with PARP-1 and XRCC1. *J. Biol. Chem.* **277**, 23028–23036 (2002).
133. Orta, M. L. *et al.* The PARP inhibitor Olaparib disrupts base excision repair of 5-aza-2'-deoxycytidine lesions. *Nucleic Acids Res.* **42**, 9108–9120 (2014).
134. Murai, J. &Pommier, Y. Classification of PARP Inhibitors Based on PARP Trapping and Catalytic Inhibition, and Rationale for Combinations with Topoisomerase I Inhibitors and Alkylating Agents. in *PARP Inhibitors for Cancer Therapy, Cancer Drug Discovery and Development* **169**, 261–274 (2015).
135. Lu, Y., Liu, Y., Pang, Y., Pacak, K. &Yang, C. Double-barreled gun: Combination of PARP inhibitor with conventional chemotherapy. *Pharmacology and Therapeutics* **188**, 168–175 (2018).
136. Shih, K. *et al.* Phase 1b/2 study to access the clinical effectos of Pamiparib (BGB-290) in combination with radiation therapy (RT) and/or Temozolomide (TMZ) in patient with newly diagnosed or recurrent/refractory Glioblastoma (GBM). *Neuro. Oncol.* **20**, vi17–vi18 (2018).

137. Pommier, Y. &Murai, J. Classification of PARP inhibitors based on PARP trapping and catalytic inhibition, and rationale for combinations. *Ann. Oncol.* **26**, ii8–ii8 (2015).
138. Laird, J. H. *et al.* Talazoparib is a potent radiosensitizer in small cell lung cancer cell lines and xenografts. *Clin. Cancer Res.* **24**, 5143–5152 (2018).
139. Zimmermann, M. *et al.* CRISPR screens identify genomic ribonucleotides as a source of PARP-trapping lesions. *Nature* **559**, 285–289 (2018).
140. Koh, S. H. *et al.* The effect of PARP inhibitor on ischaemic cell death, its related inflammation and survival signals. *Eur. J. Neurosci.* **20**, 1461–1472 (2004).
141. Somnay, Y., Lubner, S., Gill, H., Matsumura, J. B. &Chen, H. The PARP inhibitor ABT-888 potentiates dacarbazine-induced cell death in carcinoids. *Cancer Gene Ther.* **23**, 348–354 (2016).
142. Drabycz, S. *et al.* An analysis of image texture, tumor location, and MGMT promoter methylation in glioblastoma using magnetic resonance imaging. *Neuroimage* **49**, 1398–1405 (2010).
143. Khwaja, F. W. &VanMeir, E. G. Proteomic Discovery of Biomarkers in the Cerebrospinal Fluid of Brain Tumor Patients. in *CNS Cancers* 577–613 (2010). doi:10.1002/0471266949.bmc223
144. Clarke, R. H. *et al.* Sustained radiosensitization of hypoxic glioma cells after oxygen pretreatment in an animal model of glioblastoma and in vitro models of tumor hypoxia. *PLoS One* **9**, (2014).
145. Munoz, J. L., Walker, N. D., Scotto, K. W. &Rameshwar, P. Temozolomide competes for P-glycoprotein and contributes to chemoresistance in glioblastoma cells. *Cancer Lett.* **367**, 69–75 (2015).
146. Liu, X. &Raju, P. In Vitro Cancer Model for Drug Testing. in *Comprehensive Biotechnology, Second Edition* **5**, 543–549 (Elsevier B.V., 2011).
147. Chiew, G. G. Y., Wei, N., Sultania, S., Lim, S. &Luo, K. Q. Bioengineered three-dimensional co-culture of cancer cells and endothelial cells: A model system for dual analysis of tumor growth and angiogenesis. *Biotechnol. Bioeng.* **114**, 1865–1877 (2017).
148. Vora, P., Venugopal, C., McFarlane, N. &Singh, S. K. Culture and isolation of brain tumor initiating cells. *Curr. Protoc. Stem Cell Biol.* **2015**, 3.3.1-3.3.13 (2015).
149. Mischel, P. S., Nelson, S. F. &Cloughesy, T. F. Molecular Analysis of Glioblastoma: Pathway Profiling and Its Implications for Patient Therapy. *Cancer Biol. Ther.* **2**, 242–247 (2003).
150. Kirschner, S. *et al.* In vivo micro-CT imaging of untreated and irradiated orthotopic glioblastoma xenografts in mice: capabilities, limitations and a comparison with bioluminescence imaging. *J. Neurooncol.* **122**, 245–254 (2015).
151. Irtenkauf, S. M. *et al.* Optimization of glioblastoma mouse orthotopic xenograft models for translational research. *Comp. Med.* **67**, 300–314 (2017).
152. Tso, K. Y., Lee, S. D., Lo, K. W. &Yip, K. Y. Are special read alignment strategies necessary and cost-effective when handling sequencing reads from patient-derived tumor xenografts? *BMC Genomics* **15**, 1–11 (2014).

153. Seyfried, T. N., Shelton, L. M. &Huysentruyt, L. C. The VM Mouse Model of Glioblastoma Multiforme. in *Molecular Imaging in the Clinical Neurosciences* **1971**, 39–55 (2012).
154. Lau, J. &Weiss, W. A. Medulloblastoma Model. *Mol. Imaging Clin. Neurosci.* **1971**, 83–140 (2012).
155. Oh, T. *et al.* Immunocompetent murine models for the study of glioblastoma immunotherapy. *Journal of Translational Medicine* **12**, 1–10 (2014).
156. Zhang, M. *et al.* Proteome alteration of U251 human astrocytoma cell after inhibiting retinoic acid synthesis. *Mol. Cell. Biochem.* **323**, 185–193 (2009).
157. Larson, B. &Instruments, B. Automated Comet Assay Imaging and Dual-Mask Analysis to Determine DNA Damage on an Individual Comet Basis. (2016).
158. Larson, B., Sinha, A. &Katyal, S. Automated Imaging and Dual-Mask Spot Counting of γ H2AX Foci to Determine DNA Damage on an Individual Cell Basis. (2017).
159. Lee, Y. *et al.* Neurogenesis requires TopBP1 to prevent catastrophic replicative DNA damage in early progenitors. *Nat. Neurosci.* **15**, 819–26 (2012).
160. Rosso, L. *et al.* A new model for prediction of drug distribution in tumor and normal tissues: Pharmacokinetics of temozolomide in glioma patients. *Cancer Res.* **69**, 120–127 (2009).
161. Liu, L., Nakatsuru, Y. &Gerson, S. L. Base excision repair as a therapeutic target in colon cancer. *Clin. Cancer Res.* **8**, 2985–2991 (2002).
162. Wallace, S. S., Murphy, D. L. &Sweasy, J. B. Base excision repair and cancer. *Cancer Letters* **327**, 73–89 (2012).
163. Pommier, Y. *et al.* Tyrosyl-DNA-phosphodiesterases (TDP1 and TDP2). *DNA Repair (Amst).* **19**, 114–129 (2014).
164. Wu, S. *et al.* EGFR amplification induced increasesed DNA damage response and predicted selective sensitivity to Talazoparib (PARP inhibitor) in Glioblastoma stem-like cells. *Neuro. Oncol.* **20**, vi69–vi69 (2018).
165. Fraietta, I. &Gasparri, F. The development of high-content screening (HCS) technology and its importance to drug discovery. *Expert Opin. Drug Discov.* **11**, 501–514 (2016).
166. Bickle, M. The beautiful cell: High-content screening in drug discovery. *Analytical and Bioanalytical Chemistry* **398**, 219–226 (2010).
167. Huang, B. S. *et al.* MiR-223/PAX6 Axis Regulates Glioblastoma Stem Cell Proliferation and the Chemo Resistance to TMZ via Regulating PI3K/Akt Pathway. *J. Cell. Biochem.* **118**, 3452–3461 (2017).
168. Jhaveri, N. *et al.* Noscapine inhibits tumor growth in TMZ-resistant gliomas. *Cancer Lett.* **312**, 245–252 (2011).
169. Nogales-Gomez, P. *et al.* DRES-12. FUNCTIONAL GENETIC APPROACHES TO OVERCOME TEMOZOLOMIDE RESISTANCE IN GLIOBLASTOMA. *Neuro. Oncol.* **20**, vi78–vi78 (2018).
170. Cui, B. *et al.* Decoupling of DNA damage response signaling from DNA damages underlies temozolomide resistance in glioblastoma cells. *J. Biomed. Res.* **24**, 424–435 (2010).

171. Agnihotri, S. *et al.* Alkylpurine-DNA-N-glycosylase confers resistance to temozolomide in xenograft models of glioblastoma multiforme and is associated with poor survival in patients. *J. Clin. Invest.* **122**, 253–266 (2012).
172. Yamamoto, Y. *et al.* Involvement of Intracellular Cholesterol in Temozolomide-Induced Glioblastoma Cell Death. *Neurol. Med. Chir. (Tokyo).* **58**, 296–302 (2018).
173. Tappuni, S., Noonan, J. &Murphy, B. Inducing cell death in Glioblastoma. *BMC Proc.* **9**, 6561 (2015).
174. Kitange, G. J. *et al.* Evaluation of MGMT promoter methylation status and correlation with temozolomide response in orthotopic glioblastoma xenograft model. *J. Neurooncol.* **92**, 23–31 (2009).
175. Magni, M. *et al.* CCAR2/DBC1 is required for Chk2-dependent KAP1 phosphorylation and repair of DNA damage. *Oncotarget* **6**, (2015).
176. Bhatia, N. *et al.* MAGE-C2 promotes growth and tumorigenicity of melanoma cells, phosphorylation of KAP1, and DNA damage repair. *J. Invest. Dermatol.* **133**, 759–767 (2013).
177. Markkanen, E., Fischer, R., Ledentcova, M., Kessler, B. M. &Dianov, G. L. Cells deficient in base-excision repair reveal cancer hallmarks originating from adjustments to genetic instability. *Nucleic Acids Res.* **43**, 3667–3679 (2015).
178. Li, Q., Ma, R. &Zhang, M. XRCC1 rs1799782 (C194T) polymorphism correlated with tumor metastasis and molecular subtypes in breast cancer. *Onco. Targets. Ther.* **11**, 8435–8444 (2018).
179. Colicchia, V. *et al.* PARP inhibitors enhance replication stress and cause mitotic catastrophe in MYCN-dependent neuroblastoma. *Oncogene* **36**, 4682–4691 (2017).
180. Montariello, D. *et al.* Effect of poly(ADP-ribose)polymerase and DNA topoisomerase i inhibitors on the p53/p63-dependent survival of carcinoma cells. *Biochem. Pharmacol.* **94**, 212–219 (2015).
181. D'Onofrio, G. *et al.* Poly(ADP-ribose) polymerase signaling of topoisomerase 1-dependent DNA damage in carcinoma cells. *Biochem. Pharmacol.* **81**, 194–202 (2011).
182. Murai, J. *et al.* Stereospecific PARP Trapping by BMN 673 and Comparison with Olaparib and Rucaparib. *Mol. Cancer Ther.* **13**, 433–443 (2014).
183. Qian, X. *et al.* Identification of biomarkers for pseudo and true progression of GBM based on radiogenomics study. *Oncotarget* **7**, (2016).
184. Patel, A. P. *et al.* Single-cell RNA-seq highlights intratumoral heterogeneity in primary glioblastoma. *Science (80-.).* **344**, 1396–1401 (2014).

11. Supplemental Data

Notes

Controller Notes

YUA9229_RNA

Gel Image

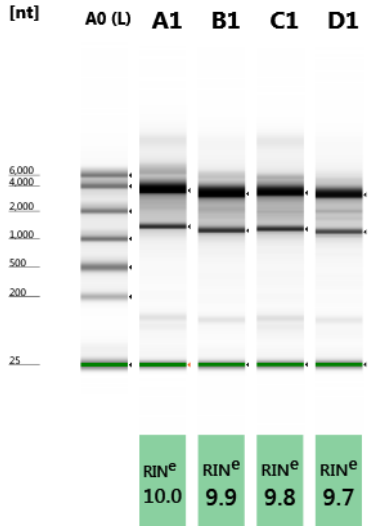

,RNA

Contrast: 0.50

Figure S1, Image of the RNA electrophoresis gel showing RNA sample purity of SG (lane A), SG(TMZ treated 72 hours, lane B), TRR (lane C), and TRR(TMZ treated, 72 hours, lane D)

Sample Info

Table S1. Table showing the purity and concentration of RNA samples at the stated concentrations.

Well	RIN^e	28S/18S (Height)	28S/18S (Area)	Conc. [ng/µl]	Sample Description	Alert	Observations	Total RNA Area	rRNA Area
A0	-	-	-	137			Ladder	-	-
A1	10.0	2.4	3.8	287	SG_diluted 5x			11.77	4.14
B1	9.9	2.2	3.3	261	SG (T)_diluted 2x			10.69	4.06
C1	9.8	2.0	3.0	252	TRR_diluted 4x			10.32	3.63
D1	9.7	2.1	3.0	190	TRR(T)_diluted 2x			7.77	2.79

A0

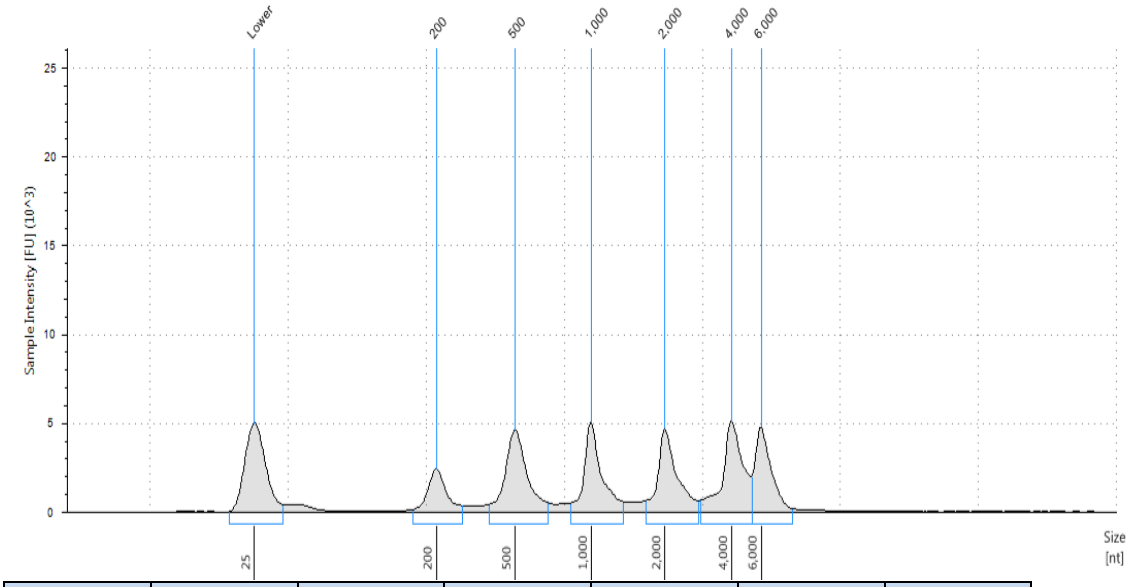

Size [nt]	Calibrated Conc. [ng/µl]	Assigned Conc. [ng/µl]	Peak Molarity [nmol/l]	% Integrated Area	Peak Comment	Observations
25	47.5	47.5	5590	-		Lower Marker
200	11.2	-	164	8.91		
500	24.8	-	146	19.84		
1,000	21.8	-	64.0	17.39		
2,000	22.2	-	32.6	17.72		
4,000	25.4	-	18.7	20.31		
6,000	19.8	-	9.71	15.83		

Figure S2. Graph showing RNA contents of the SG RNA sample.

A1

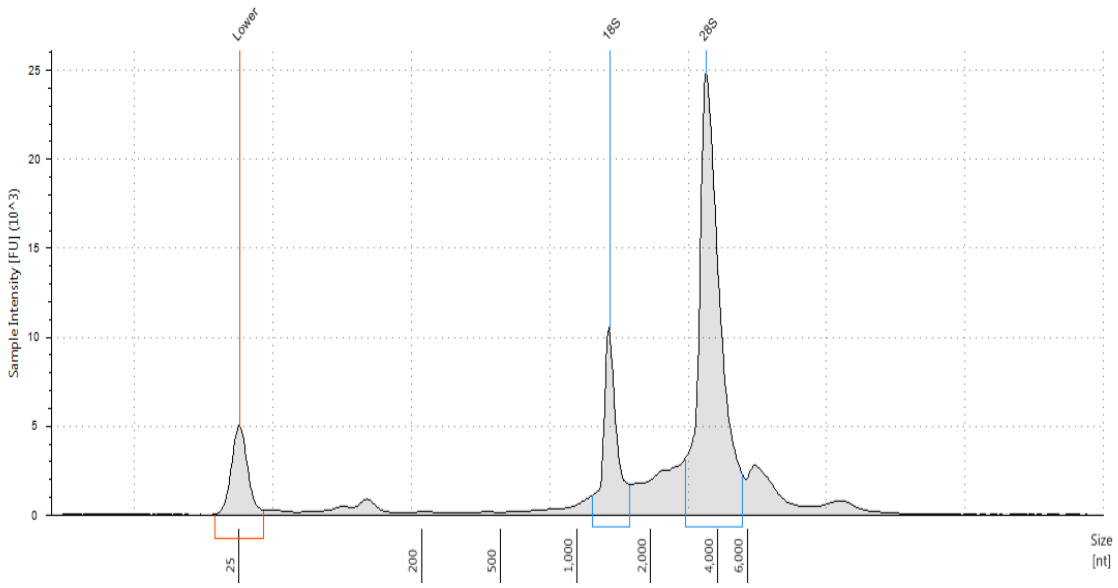

SG_diluted 5x

Size [nt]	Calibrated Conc. [ng/µl]	Assigned Conc. [ng/µl]	Peak Molarity [nmol/l]	% Integrated Area	Peak Comment	Observations
25	47.5	47.5	5590	-		Lower Marker
1,349	40.9	-	89.1	20.79		18S
3,533	156	-	130	79.21		28S

Figure S3. Graph showing RNA contents of the SG (5x dilution) sample.

B1

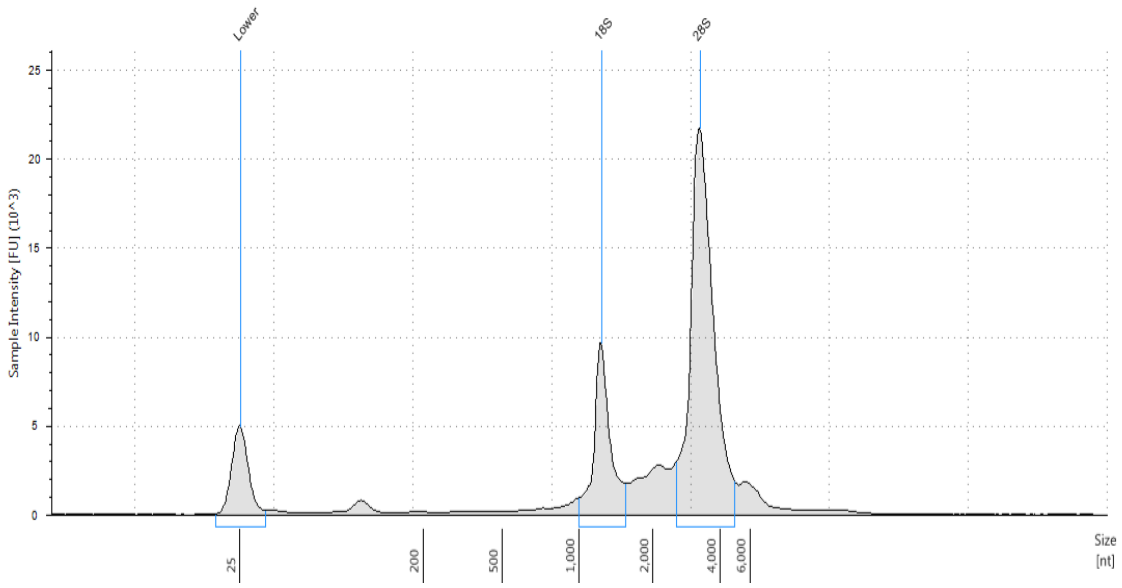

SG (T)_diluted 2x

Size [nt]	Calibrated Conc. [ng/µl]	Assigned Conc. [ng/µl]	Peak Molarity [nmol/l]	% Integrated Area	Peak Comment	Observations
25	47.5	47.5	5590	-		Lower Marker
1,226	45.2	-	108	23.45		18S
3,233	148	-	134	76.55		28S

Figure S4. Graph showing RNA contents of the SG(Treated) (2x dilution) sample.

C1

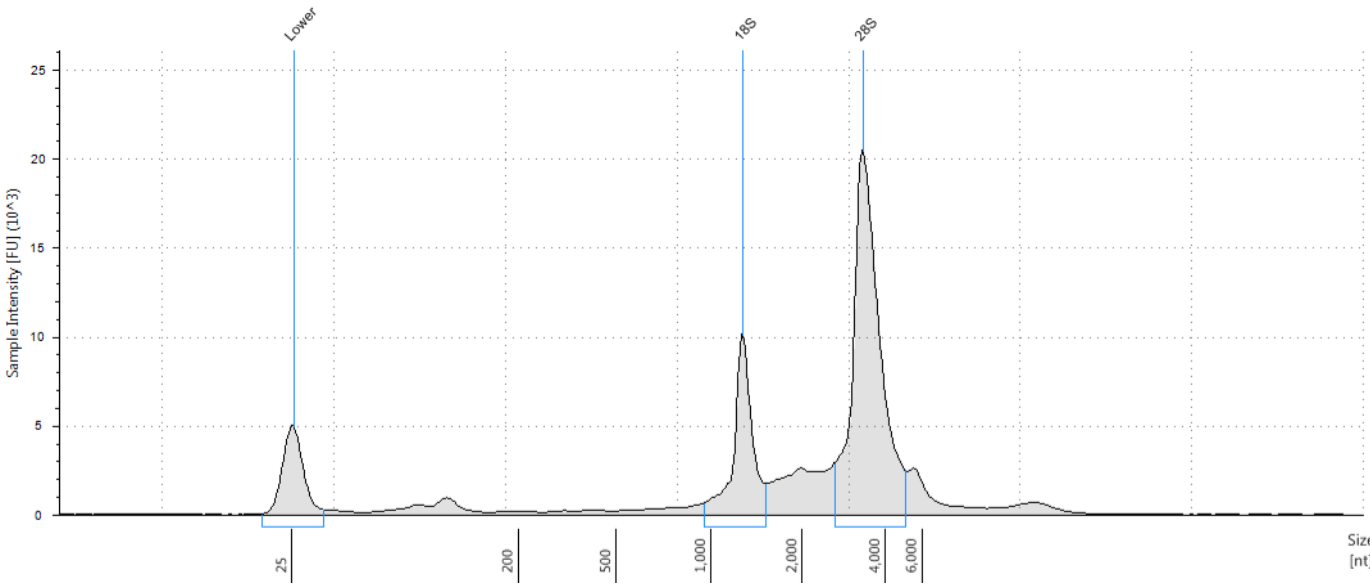

TRR_diluted 4x

Size [nt]	Calibrated Conc. [ng/µl]	Assigned Conc. [ng/µl]	Peak Molarity [nmol/l]	% Integrated Area	Peak Comment	Observations
25	47.5	47.5	5590	-		Lower Marker
1,266	43.6	-	101	25.25		18S
3,313	129	-	115	74.75		28S

Figure S5. Graph showing RNA contents of the TRR (4x dilution) sample.

D1

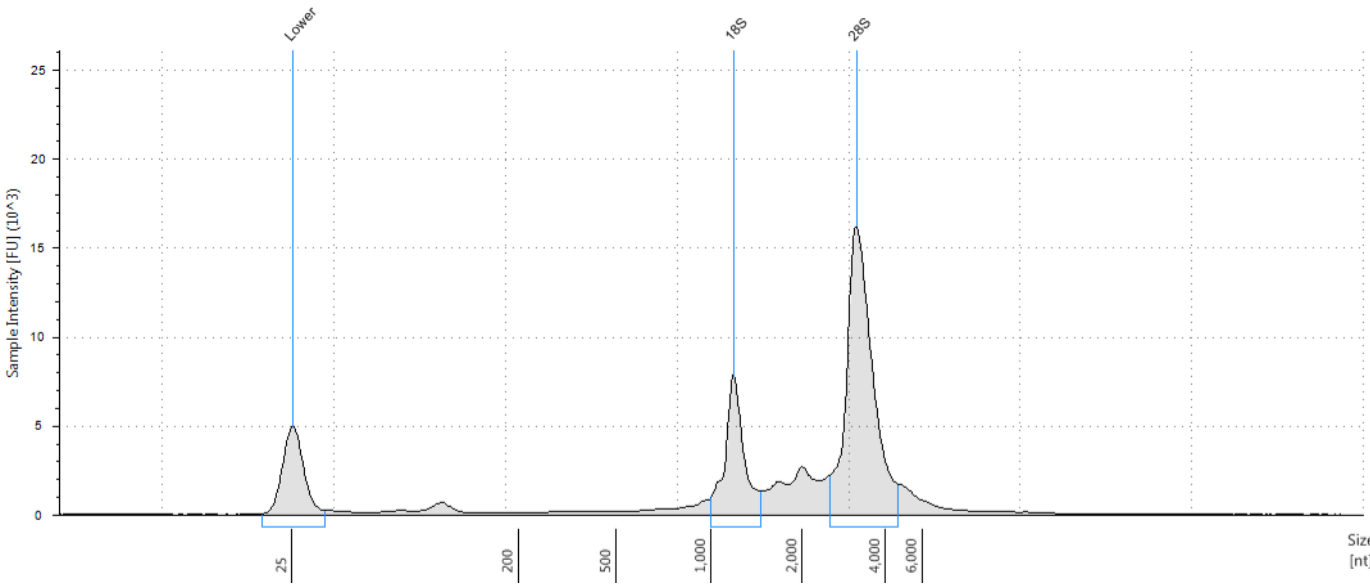

TRR(T)_diluted 2x

Size [nt]	Calibrated Conc. [ng/µl]	Assigned Conc. [ng/µl]	Peak Molarity [nmol/l]	% Integrated Area	Peak Comment	Observations
25	47.5	47.5	5590	-		Lower Marker
1,180	33.5	-	83.4	25.26		18S
3,143	99.0	-	92.6	74.74		28S

Figure S6. Graph showing RNA contents of the TRR(Treated) (2x dilution) sample.